DEVELOPMENT OF AN ACCURATE WIDE RANGE ULTRA HIGH VACUUM GAUGE CALIBRATION METHOD

By Peter Fowler and F. J. Brock

Prepared under Contract No. NAS5-3967 by
NATIONAL RESEARCH CORPORATION
Cambridge, Massachusetts

for

NATIONAL AERONAUTICS AND SPACE ADMINISTRATION

TABLE OF CONTENTS

		Page
	SUMMARY	1
1.	INTRODUCTION	2
2.	THEORY OF CALIBRATION SYSTEM	3
	2.1 Gauge Enclosure Method	6
	2.2 Analysis of Gauge Enclosure Method	8
	2.3 Probable Error in Calculated Pressure	13
3.	POROUS PLUG	19
	3.1 Porous Vycor Glass	19
	3.2 Porous Plug Conductance Measurement Technique	21
	3.3 Determination of Porous Glass Flow Properties	22
4.	INVESTIGATION OF MOLECULAR BEAM SOURCES	46
	4.1 Deviations From Free Molecular Flow of an Orifice	46
	4.2 Experimental Measurement of Conductance	50
	4.3 Scattering Effects in Molecular Beam Sources	63
	4.4 Non-Equilibrium Effects in Molecular Beam Sources	65
5.	CALIBRATION EXPERIMENT OF PROTOTYPE SYSTEM	66
6.	DISCUSSION, RESULTS, AND CONCLUSIONS	73
	6.1 Porous Plug	73
	6.2 Beam Orifice	75
	6.3 Molecular Furnace Equilibrium	77
	6.4 Time to Establish Calibration System Equilibrium	78
	6.5 Gas Properties	80
	6.5.1 Pressure-Volume-Temperature Relation for Gas	81
	6.5.2 Adsorption and Desorption of Gas	81

TABLE OF CONTENTS (Continued)

	Page
6.5.3 Background Gas Pressure	87
6.6 Application of Results to Design Principles	88
6.7 Probable Error in Gauge Pressure	92
7. RECOMMENDATIONS FOR FUTURE WORK	94
APPENDIX 1. MEAN MOLECULAR VELOCITY IN MOLECULAR BEAM	98
APPENDIX 2. ANALYSIS OF ORIFICE CONDUCTANCE EXPERIMENT	100
REFERENCES	105

LIST OF FIGURES

		PAGE
1.	Ultra High Vacuum Gauge Calibration System. (Schematic)	7
2.	Molecular Beam and Enclosure Apertures. (Schematic)	9
3.	Gas Source Chamber Volume Measurement Apparatus. (Schematic)	17
4.	Porous Plug #1.	23
5.	Porous Plug #2.	24
6.	Porous Plug #2 in Compression Mounting.	25
7.	Porous Plug #1 Mounted in Heat Treatment Furnace.	26
8.	Porous Plug #2 Mounted in Heat Treatment Furnace.	27
9.	Flow System for Porous Plug Conductance Measurement. (Schematic)	29
10.	Rotating Piston Gauge and Auxiliary Equipment.	30
11.	Gas Source Chamber and Molecular Furnace Prior to Joining.	31
12.	Porous Plug Conductance Measurement Experimental Apparatus.	33
13.	Porous Plug Conductance Measurement Run 1-1.	34
14.	Porous Plug Conductance Measurement Run 1-3.	35
15.	Porous Plug Conductance Measurement Run 1-4.	36
16.	Porous Plug Conductance Measurement Run 1-5.	37
17.	Porous Plug Conductance Measurement Run 1-6.	38
18.	Porous Plug Conductance Measurement Run 1-7.	39

LIST OF FIGURES (Continued)

		PAGE
19.	Porous Plug Conductance Measurement Run 1-8.	40
20.	Gas Source Chamber Volume Measurement Experimental Apparatus.	44
21.	Flux Distribution of Molecular Beam with $\ell/d = 0,1$ . .	49
22.	Orifice Conductance Measurement Experiment.. . . . . (Schematic).	51
23.	Orifice Conductance Measurement Experiment	56
24.	Orifice #1 Mounted on Gold O-Ring Seal Flange.	57
25.	Orifice #2 100X Magnified	58
26.	Orifice Conductance Measurement Run 1-6.	60
27.	Orifice Conductance Measurement Run 1-7.	61
28.	Calculated and Measured Deviation from Free Molecular Flow Through an Orifice.	62
29.	Calibration Run of Prototype System. a) Gauge and Enclosure in Cryopumped Chamber.	67
	b) Molecular Furnace and Gas Source Chamber Mounted on Cryopumping Chamber Wall.	67
30.	Auxiliary Apparatus for Calibration Run of Prototype System	68
31.	Calibration Data for Suppressor Grid Gauge	71
32.	Signal-to-Background Gas Pressure Ratio and Cryopump Temperature During Calibration Run	72
33.	Orifice #2 Mounted on Gold O-Ring Seal Flange.	76
34.	Argon Relative Coverage Versus Temperature for a 10 cm. Radius Spherical Cavity	84
35.	Maximum Gauge Enclosure Pressure Versus Beam Aperture Diameter for Various Constraining Conditions	89

LIST OF FIGURES (Concluded)

		PAGE
36.	Percentage Increase of Furnace Gas Density Due to Emergent Flux from Enclosure Versus ℓ	93
37.	Orifice Conductance Measurement Experiment. (Schematic)	100

LIST OF TABLES

No.		Page
1	LEAST SQUARES SLOPE SUMMARY FOR POROUS PLUGS	42
2	LEAST SQUARES ANALYSIS FOR POROUS PLUG EXPERIMENT 1-5	43
3	DATA OBTAINED ON CALIBRATION OF SUPPRESSOR GRID GAUGE	70
4	MAXIMUM FURNACE PRESSURE AND POROUS PLUG CONDUCTANCE FOR VARIOUS ALLOWED KNUDSEN NUMBERS	90

DEVELOPMENT OF AN ACCURATE WIDE RANGE ULTRA HIGH VACUUM GAUGE CALIBRATION METHOD

By Peter Fowler and F. J. Brock

SUMMARY

During the past year and one-half, under National Aeronautics and Space Administration Contract No. NAS5-3967, the National Research Corporation has been working on the development of an accurate, wide range, vacuum gauge calibration method. This method of calibration applies pressure attenuation, atomic beam, and cryopumping techniques to a system such that in a volume having extremely low background gas density, is formed an atomic beam having a precisely known density which is variable over the useful range of operation of ion gauges and mass spectrometers. Under the program, an analysis of the conceptual design of the calibration system and its components was made. A kinetic theory analysis of the gas flow in each component of the system was made to determine the important system parameters and establish their optimum value or required range such that the maximum dynamic range of beam density was obtained and the background density was minimized.

A prototype apparatus was constructed in order to experimentally evaluate the components of the system. Two types of porous Vycor glass plugs were made and their conductance measured with a probable error of less than 0.5%. The conductance of porous Vycor was determined to be independent of pressure to within 0.5% up to a pressure of 5200 Torr, which corresponds to a Knudsen number of 1.7. This implies a dynamic range of pressure in the calibration system gas source of at least 350.

Measurement of orifice conductance for nearly ideal apertures was made at pressures corresponding to Knudsen numbers as small as 0.75. The orifice conductance was found to deviate less than 1% from that expected for free molecular flow for Knudsen numbers greater than 12. The deviation from free molecular flow for a Knudsen number of 0.75 was measured to be $\sim$7.5%.

The prototype calibration system was installed in an extreme high vacuum system and its performance evaluated. The signal-to-noise ratio (beam to background pressure ratio) for argon was

found to be of the order of 460 for a cryopump temperature of 11°K and 40 for 12°K. These ratios indicate that a sufficiently low background gas density for proper calibration system performance can be maintained in a cavity cooled to the temperature of liquid helium (4.2°K).

An accumulative error analysis of the calibration system was made to establish the absolute calibration accuracy attainable. In this analysis, the maximum probable deviation of the actual performance from the predicted performance was determined and evaluated in terms of the accuracy of measurement of individual system parameters and the accuracy with which the constraints were satisfied. The analysis showed that for the average probable error found to be attainable in the individual parameters, the accumulated probable error of the calibration system could be maintained less than 5%.

In the work completed to date, considerable confidence has been developed that the proposed method of calibration will have the desired accuracy and range. However, additional research is required to determine: 1) the flow properties of gases other than argon through porous glass, 2) the minimum attainable background pressure in the cryopump and gauge enclosure, 3) the angular distribution of molecules in the molecular beam, and 4) the orifice conductance, accurately, for small Knudsen numbers.

1. INTRODUCTION

The pressure gauges and mass spectrometers for use in analyzing upper atmosphere and interplanetary gases must have a known response over a wide pressure range. It is thus required that there exist an accurate calibration method to cover this wide pressure range and that the calibrations performed have reference to a widely accepted absolute pressure standard. The purpose of this investigation is to develop and test the elements of such a calibration method.

Ideally, it is preferable to place a vacuum gauge in a perfectly clean, empty, inert vacuum system, into which may be introduced an accurately known, controllable, gas pressure. The nearest actual approach to this ideal is to place the gauge in an accurately known flux of a molecular beam, operating in an extreme high vacuum system.

Such a system has been investigated. It consists of a high pressure gas source which supplies gas through a porous plug to a molecular furnace from which is extracted the molecular beam to be injected into a cryopumped gauge calibration cavity. The pressure range over which the gas source is operated is within the measurement range of a precision rotating piston gauge for which the National Bureau of Standards will provide certification.

2. THEORY OF CALIBRATION SYSTEM

Consider a chamber which serves as a gas pressure source, maintained at pressure p_o from which the gas effuses in molecular flow through a porous plug, having a conductance C_p. The quantity of gas effusing is then

$$Q_p = C_p p_o. \qquad (2.0.1)$$

Consider further the effusing gas to enter a second chamber, the molecular furnace, in one wall of which is a molecular beam forming aperture that is a plane, circular, ideal aperture of area S_a and conductance C_a. It is assumed that the gas density outside of S_a is maintained negligibly small. If the pressure, p, in the molecular furnace is maintained low enough such that flow through the aperture is free molecular effusion, Knudsen[1] has shown that for a gas in thermal equilibrium with molecular furnace walls, the quantity of gas passing outward through S_a per second is

$$Q_f = pC_a = p\frac{\bar{v}S_a}{4}, \qquad (2.0.2)$$

where $\bar{v}$ is the mean molecular speed in the furnace. Deviations from this behavior for high pressures and flow rates will be discussed in later sections.

When conditions of steady flow have been established, the flow rate into the furnace must be equal to that out of the furnace, or

$$p_o C_p = p C_a . \qquad (2.0.3)$$

Anticipating the requirements of a wide range calibration system, and therefore a large pressure attenuation between the gas source and the molecular furnace, a second aperture of conductance, C is introduced in the molecular furnace wall so that in place of Equation (2.0.3), we have

$$p_o C_p = p(C + C_a). \qquad (2.0.4)$$

Out of the beam aperture in the furnace, the molecules effuse into the half space beyond with a flux distribution, in the limit that the mean free path of furnace molecules is very large compared to the aperture dimensions, given by[2]

$$\dot{N} = S_a \bar{v}\, n \cos\theta \, \frac{d\omega}{4\pi} , \qquad (2.0.5)$$

where $d\omega$ is the elementary solid angle at an angle θ with the axis of the beam (aperture normal).

Now, for a detector of area A_b distant ℓ along the normal to the orifice, the above flux also is given by

$$\dot{N} = n_b A_b \bar{v}_b , \qquad (2.0.6)$$

where n_b is the beam density and $\bar{v}_b$ is the mean beam velocity. Expression (2.0.6) is seen to hold for ℓ sufficiently large that the molecular velocity is axial. Quantitatively, the requirement is that the cosine of the half angle subtended at orifice S_a by the detector be sufficiently close to unity. For most gauges it is thus required that $\ell \geq 20$ cm for the cosine to differ from unity by less than 1/2%. The method of dealing with smaller ℓ will be discussed below.

Comparing Equations (2.05) and (2.06) and noting that the solid angle subtended by A_b is A_b/ℓ^2, it is found that the molecular beam density on the axis of the beam is

$$n_b = \frac{1}{4\pi} \frac{S_a}{\ell^2} \frac{\bar{v}}{\bar{v}_b} n. \qquad (2.0.7)$$

As is shown in Appendix I, the mean molecular speed in the furnace is related to that in the beam by

$$\bar{v} = \frac{8}{3\pi} \bar{v}_b. \qquad (2.0.8)$$

Substitution of Equation (2.0.8) into Equation (2.0.7) gives, for a circular aperture of radius r_a,

$$n_b = \frac{2}{3\pi} \left(\frac{r_a}{\ell}\right)^2 n. \qquad (2.0.9)$$

Although the gas molecules have a mean velocity $\bar{v}_b$ with respect to a stationary observer (i.e., the gauge to be calibrated), this velocity is negligible compared to the velocity of the ionizing electrons which generate the gauge ion current. Thus, the gas molecules appear stationary in comparison to dynamic operation of the gauge. In addition, for ordinary molecular beam velocities, the average kinetic energy that an ion has immediately after ionization is not substantially different from the average kinetic energy that an ion formed from an equilibrium gas molecule would have. Therefore, the ion collection efficiency of the gauge is the same for beam molecules as for equilibrium gas molecules. The ionization gauge, which measures molecular density, therefore cannot distinguish between a non-equilibrium gas such as in a moderate temperature molecular beam and an equilibrium gas. Thus, although Equation (2.0.9) was derived in terms of density, the ideal gas law,

$$p = nkT, \qquad (2.0.10)$$

may be used to restate Equation (2.0.9) in terms of the equilibrium pressure of a gas of density equal to the beam density. Thus,

$$p_b = \frac{2}{3\pi} \left(\frac{r_a}{\ell}\right)^2 p. \qquad (2.0.11)$$

Finally, combining Equations (2.0.4) and (2.0.11) yields an equation that may be considered the calibration equation:

$$p_b = \frac{2}{3\pi} \left(\frac{r_a}{\ell}\right)^2 \frac{C_p}{C + C_a} p_o. \qquad (2.0.12)$$

2.1 Gauge Enclosure Method

An assumption implicit in this derivation has been that the beam density is constant over the volume of the gauge ion collecting structure (e.g., within the grid cage of a Bayard-Alpert gauge). Considering separately the density variations perpendicular to and parallel to the beam axis, the former is seen from Equation (2.0.5) to be negligible as long as $\cos \frac{\theta_g}{2}$ is sufficiently close to unity, where θ_g is the angle at the aperture subtended by the gauge, while the latter may be investigated by applying Equation (2.0.9) to two different values of ℓ. Let ℓ_1 and ℓ_2 represent, for example, the midpoint and one extremity of the ionizing region of length L. The ratio of densities at these points is given by (for large ℓ)

$$\frac{n(\ell_2)}{n(\ell_1)} = \frac{\ell_1^2}{\left(\ell_1 + \frac{L}{2}\right)^2} \approx 1 - \frac{L}{\ell_1}. \qquad (2.1.1)$$

Thus, there exists a minimum distance of approach of the gauge to the molecular beam aperture if an unacceptable non-uniformity in the gas density distribution within the gauge is to be avoided. But to obtain a sufficiently large variation in beam density by varying ℓ, the calibration apparatus becomes long and cumbersome, since the range of beam density variation is proportional to

$$\frac{\ell_{max}^2}{\ell_{min}^2}. \qquad (2.1.2)$$

For example, if less than 1/2% error is required in this term, then for L = 4 cm, $\ell_1 > 800$ cm. The error at ℓ = 200 cm is 2%.

As an alternative method, an isothermal enclosure can be placed around the gauge such that the molecular beam is transformed to an equilibrium gas upon entering the enclosure, thus eliminating the density variation associated with the non-equilibrium beam. This has the further desirability that it may be used in calibrating gauges that would otherwise, due to their geometry, strongly scatter the molecular beam.

Figure 1 is a schematic of such a calibration system as described above. In the next two sections, a mathematical analysis of that calibration system and of the accumulated probable error in the gauge enclosure pressure will be presented.

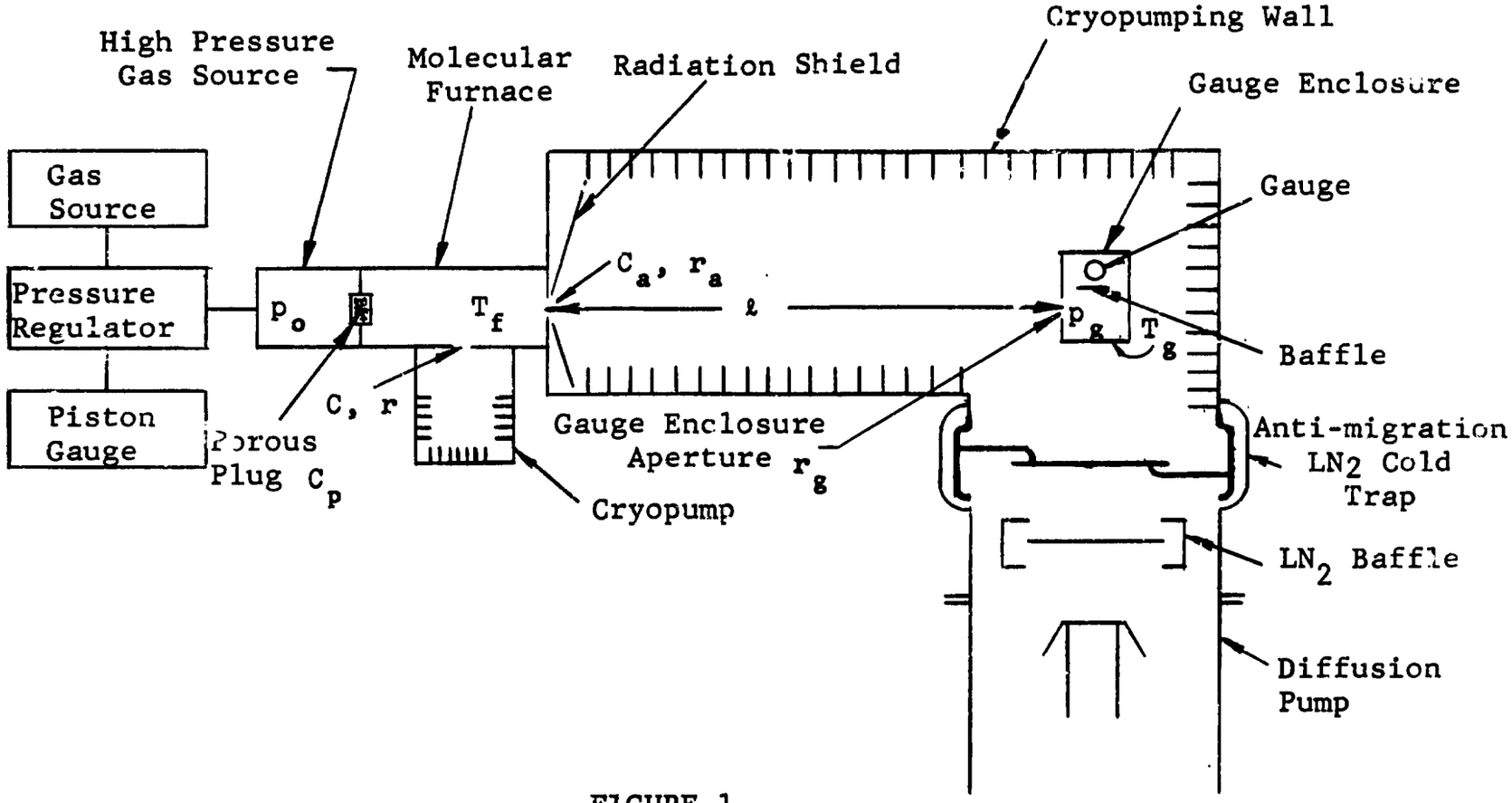

FIGURE 1

ULTRA HIGH VACUUM GAUGE CALIBRATION SYSTEM (SCHEMATIC)

2.2 Analysis of Gauge Enclosure Method

As is shown in Appendix 1, following Kennard,[49] for a gas in equilibrium at temperature T the number of molecules per second, $d\Gamma_v$, moving with speeds in the range dv crossing from one side through unit area of S_1 and passing into a solid angle $d\omega$ whose axis makes an angle ϕ with the normal to S_1 is

$$d\Gamma_v = n\left(\frac{m}{2\pi kT}\right)^{1/2} v^3 e^{-\frac{mv^2}{2kT}} \cos\phi \, dv d\omega. \qquad (2.2.1)$$

where

n = density in the molecular furnace,
m = mass of gas atom,
k = Boltzmann constant.

If a small, ideal aperture, S_1, is made in the wall of a vessel containing an equilibrium gas and if the mean free path of the gas is large compared with the aperture diameter, then $d\Gamma_v$ is the number of molecules per unit area and unit time with speeds in the range dv passing through the aperture into $d\omega$.

Consider this Maxwellian effusive stream after emanating from S_1 to enter an ideal aperture S_2 in a wall distant ℓ cm along the normal to S_1, as shown in Figure 2. Since the mean free path of the gas is long, there are a negligible number of molecular collisions in the space between S_1 and S_2, so that those molecules moving into $d\omega$ from dS_1 pass through elementary area dS_2 where

$$d\omega = \frac{\cos\phi \, dS_2}{Z^2}, \qquad (2.2.2)$$

$$Z^2 = \ell^2 + R^2 + r^2 - 2Rr\cos\theta \qquad (2.2.3)$$

and

$$\cos\phi = \frac{\ell}{Z}. \qquad (2.2.4)$$

Thus, Equation (2.2.1) becomes

$$d\Gamma_v = n\ell^2\left(\frac{m}{2\pi kT}\right)^{1/2} v^3 e^{-\frac{mv^2}{2kT}} \frac{dS_2}{Z^4} dv. \qquad (2.2.5)$$

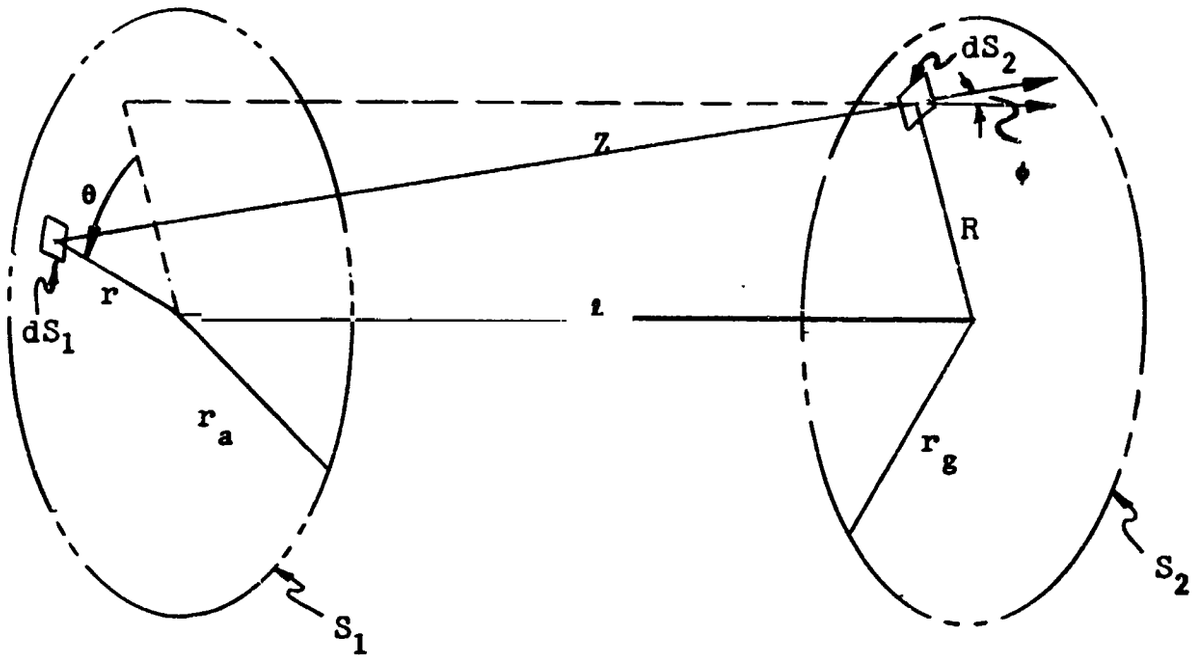

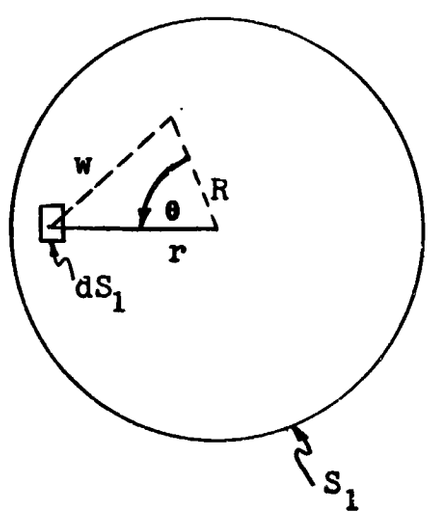

$$Z^2 = \ell^2 + w^2$$

$$w^2 = r^2 + R^2 - 2rR \cos \theta$$

FIGURE 2

MOLECULAR BEAM AND ENCLOSURE APERTURES (SCHEMATIC)

Integrating over the velocity spectrum gives the total number of molecules per unit area and per second, $d\Gamma$, leaving dS_1 and entering dS_2

$$d\Gamma = \int_0^\infty \frac{d\Gamma_v}{dv}\, dv = \frac{n\ell^2}{4\pi}\left(\frac{8kT}{\pi m}\right)^{1/2} \frac{dS_2}{Z^4} \qquad (2.2.6)$$

Now, as shown in Appendix 1, the mean molecular speed in the furnace is

$$\bar{v}_f = \left(\frac{8kT_f}{\pi m}\right)^{1/2};$$

therefore,

$$d\Gamma = \frac{n\bar{v}_f}{4\pi} \frac{\ell^2\, dS_2}{(\ell^2 + R^2 + r^2 - 2Rr\cos\theta)^2}. \qquad (2.2.7)$$

The total molecular flux contribution into dS_2 from all the aperture area S_1 is then,

$$dv = \int_{S_1} d\Gamma\, dS_1 = \frac{n\bar{v}_f \ell^2\, dS_2}{4\pi} \int_0^{r_a}\int_0^{2\pi} \frac{r\, dr\, d\theta}{(\ell^2 + R^2 + r^2 - 2Rr\cos\theta)^2}. \qquad (2.2.8)$$

Using Dwight 446.03 and 859.2, and integrating with respect to gives

$$\frac{dv}{dS_2} = \frac{n\bar{v}_f}{4\pi}\ell^2 \int_0^{r_a} \left(\frac{1}{\left[\ell^2 + R^2 + r^2\right]^2 - 4R^2r^2}\right) \left(\frac{2\pi r\, dr}{1 - \frac{4R^2r^2}{\left[\ell^2 + R^2 + r^2\right]^2}}\right)^{1/2} \qquad (2.2.9)$$

After some manipulation and change of variables to

$$u = R^2 - \ell^2 - r^2, \qquad (2.2.10)$$

Equation (2.2.9) may be written

$$\frac{dv}{dS_2} = \frac{n\bar{v}_f}{4}\ell^2 \int_{u(R^2-\ell^2)}^{u(R^2-\ell^2-r_a^2)} \frac{(u - 2R^2)du}{(u^2 + 4R^2\ell^2)^{3/2}}. \qquad (2.2.11)$$

Using Dwight 200.03 and 201.03 to evaluate this integral, gives

$$\frac{dv}{dS_2} = \frac{n\bar{v}_f}{8}\left(1 - \frac{R^2 + \ell^2 - r_a^2}{\left[(R^2 + \ell^2 + r_a^2)^2 - 4R^2r_a^2\right]^{1/2}}\right). \qquad (2.2.12)$$

Now, integrating the molecular flux into dS_2, over all of aperture S_2, gives the total number of molecules entering S_2 per unit time

$$\dot{N}_{S_{2(In)}} = \int_{S_2} \left(\frac{dv}{dS_2}\right) dS_2 \tag{2.2.13}$$

$$= \frac{n\bar{v}_f}{8} \int_0^{r_g} \left(1 - \frac{R^2 + \ell^2 - r_a^2}{\left[(R^2 + \ell^2 + r_a^2)^2 - 4R^2 r_a^2\right]^{1/2}}\right) 2\pi R dR.$$

Changing variables to $u = R^2 + \ell^2 + r_a^2$ and using Dwight 380.011 to evaluate the integral gives

$$\dot{N}_{S_{2(In)}} = \frac{n\bar{v}_f}{8} \pi(r_a^2 + r_g^2 + \ell^2)\left\{1 - \left[1 - \frac{4r_a^2 r_g^2}{(r_a^2 + r_g^2 + \ell^2)^2}\right]^{1/2}\right\}. \tag{2.2.14}$$

In this application, the enclosure radius r_g must be maintained large enough that ionic pumping does not introduce large errors in enclosure pressure. For a Bayard-Alpert structure this requires $r_g \approx 0.8$ cm and for a Redhead structure, $r_g \approx 3.1$ cm. If, to minimize scattering, the closest approach of the enclosure to the furnace aperture is fixed at 9 cm and the practical upper limit for the furnace aperture is fixed at $r_a \approx .75$ cm, then the quantity in square brackets in Equation (2.2.14) is approximately equal to one, since

$$\frac{4r_a^2 r_g^2}{(r_a^2 + r_g^2 + \ell^2)^2} \leq \frac{1}{300} \tag{2.2.15}$$

Therefore, to better than 1/4% the square bracket in Equation (2.2.14) may be expanded in a binomial series in which all but the first two terms are neglected. Equation (2.2.14) then becomes

$$\dot{N}_{S_{2(In)}} = \frac{n\bar{v}_f \pi}{4} \frac{r_a^2 r_g^2}{(r_a^2 + r_g^2 + \ell^2)} . \qquad (2.2.16)$$

The beam molecules, after being randomized in the gauge enclosure at temperature T_g, then re-emerge from the enclosure aperture as a molecular beam. The number of molecules effusing per second is[1]

$$\dot{N}_{S_{2(Out)}} = \frac{1}{4} n_g \bar{v}_g \pi r_g^2 . \qquad (2.2.17)$$

In addition, in the process of its operation, an ion gauge drives gas into the gauge elements with an effective pumping speed, $S(cm^3/sec)$, so that when the molecular density in the gauge enclosure reaches equilibrium,

$$\dot{N}_{S_{2(In)}} = \dot{N}_{S_{2(Out)}} + Sn_g . \qquad (2.2.18)$$

Therefore, substituting Equations (2.2.16), (2.2.17) into Equation (2.2.18), it is found that

$$\left(1 + \frac{4S}{\pi r_g^2 \bar{v}_g}\right) n_g = \frac{\bar{v}_f}{\bar{v}_g} \frac{r_a^2}{r_a^2 + r_g^2 + \ell^2} n_o . \qquad (2.2.19)$$

But the constraint has already been imposed that

$$\frac{\bar{v}_g \pi}{4} r_g^2 >> S . \qquad (2.2.20)$$

Therefore, Equation (2.2.19) may be written

$$n_g = \frac{\bar{v}_f}{\bar{v}_g} \frac{r_a^2}{r_g^2 + r_g^2 + \ell^2} n_o . \qquad (2.2.21)$$

Now, Appendix 1 shows

$$\frac{\bar{v}_f}{\bar{v}_g} = \left(\frac{T_f}{T_g}\right)^{1/2} , \qquad (2.2.22)$$

and since the molecular density in the furnace is related to that in the isothermal gas source by (Equation (2.0.4))

$$n = \frac{C_p}{C + C_a} n_o , \qquad (2.2.23)$$

where,

C_p = porous plug conductance,

C = furnace attenuation aperture conductance, and

C_a = furnace beam aperture conductance,

then, the steady state molecular density in the gauge enclosure is given by

$$n_g = \left(\frac{T_f}{T_g}\right)^{1/2} \frac{r_a^2}{r_a^2 + r_g^2 + \ell^2} \frac{C_p}{C + C_a} n_o. \qquad (2.2.24)$$

Following the reasoning in Section 2.0, Equation (2.2.24) may be expressed in terms of pressure using Equation (2.0.10), so that finally

$$p_g = \left(\frac{T_f}{T_g}\right)^{1/2} \frac{r_a^2}{r_a^2 + r_g^2 + \ell^2} \frac{C_p}{C + C_a} p_o. \qquad (2.2.25)$$

2.3 Probable Error in Calculated Pressure

Equation (2.2.25) is the expression for the pressure in the gauge enclosure. If R_{p_g} is the probable error in the mean value of the pressure, then the relative probable error, $r_{p_g} = R_{p_g}/p_g$, in the mean value of p_g is

$$r_{p_g} = \frac{1}{p_g} \left\{ \left(\frac{\partial p_g}{\partial r_a}\right)^2 R_{r_a}^2 + \left(\frac{\partial p_g}{\partial \ell}\right)^2 R_\ell^2 + \left(\frac{\partial p_g}{\partial C_p}\right)^2 R_p^2 + \left(\frac{\partial p_g}{\partial C}\right)^2 R_C^2 \right. \qquad (2.3.1)$$

$$\left. + \left(\frac{\partial p_g}{\partial C_a}\right)^2 R_{C_a}^2 + \left(\frac{\partial p_g}{\partial p_o}\right)^2 R_{p_o}^2 + \left(\frac{\partial p_g}{\partial r_g}\right)^2 R_{r_g}^2 + \left(\frac{\partial p_g}{\partial T_f}\right)^2 R_{T_f}^2 + \left(\frac{\partial p_g}{\partial T_g}\right)^2 R_{T_g}^2 \right\}^{1/2}.$$

In Equation (2.3.1) and what follows, the mean value is to be inferred for each variable; however, the mean value notation (e.g., $\bar{x}$) will be deleted.

Calculating from Equation (2.2.25), the partial derivatives required in Equation (2.3.1), and dividing by p_g yields

$$\frac{1}{p_g}\frac{\partial p_g}{\partial r_a} = \frac{2}{r_a}\frac{r_g^2 + \ell^2}{(r_a^2 + r_g^2 + \ell^2)} \qquad \frac{1}{p_g}\frac{\partial p_g}{\partial T_g} = -\frac{1}{2T_g}$$

$$\frac{1}{p_g}\frac{\partial p_g}{\partial r_g} = \frac{-2r_g}{r_a^2 + r_a^2 + \ell^2} \qquad \frac{1}{p_g}\frac{\partial p_g}{\partial C_p} = \frac{1}{C_p}$$

$$\frac{1}{p_g}\frac{\partial p_g}{\partial \ell} = \frac{-2\ell}{r_a^2 + r_g^2 + \ell^2} \qquad \frac{1}{p_g}\frac{\partial p_g}{\partial C} = -\frac{1}{C + C_a}$$

$$\frac{1}{p_g}\frac{\partial p_g}{\partial T_f} = \frac{1}{2T_f} \qquad \frac{1}{p_g}\frac{\partial p_g}{\partial C_a} = -\frac{1}{C + C_a}$$

$$\frac{1}{p_g}\frac{\partial p_g}{\partial p_o} = \frac{1}{p_o}$$

(2.3.2)

Substituting these into Equation (2.3.1) and remembering that $r_x = R_x/x$, it is found, assuming for the length measurements $r_{r_a} = r_{r_g} = r_\ell$ and for the temperature measurements $r_{T_f} = r_{T_g}$, that

$$r_{p_g} = \left\{ \frac{8(\ell^4 + r_g^2\ell^2 + r_g^4)}{(\ell^2 + r_a^2 + r_g^2)^2} r_{r_a}^2 + \frac{1}{2} r_{T_f}^2 + r_{C_p}^2 + \frac{1}{(C + C_a)^2} (C^2 r_C^2 + C_a^2 r_{C_a}^2) \right.$$

$$\left. + r_{p_o}^2 \right\}^{1/2} . \qquad (2.3.3)$$

Now $$C_a = bT_f^{1/2} r_a^2, \text{ where } b \text{ is a constant,} \qquad (2.3.4)$$

so, following the procedure of Equation (2.3.1) gives

$$r_{C_a}^2 = 1/4\ r_{T_f}^2 + 4r_{r_a}^2 , \qquad (2.3.5)$$

and since assuming that since the measurements are similar,

$$r_{C_a} = r_C . \qquad (2.3.6)$$

Now, since

$$\frac{C^2 + C_a^2}{(C + C_a)^2} \leq 1, \qquad (2.3.7)$$

it is seen that Equation (2.3.3) becomes

$$r_{p_g} \leq \left\{ \left[\frac{8(\ell^4 + r_g^2\ell^2 + r_g^4)}{(r_a^2 + r_g^2 + \ell^2)^2} + 4 \right] r_{r_a}^2 + \frac{3}{4} r_{T_f}^2 + r_{C_p}^2 + r_{p_o}^2 \right\}^{1/2} . \qquad (2.3.8)$$

Now, as will be more fully described in Section 3, C_p is obtained from the decay of pressure p_o in the gas source volume, V, from times 0 to τ, that is,

$$C_p = \frac{V}{\tau} \ln \frac{p_o(0)}{p_o(\tau)} . \qquad (2.3.9)$$

Therefore, following the procedure of Equation (2.3.1) and assuming for both pressure measurements that $r_{p_o}(0) = r_{p_o}(\tau) = r_{p_o}$ gives

$$r_{C_p}^2 = r_V^2 + r_\tau^2 + 2\left[\ln \frac{p_o(0)}{p_o(\tau)}\right]^{-2} r_{p_o}^2 . \qquad (2.3.10)$$

As will also be described in Section 3, the volume, V, of the pressure source is determined by measuring the pressure change $\Delta p = p_1 - p_2$ when the volume of the system is changed by $\Delta V = V_1 - V_2$ by means of a precision burette. A schematic of the experimental setup is shown in Figure 3. The initial volume of the system is

$$V_1 = V + V' = \frac{NkT_1}{p_1} , \qquad (2.3.11)$$

and the volume after increasing the diffusion pump oil level in the precision burette is

$$V_2 = V + V' - \Delta V = \frac{NkT_2}{p_2} , \qquad (2.3.12)$$

where V' is the unused volume of the burette during measurement of p_1. Simultaneous solution of (2.3.11) and (2.3.12) yields

$$V = \frac{\Delta V}{\left(1 - \frac{p_1 T_2}{p_2 T_1}\right)} - V' . \qquad (2.3.13)$$

Thus, following the procedure of Equation (2.3.1), we have

$$r_V^2 = \frac{1}{\left[\left(\frac{2T_2p_1 - T_1p_2}{T_1p_2 - p_1T_2}\right)\Delta V - V'\right]^2}\left[\left(\frac{T_1p_2}{T_1p_2 - p_1T_2}\right)^2 R_{\Delta V}^2\right.$$

$$+ (\Delta V)^2 p_2^2 \left(\frac{p_1T_2}{(T_1p_2 - p_1T_2)2}\right)^2 R_{T_1}^2 + (\Delta V)^2 T_1^2 \left(\frac{p_1T_2}{(T_1p_2 - p_1T_2)2}\right)^2 R_{p_2}^2$$

$$\left. + \frac{(\Delta V)^2 T_1^2 p_2^2 p_1^2}{(T_1p_2 - p_1T_2)^4} R_{T_2}^2 + \frac{(\Delta V)^2 T_1^2 p_2^2 T_2^2}{(T_1p_2 - p_1T_2)^4} R_{p_1}^2 + R_{V'}^2\right] . \qquad (2.3.14)$$

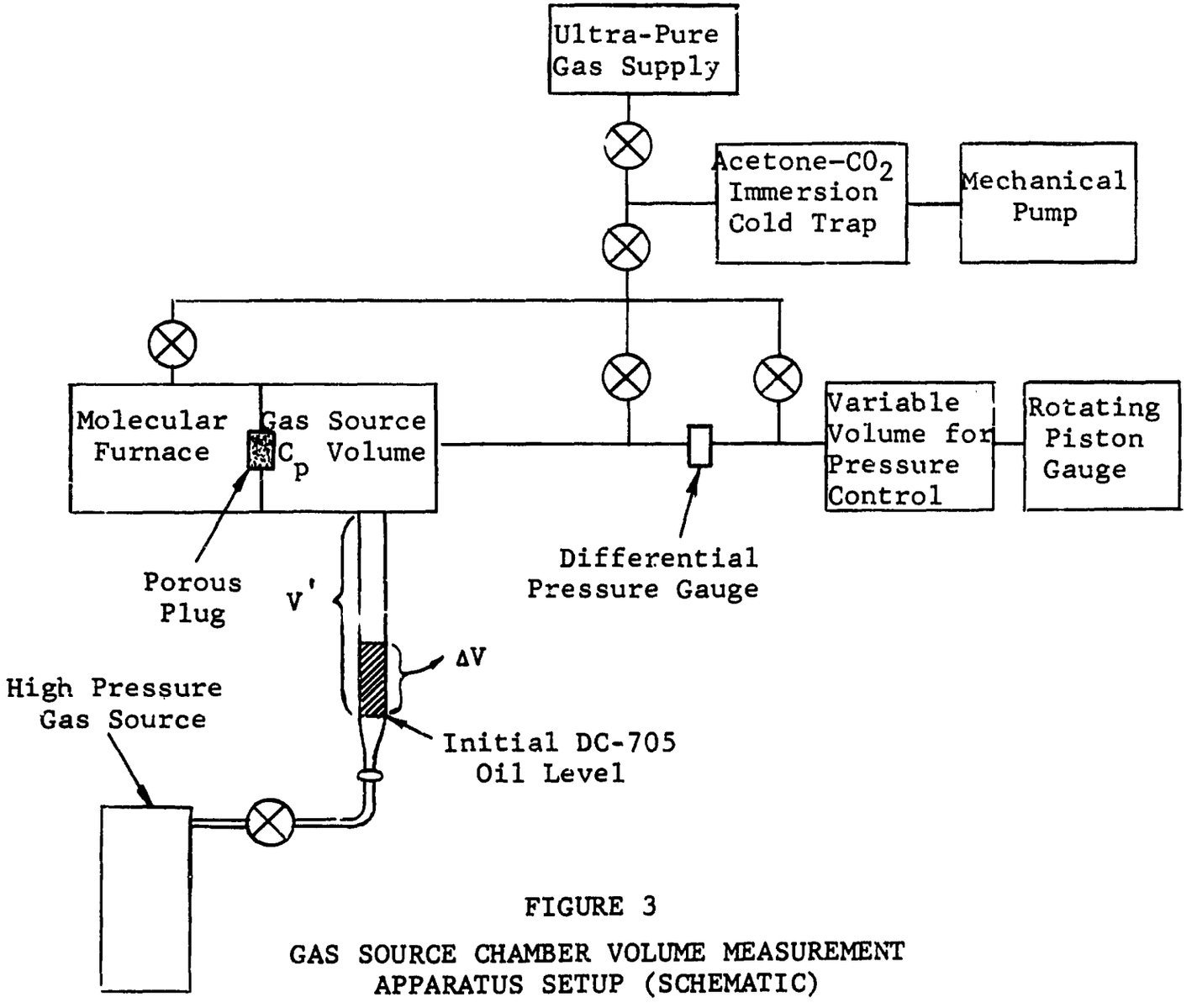

FIGURE 3

GAS SOURCE CHAMBER VOLUME MEASUREMENT
APPARATUS SETUP (SCHEMATIC)

Now, since they are similar measurements, we may take $R_{T_1} = R_{T_2}$ and $R_{p_1} = R_{p_2}$ and then Equation (2.3.14) becomes

$$r_V^2 = \frac{1}{\left[\left(\frac{2T_2p_1 - T_1p_2}{T_1p_2 - p_1T_2}\right)\Delta V - V'\right]^2}\left\{\left(\frac{T_1p_2\,\Delta V}{T_1p_2 - p_1T_2}\right)^2 r_{\Delta V}^2 + 2\,\frac{(p_1p_2T_1T_2\,\Delta V)^2}{(T_1p_2 - p_1T_2)^4}\left[r_{T_1}^2 + r_{p_1}^2\right] + V'^2\, r_{V'}^2\right\}. \qquad (2.3.15)$$

Thus, finally, substituting Equations (2.3.10) and (2.3.15) into Equation (2.3.8) gives the relative probable error r_{p_g} in the mean value of the gauge enclosure pressure:

$$r_{p_g} \le \left\{\left[\frac{8(\ell^4 + r_g^2\ell^2 + r_g^4)}{(r_a^2 + r_g^2 + \ell^2)^2} + 4\right] r_{r_a}^2 + \frac{3}{4}\, r_{T_f}^2 + \left[1 + 2\left(\ln\frac{p_o(0)}{p_o(\tau)}\right)^{-2}\right] r_{p_o}^2 + r_\tau^2 + \frac{1}{\left[\left(\frac{2T_2p_1 - T_1p_2}{T_1p_2 - p_1T_2}\right)\Delta V - V'\right]^2}\left[\left(\frac{T_1p_2\,\Delta V}{T_1p_2 - p_1T_2}\right)^2 r_{\Delta V}^2 + 2\,\frac{(p_1p_2T_1T_2\,\Delta V)^2}{(T_1p_2 - p_1T_2)^4}\left[r_{T_1}^2 + r_{p_1}^2\right] + V'^2\, r_{V'}^2\right]\right\}^{1/2}. \qquad (2.3.16)$$

A numerical estimate of the accumulated probable error was made from Equation (2.3.16), based on the assumption that the probable errors in the individual measurements can be maintained at the following levels: length $\leq$ 0.5%, time $\leq$ 0.1%, temperature $\leq$ 0.5%, and pressure $\leq$ 0.03%. Experience with the development of this calibration system indicates that such probable errors can be maintained in practice. It was assumed that the data formed an adequate statistical sample. The results indicate that an accumulated probable error of calibration of not greater than 5% is attainable.

3. POROUS PLUG

As discussed in Section 2, a porous plug is introduced between the gas pressure source and molecular furnace to provide pressure attenuation. The flow properties of porous materials have been extensively studied.[3, 4, 5, 14, 15, 19] In many porous media, the character of the flow makes the transition from viscous to molecular flow as gas proceeds through the porous material. Such a transition naturally depends upon the upstream and downstream pressure and the characteristic dimensions of the pores. By choosing a material with an effective pore diameter, d_p, sufficiently small compared to the mean free path, λ, of the gas at the upstream surface of the porous plug, molecular flow conditions can be maintained throughout the entire porous plug; thus, the throughput is a linear function of the pressure differential across the porous material. This latter condition of linearity is highly desirable in a gauge calibration system.

3.1 Porous Vycor Glass

One of the stages in the development of Vycor is a porous silicic network obtained by leaching of borosilicate glass.[6] After once cycling to high temperatures (up to about 700°C), this porous structure is reported[7, 8] to be stable with respect to repeated cycles to lower temperatures. Because of its temperature stability, porous Vycor is a very suitable material for a pressure attenuator in a wide range calibration system since high temperature degassing is essential to proper system performance.

Porous Vycor (Corning 7930) has been estimated[9,10,11,12,15,21] to have an effective pore diameter of about 60 angstroms, as determined from its adsorptive and desorptive properties. As will be discussed more fully in Section 4, departures from molecular flow conditions may become large when the mean free path finally decreases such that $\lambda \approx d_p$. Since the mean free path of argon at 298°K is given by Dushman[13] to be

$$\lambda = \frac{5.31 \times 10^{-3}}{p}, \qquad (3.1.1)$$

where p = pressure in Torr; molecular flow conditions in porous Vycor are expected to hold for upstream pressures approaching

$$p(\lambda \approx d_p) \approx 10^4 \text{ Torr.} \qquad (3.1.2)$$

In a channel of length large compared with its diameter, the flow remains free molecular for much smaller ratios of Knudsen number $M = \lambda/d$ than for the short tubes or apertures which will be discussed in Section 4. Porous glass would be expected to have more of the character of long capillaries than apertures or short tubes.

In the case of many porous materials, surface flow has been shown to be a large component of the total flow.[14] For example, Carman and Malherbe[14] have shown it is the major contribution to the flow in the case of Linde silica and Carbolac 1. Barrer and Barrie[15] show for porous Vycor glass, however, that after the blind pores which contribute most to the internal surface area are filled up and the steady state established, surface flow contributes little to the total flow. They show that although in the transient approach to steady flow the adsorption of argon is very marked compared to that of helium, in the steady state the ratio of flow rates for the two gases is

$$\left(\frac{C_{He}}{C_{Ar}}\right) = 3.29. \qquad (3.1.3)$$

The prediction of molecular flow theory is

$$\frac{C_{He}}{C_{Ar}} = \left(\frac{M_{Ar}}{M_{He}}\right)^{1/2} = 3.16 \qquad (3.1.4)$$

which differs from the value given in expression (3.1.3) by 4%. They also find that C is very closely proportional to $T^{\frac{1}{2}}$ as expected for molecular flow, for all gases investigated except ethane.

Considering the above possibilities for deviation from molecular flow in porous plugs, it is necessary to determine the minimum value of M that may be used such that throughput deviation from linearity with pressure remains less than some prescribed value. The minimum usable value of M corresponds to the maximum allowed value of p_o in the gas source and thus determines the upper limit of the gas source dynamic range.

3.2 Porous Plug Conductance Measurement Technique

Assume for the moment that molecular flow occurs throughout the entire volume of a porous plug separating the chamber of volume V at pressure p from one at pressure $p' << p$. If C_p is the conductance of the plug, then after molecular sinks not contributing to steady state flow have been filled, and since sources such as wall desorption are not important at the pressures involved, particle conservation requires:

$$- V \frac{dp}{dt} = C_p p. \qquad (3.2.1)$$

The solution to Equation (3.2.1) for $p = p_o$ at time zero is

$$p = p_o e^{- \frac{C_p t}{V}}, \qquad (3.2.2)$$

so that on a plot of $\ell n\ p$ vs. t the slope will be given by

$$\text{Slope} = - \frac{C_p}{V}. \qquad (3.2.3)$$

At the other extreme, if the porous plug flow is completely viscous, the conservation equation becomes

$$- V \frac{dp}{dt} = Dp^2, \qquad (3.2.4)$$

where D depends upon the temperature and gas. The solution to Equation (3.2.4) is:

$$\frac{1}{p_o} - \frac{1}{p} = - \frac{D}{V} t. \qquad (3.2.5)$$

If the flow changes from viscous to molecular as the pressure, p, is decreased in the chamber, the data will lie on a curve which shows a transition from Equation (3.2.4) to Equation (3.2.1). If an experiment is carried out to monitor the decay of pressure in such a chamber as described above, the main characteristic of the transition from viscous to molecular flow will be a decrease

in the absolute value of the slope of $\ell n\ p$ vs. t until at low enough pressures the slope becomes constant and equal to $- C_p/V$.

3.3 Determination of Porous Glass Flow Properties

Such an experiment was carried out for two separate porous Vycor plugs. Figures 4 and 5 show the two plugs, the first of which is in the form of a porous tip on the end of a test tube structure. Several grades of glass were used in this plug, the last being Corning 7052 for sealing to a Kovar tube welded to the gold o-ring sealed flange used to join it to the gas source. The second plug, Figure 5, was in the form of a 1 inch diameter, right circular cylinder of rolled porous Vycor. The cylinder which is about 0.135 inches thick was mounted in pure indium contained in a Cajon connector VC-16. The connector brazed to a gold o-ring sealed flange is shown in Figure 6 mounted on the wall of the molecular furnace.

During the manufacture of porous plugs and while they are maintained under normal atmospheric conditions, various contaminants are adsorbed in the pores. The plugs take on a yellowish or brownish color and upon heating become dark brown.[16,17] In order to clean up this adsorbed material, Corning Glass Company, the manufacturer, advised heating the plug to 500°C in oxygen until the color clears up. The furnace shown in Figure 7, with porous plug #1 installed, was constructed so that oxygen passing through a dry ice acetone immersion cold trap was continuously forced through the porous plug, and at the same time, another similarly treated oxygen line supplied oxygen at a lower pressure to the exterior of the plug. The temperature was increased at a rate not exceeding 100°C per hour to 425°C. The temperature was measured by a thermocouple inside the porous end of the tube.

During the first 8 hours of heating in oxygen, the color of the porous glass varied among yellow, brown, and red. The heating and flushing was continued to a total of 24 hours after which time the porous glass had a translucent appearance with a slight blue color when illuminated with white light. The disc-type porous plug, #2, was similarly heat treated, being mounted in the furnace as shown in Figure 8. Both plugs were maintained in the purified oxygen environment until they were installed in the prototype calibration system and during this installation they were bathed in a flow of dry argon, nitrogen, or helium.

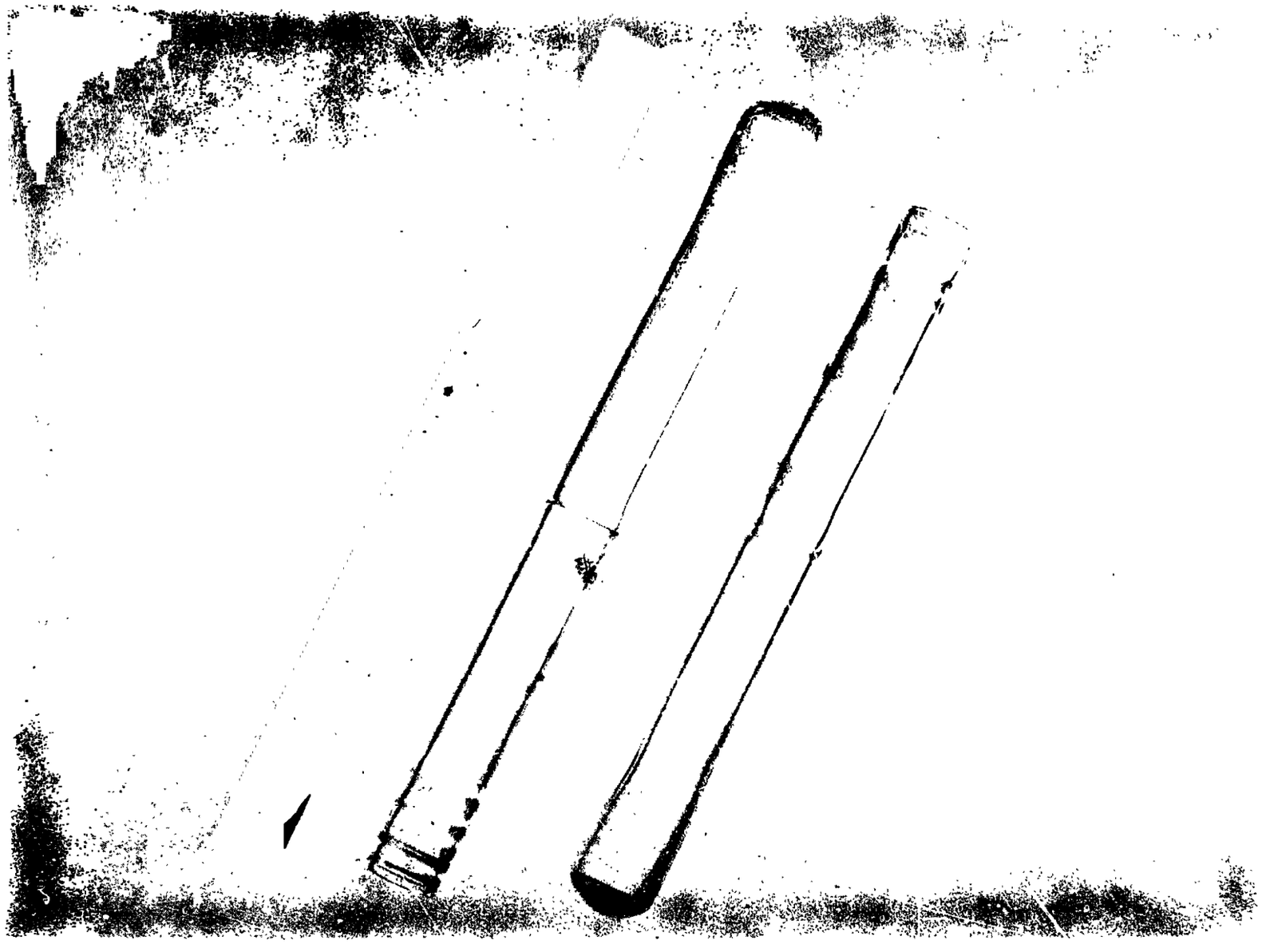

FIGURE 4
POROUS PLUG #1

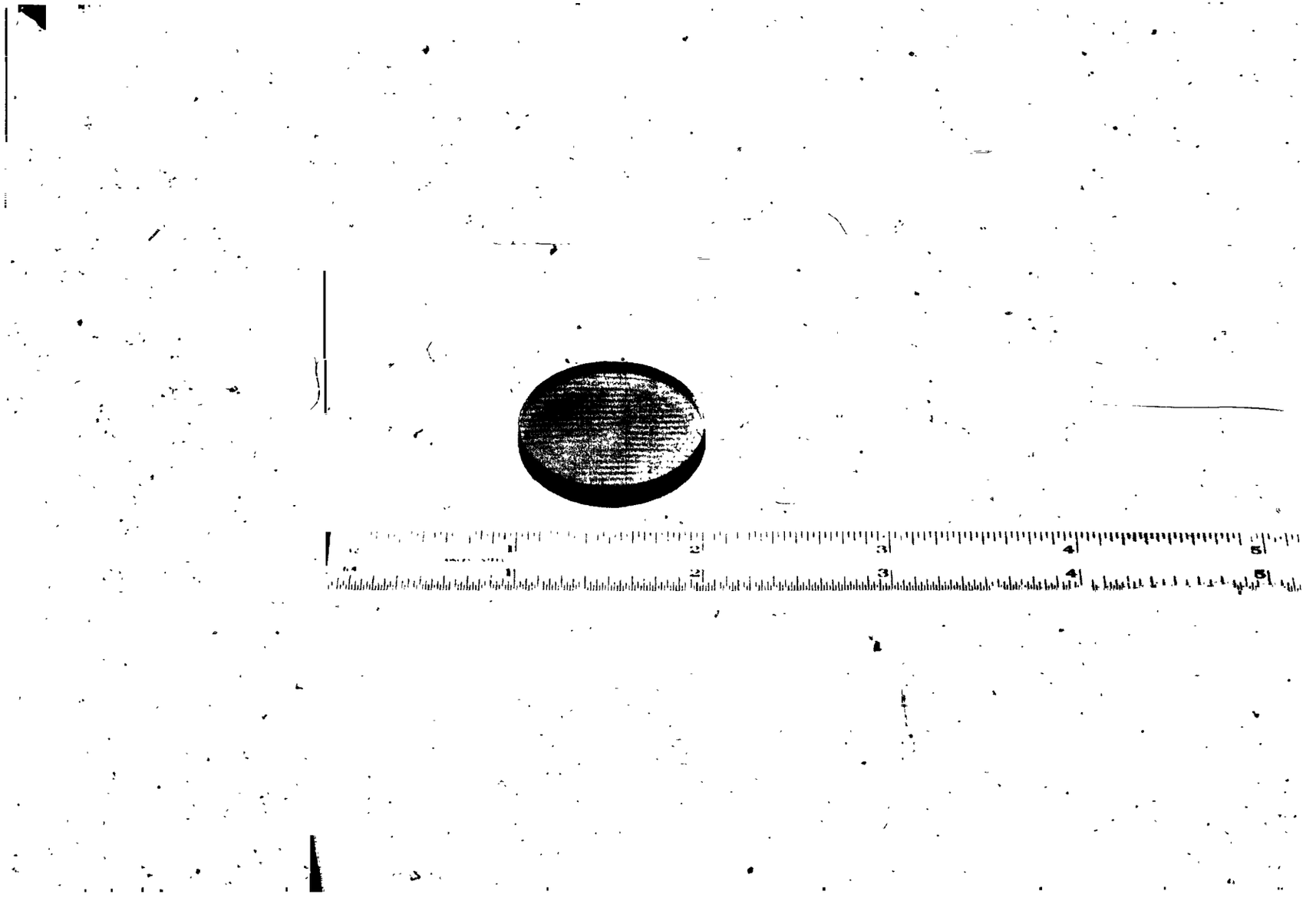

FIGURE 5
POROUS PLUG #2

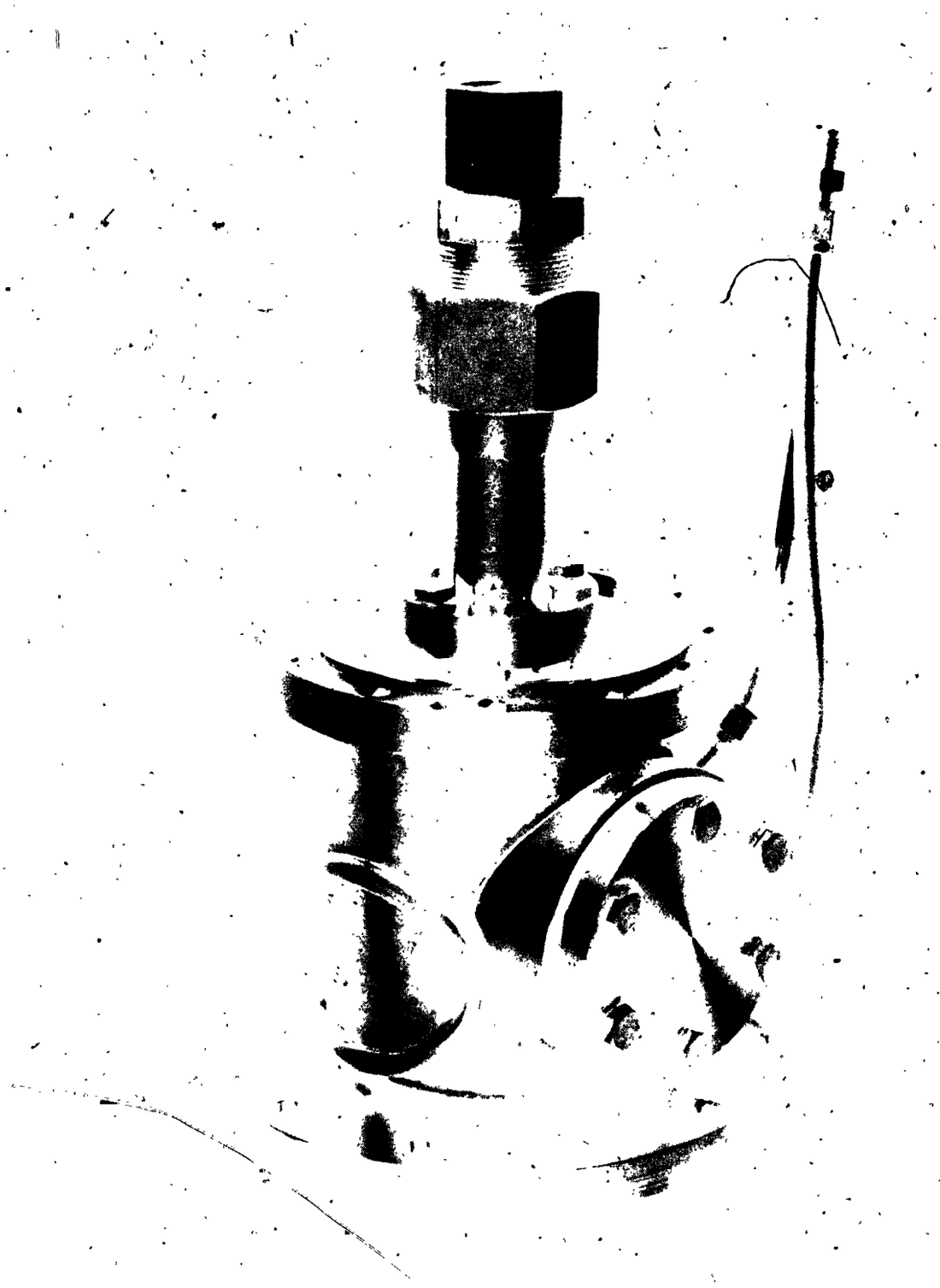

FIGURE 6
POROUS PLUG #2 IN COMPRESSION MOUNTING

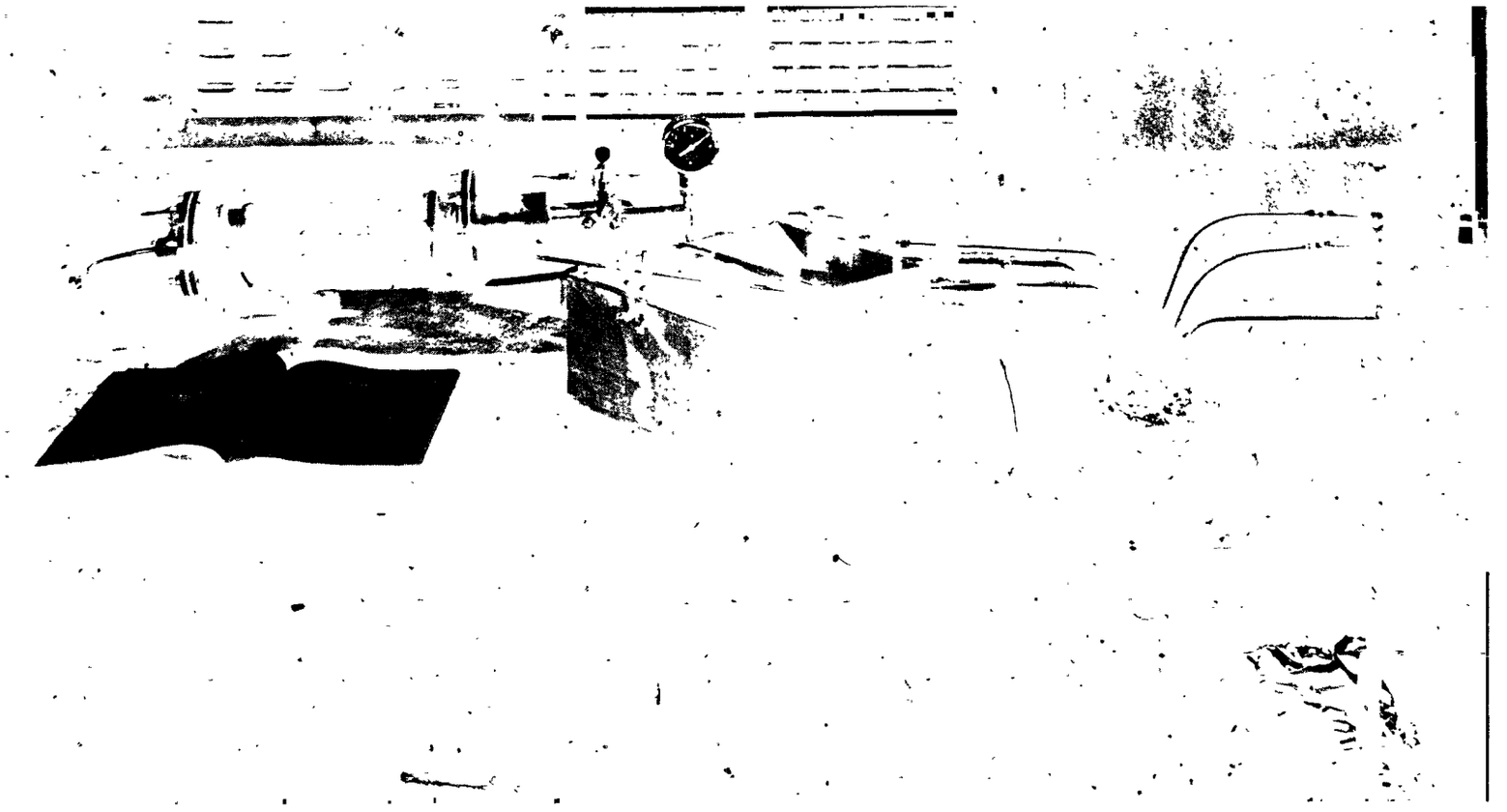

FIGURE 7
POROUS PLUG #1 MOUNTED IN HEAT TREATMENT FURNACE

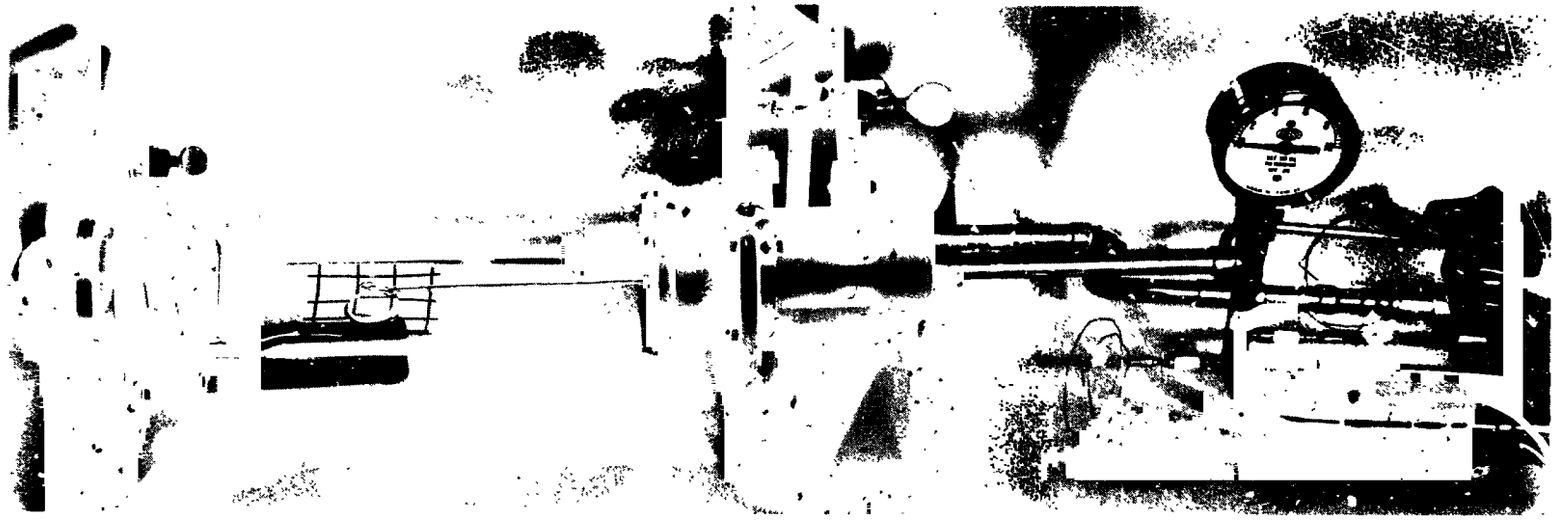

FIGURE 8
POROUS PLUG #2 MOUNTED IN HEAT TREATMENT FURNACE

The gas used for the porous plug conductance experiments was "Baker analyzed" ultra-pure argon* maintained at 304°K. In addition, in order to understand the flow mechanism more completely, an experiment was carried out with helium gas at 304°K and also with argon gas at 308°K. Figure 9 is a diagram of the flow system used. The rotating piston gauge (CEC-type 6-201-0001 Primary Pressure Standard) shown with its associated components in Figure 10 is joined by a differential pressure gauge (MKS Baratron, Type 77H-1068) to the gas source chamber. The pressure, p', below the porous plug was maintained low by a diffusion pumping system, the pumping speed of which for 304°K argon was determined to be 104 liters per second by reference to the ion gauge shown. In the steady state, the pressure ratio across the plug is given by

$$\frac{p}{p'} = \frac{S}{C_p} . \qquad (3.3.1)$$

For the plugs used, this ratio is $> 5 \times 10^6$.

Careful attention was given to the construction of joints in the system in order to prevent leaks that could contribute as much as 0.1% of the porous plug conductance. Heliarc welding of stainless steel, gold-nickel eutectic alloy brazing, and gold compression seals were used wherever possible. Figure 11 shows the gas source chamber and molecular furnace after brazing and welding but before assembly using gold seals. Although a helium mass spectrometer leak detector was used to assure the vacuum integrity of most of the system, it was not possible to do so for the porous plug structure and mounting. If a leak had been in the porous plug structure, it would have been immediately evident in the data, since from Dushman[18] it may be

---

* A typical impurity analysis of the gas used was:

O_2	< 1.4 ppm
N_2	< 1 ppm
Ne	< 1 ppm
H_2O	< 0.4 ppm
CO_2	< 1 ppm
Hydrocarbon	< 1 ppm

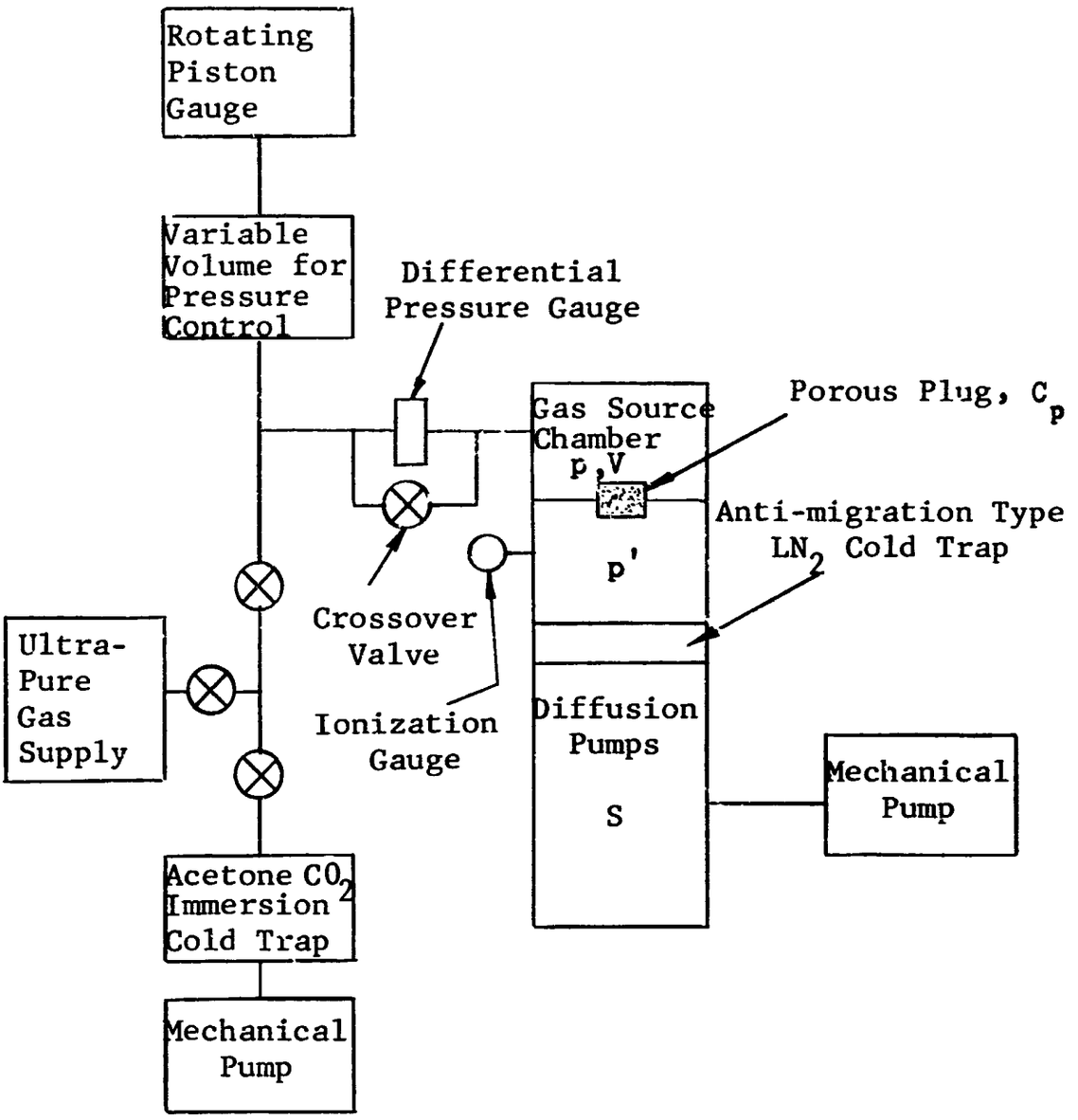

FIGURE 9

FLOW SYSTEM FOR POROUS PLUG CONDUCTANCE MEASUREMENT (SCHEMATIC)

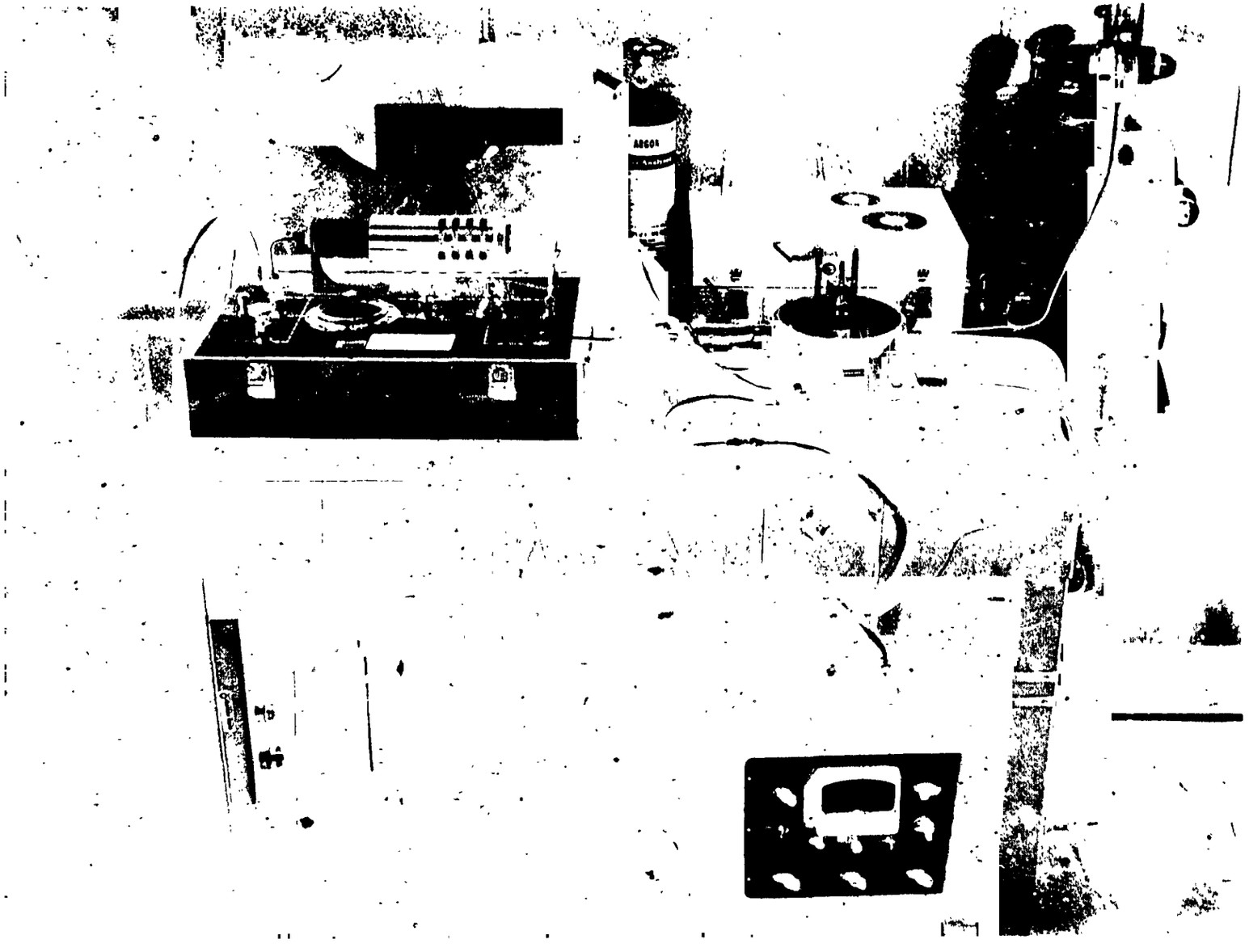

FIGURE 10
ROTATING PISTON GAUGE AND AUXILIARY EQUIPMENT

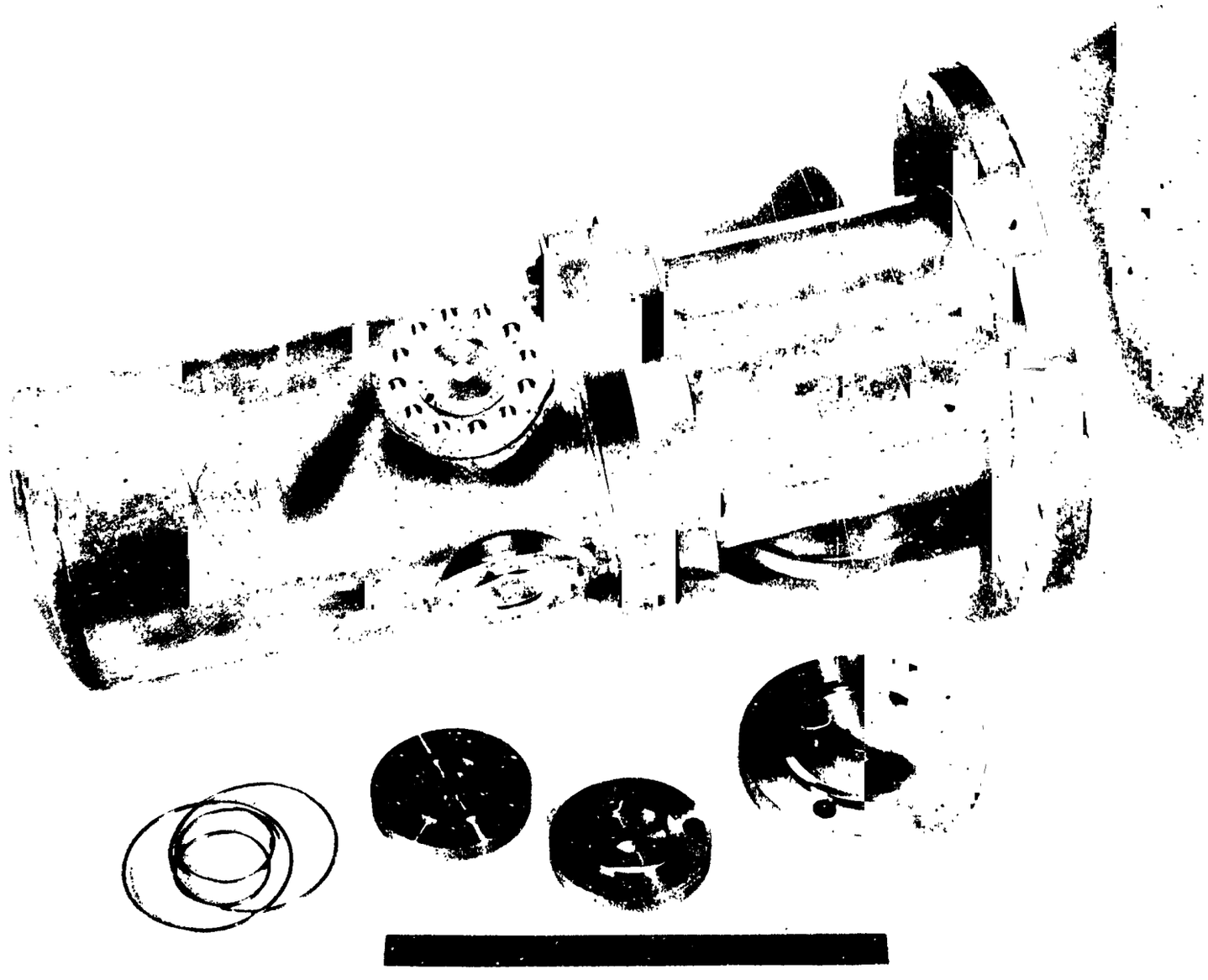

FIGURE 11
GAS SOURCE CHAMBER AND MOLECULAR FURNACE PRIOR TO JOINING

calculated that the diameter of a capillary in a 0.1 cm wall necessary to give 0.1% of the conductance of the plug used (2×10^{-5} liters/sec) is, approximately,

$$d = 6 \times 10^{-4} \text{ cm.} \qquad (3.3.2)$$

Since the mean free path in the gas source chamber is orders of magnitude smaller than this, the flow would have a definitely viscous behavior and the conductance would show large variations with pressure.

After evacuation of the gas source chamber and gauges, the entire system was pressurized with ultra-pure gas. The differential pressure gauge was then calibrated for zero differential and the crossover valve closed, isolating the gas source chamber from the rotating piston gauge through the differential pressure gauge diaphragm. This part of the procedure is necessary since the leakage between the piston and cylinder (gas lubrication) was of the same order of magnitude as the conductance of the porous plug and would introduce a very large error in the measured value of C_p if this leakage path were not blocked. As the gas diffused through the porous plug, the chamber pressure decay was monitored with the rotating piston gauge. There was not infinite resolution of pressure with the piston gauge since the measurement involves adding incremental weights to the rotated piston or cylinder. Therefore, the procedure in making the measurement was to maintain the piston floating with the appropriate weights for the next lowest pressure to be arrived at in the decay of chamber pressure. The pressure differential between the piston gauge and the chamber was monitored and the time that the differential becomes zero was observed. The zero point had been previously calibrated as mentioned above. Experience had shown that the Baratron zero drift was less than 10^{-3} Torr over an experiment lasting for several days. This procedure was then carried out for incremental decreases in weight of the piston or cylinder.

The measurements were carried out for a pressure range of 0.3 psi to 100.5 psi using porous plug #1 in the equipment shown in Figure 12. Figures 13 and 19 show on logarithmic plots the decay of pressure with time. The solid lines are least squares fits to a straight line. The relative standard error estimates for these least squares fits are less than 0.2%. The average value of the slopes of the least squares fits was determined from the results of seven separate pressure decay curves derived

FIGURE 12
POROUS PLUG CONDUCTANCE MEASUREMENT EXPERIMENTAL APPARATUS

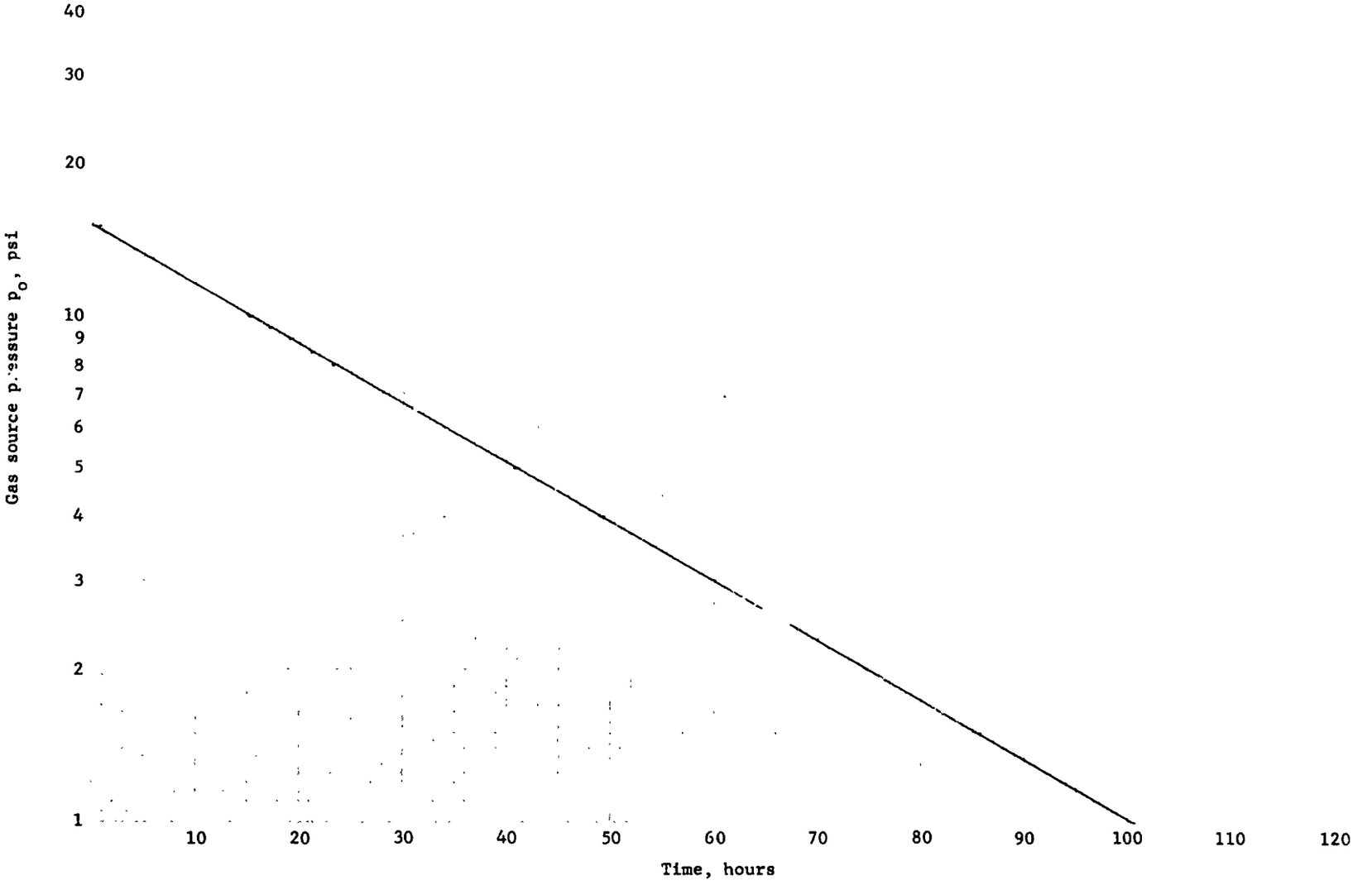

FIGURE 13. POROUS PLUG CONDUCTANCE MEASUREMENT RUN 1-1. Least squares fit to straight line.

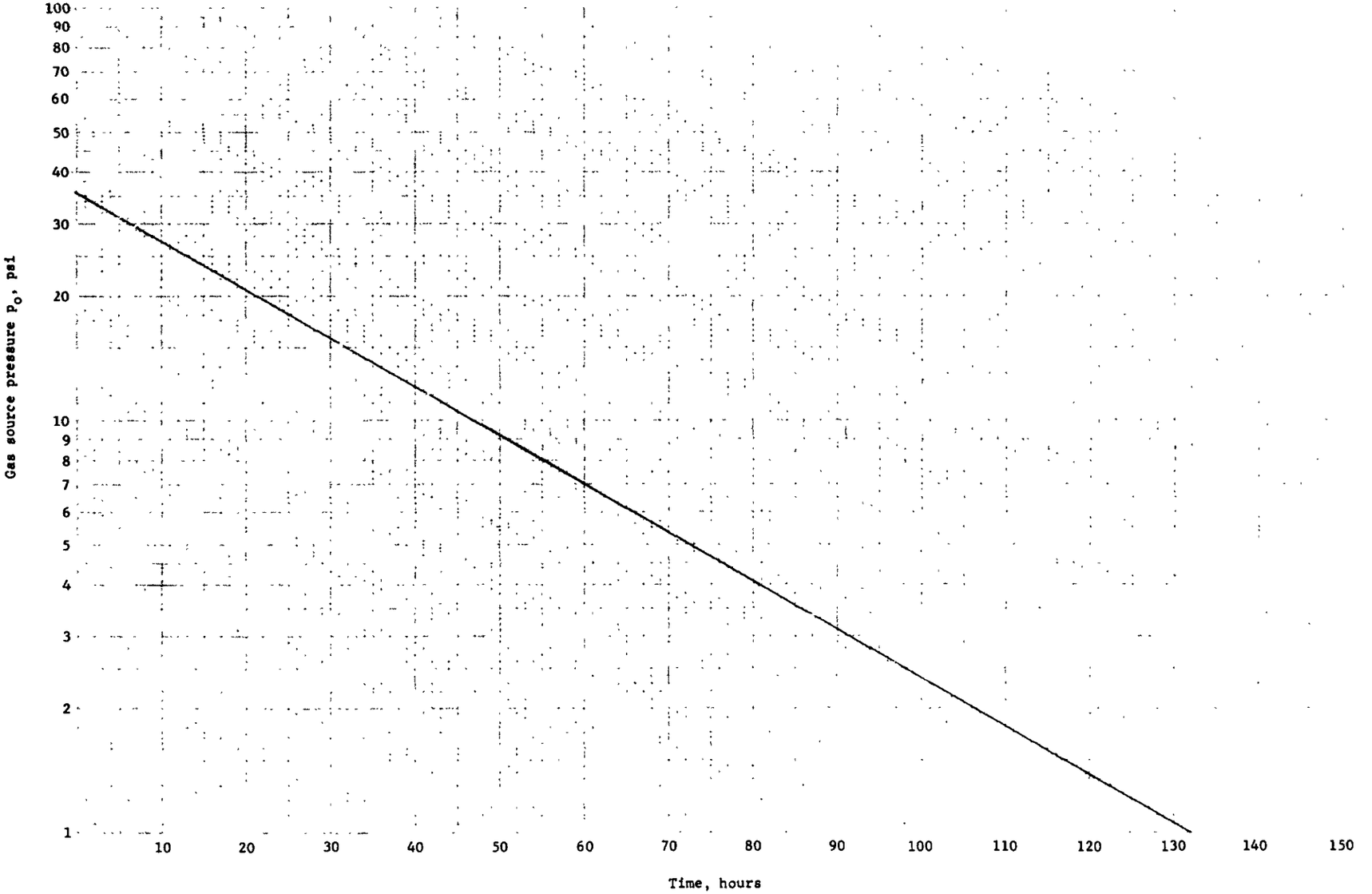

FIGURE 14. POROUS PLUG CONDUCTANCE MEASUREMENT RUN 1-3. Least squares fit to straight line.

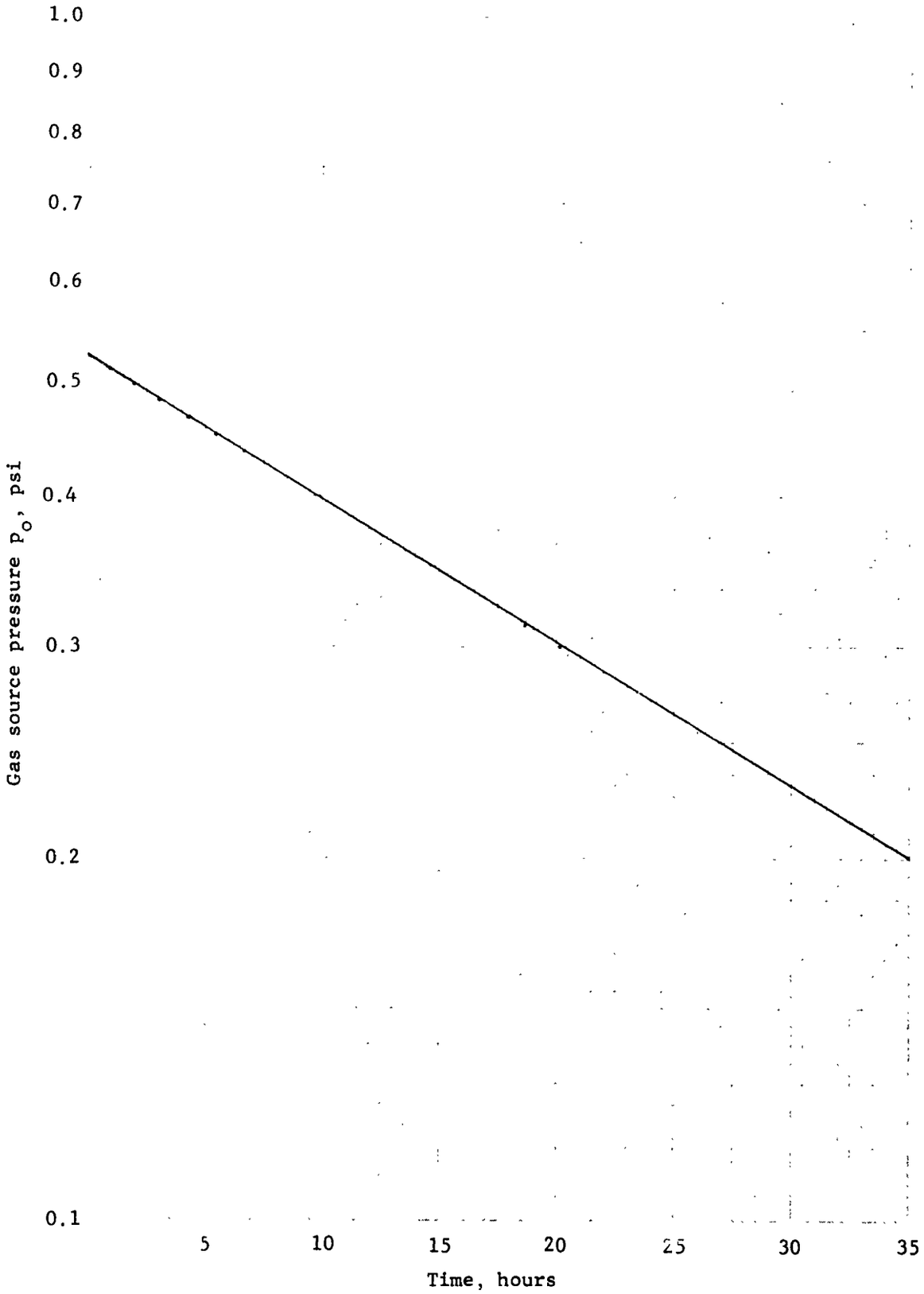

FIGURE 15. POROUS PLUG CONDUCTANCE MEASUREMENT RUN 1-4.
Least squares fit to straight line.

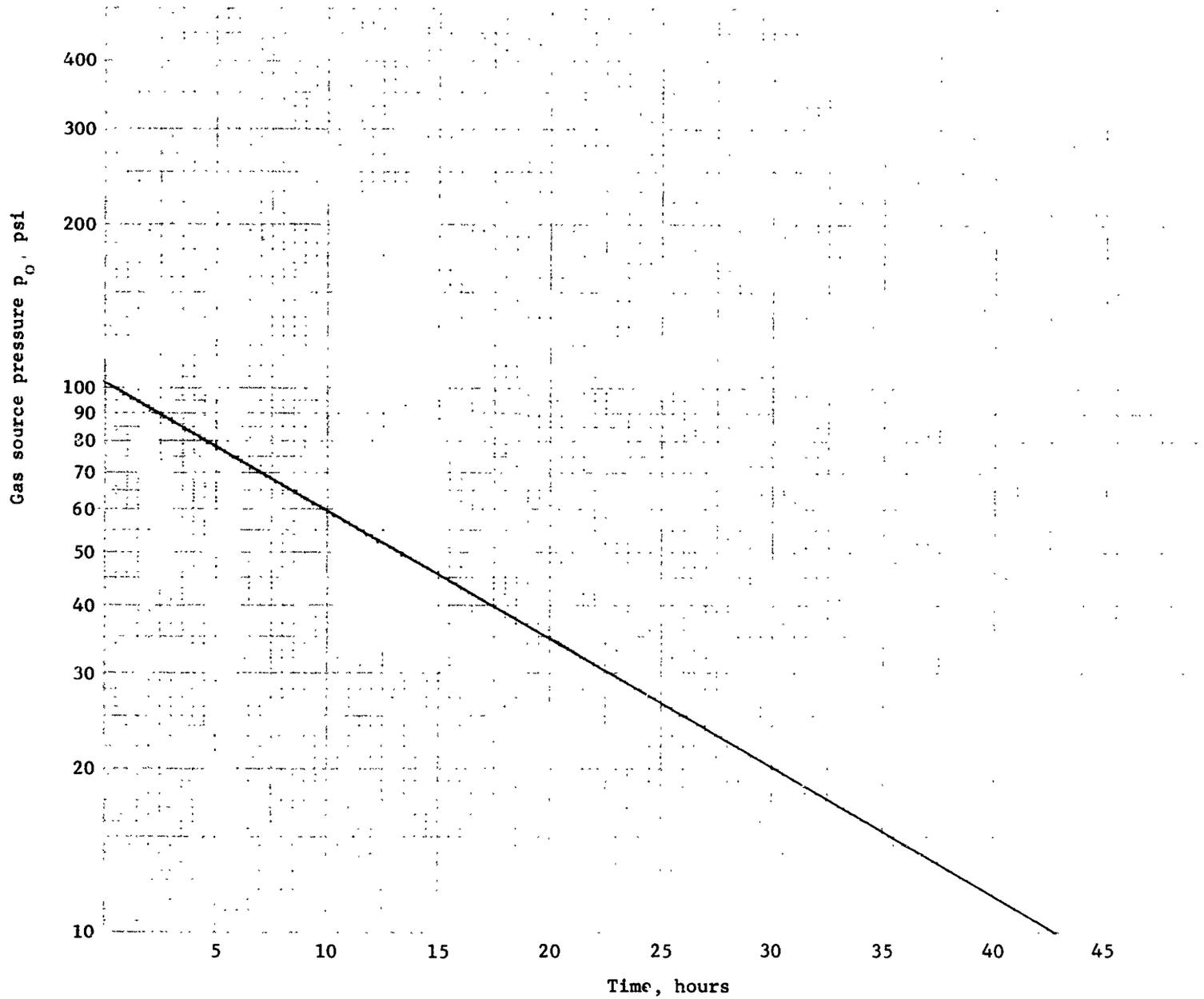

FIGURE 16. POROUS PLUG CONDUCTANCE MEASUREMENT RUN 1-5. Least squares fit to straight line.

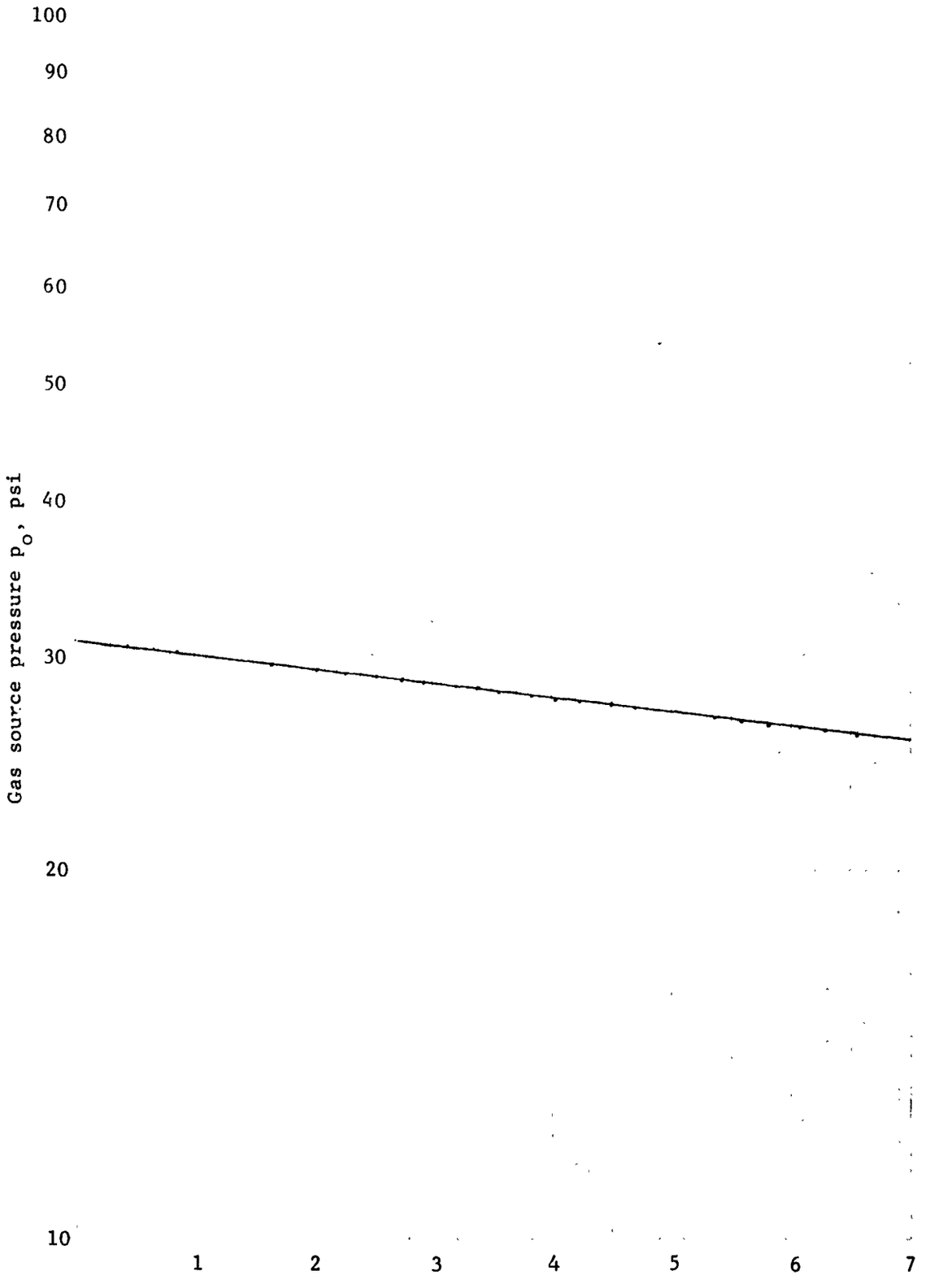

FIGURE 17. POROUS PLUG CONDUCTANCE MEASUREMENT RUN 1-6.
Least squares fit to straight line.

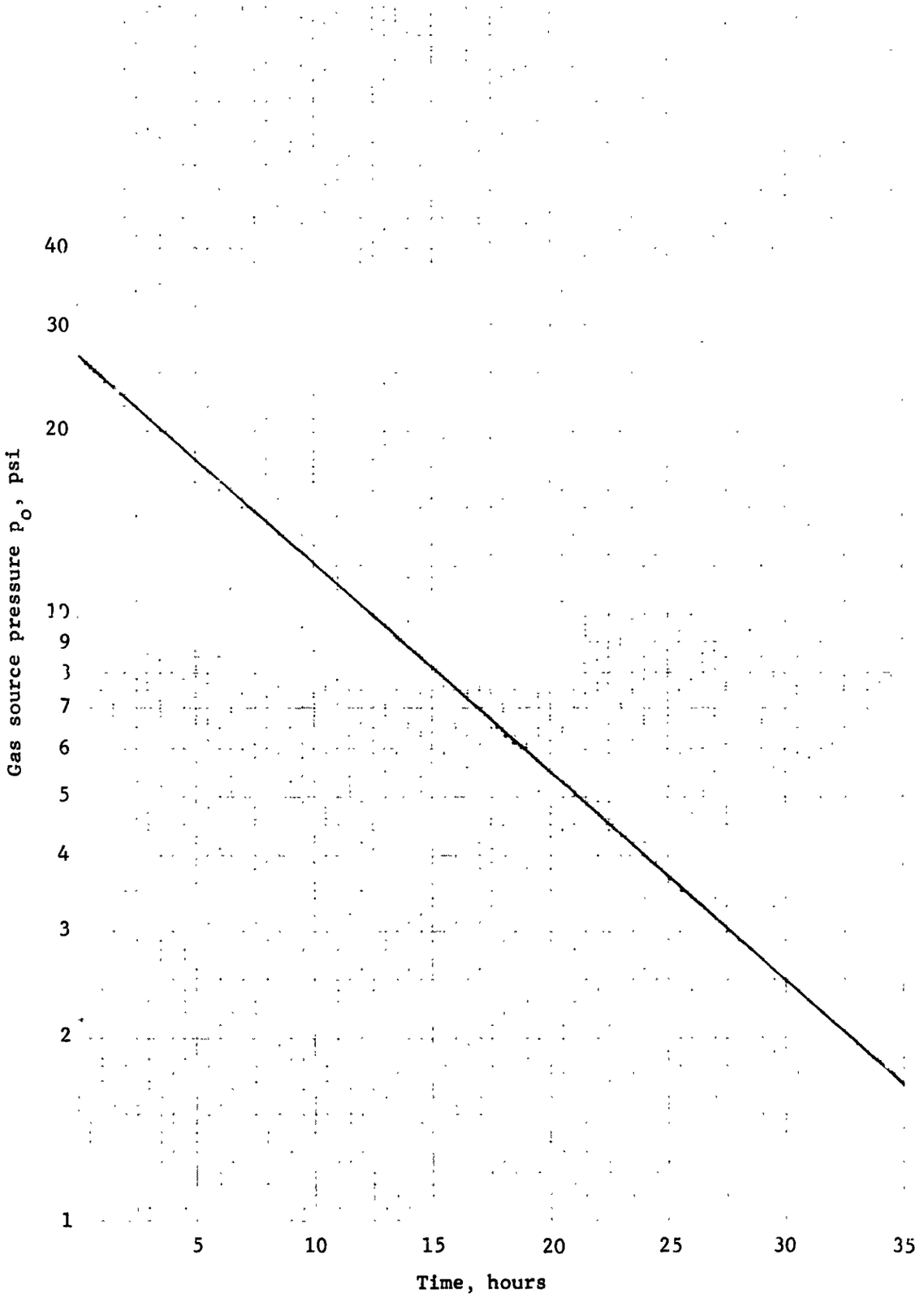

FIGURE 18. POROUS PLUG CONDUCTANCE MEASUREMENT RUN 1-7.
Least squares fit to straight line.

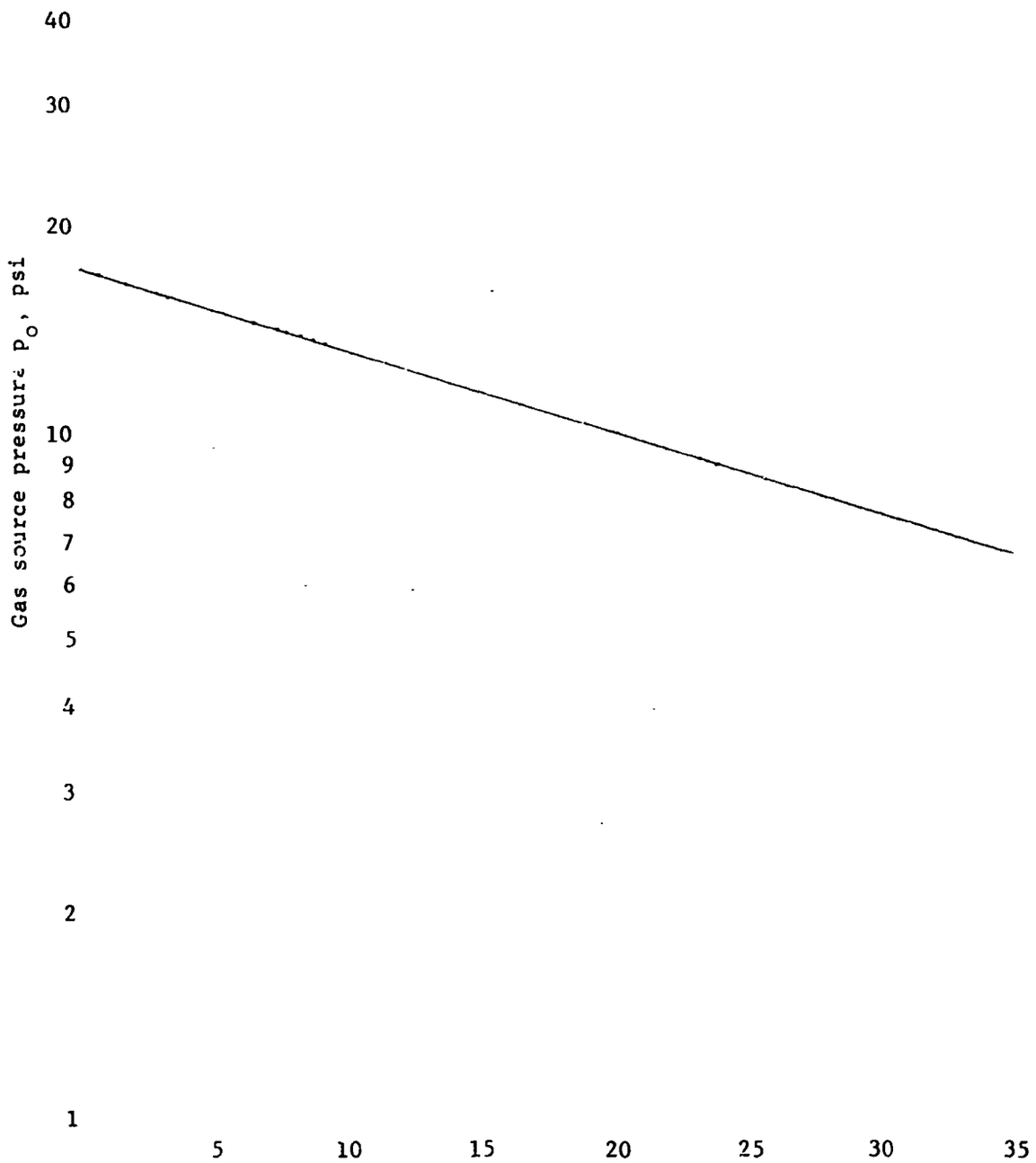

FIGURE 19. POROUS PLUG CONDUCTANCE MEASUREMENT RUN 1-8.
Least squares fit to straight line.

from 189 data points covering widely different regions within the range given above.

The gas source chamber and porous plug were maintained at 304°K + 0.5°K in six of the experiments and at 308°K + 0.5°K in one. The last pressure decay (see Figure 19) was performed after admitting atmospheric air at near 100% relative humidity for a 14 hour period. The least square slope of the experimental decay curves are given in Table 1. The average value of the least squares slopes of all decay curves is 7.55×10^{-6} per second with a relative standard error of the mean of 0.5%. The distribution of values is random showing no significant trend with pressure or temperature within the limits investigated. The last pressure decay measurement performed after the deliberate contamination of the plug showed nearly the largest deviation from the mean.

Since the transition to viscous flow will be most evident at the highest pressure, least squares analysis was carried out for the fit to a straight line of sections of the pressure decay data of the highest pressure experiment, namely 100.5 psi (see Figure 16). The slope of the least squares fit for groups of 10 points was determined and the results are shown in Table 2. It is seen that the 10 point slopes depart from the least squares slope of the complete set of data by less than 1/3%, and the deviation at the highest pressure is negative, not positive as one would expect if viscous flow phenomena were becoming evident.

It is thus found that linear flow conditions prevail for pressures such that M is smaller than 1.7. Wilson, et al[19] have reported for stainless steel plugs that deviations from linear flow were evident for M = 1.6.

In order to determine the conductance of the plug from the slope of the pressure decay curve, it is seen from Equation (3.2.3) that the volume, V, of the pressure source must be known. An experiment to determine V was carried out for each porous plug since the two different plug mountings did not displace the same volume. The experiment consisted of measuring the pressure change in the pressure source as the volume of a precision burette joined to the pressure source was varied by ΔV. An analysis of the experiment was presented in Section 2.3 as a part of error analysis. Figure 20 shows the experimental arrangement with the burette shown extending downward. The volume of gas in the burette was changed by varying the level

TABLE 1

LEAST SQUARES SLOPE SUMMARY FOR POROUS PLUGS

Porous Plug #1

Experiment	Pressure Range, psi	Least Squares Slope, hr^{-1}	Deviation* From Mean	Temperature and Gas
1-1	1.5 - 15	0.02696	-0.85%	304°K, Ar
1-2	2.3 - 24	0.02705	-0.51%	304°K, Ar
1-3	1.305 - 35	0.02709	-0.37%	304°K, Ar
1-4	0.3 - 0.51	0.02737	+0.66%	304°K, Ar
1-5	32 - 100.5	0.02717	-0.07%	304°K, Ar
1-6	25.8 - 30.5	0.02730	+0.40%	308°K, Ar
1-7	3.5 - 25.8	0.07889		304°K, He
1-8**	9 - 17	0.02739	+0.74%	304°K, Ar
	Mean*	0.02717		

Porous Plug #2

2-1	7.5 - 14.65	0.01901	+1.01%	304°K, Ar
2-2	4.15 - 6.8	0.01863	-1.01%	304°K, Ar
	Mean	0.01882		

* Run 1-7 was not considered in determining the mean; only argon runs were considered.

** Run 1-8 was carried out after 14 hours of flow of moist atmospheric air through the porous plug.

TABLE 2

LEAST SQUARES ANALYSIS FOR POROUS PLUG EXPERIMENT 1-5

Pressure Range	Slope of Least Squares Fit	Deviation from Slope* For Fit to All Points
100.5 - 84 psi (5200-4400 Torr)	2.706×10^{-2} hr^{-1}	-0.33%
82.5 - 67 psi (4260-3490 Torr)	2.715×10^{-2} hr^{-1}	0
66 - 51 psi (3410-2635 Torr)	2.723×10^{-2} hr^{-1}	+ .29%
49.5 - 33.5 psi (2560-1730 Torr)	2.715×10^{-2} hr^{-1}	0

* Slope of least squares fit for complete 100.5 - 32 psi run is 2.715×10^{-2} per hr.

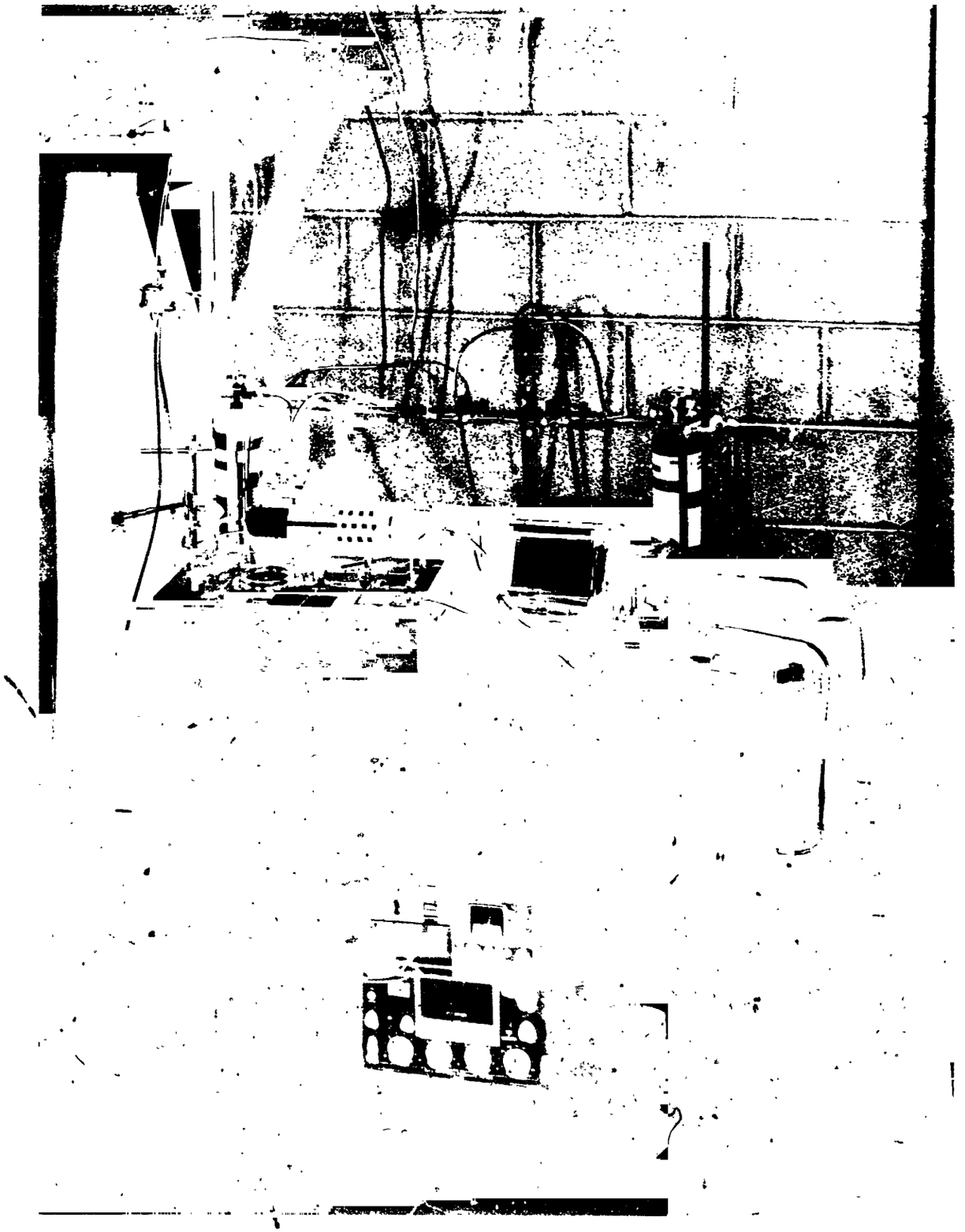

FIGURE 20
GAS SOURCE CHAMBER VOLUME MEASUREMENT EXPERIMENTAL APPARATUS

of a low vapor pressure silicone oil (Dow-Corning 705) using an external source of pressure. The pressure in the gas source volume was determined using the rotating piston gauge. As with the pressure decay measurements, to prevent the leakage in the piston gauge from affecting the measurement, the differential pressure gauge was placed between the piston gauge and gas source and the readings taken for zero pressure differential. The experiment is begun with the gas source, molecular furnace and piston gauge joined to a common manifold pressurized with ultra-high purity argon to the level required to float the piston. All metal valves are then closed to isolate the three elements. By taking care in closing the valves, the small variation in pressure in the system, due to the trapping of gas as the valve seat closes, can be kept less than 10^{-3} Torr, which is negligible in comparison to the change in pressure induced by changing the volume by ΔV. The weight of the piston is increased to correspond to a 0.5 psi ($\sim$ 26 Torr) pressure increase and the level of oil in the burette increased until the differential pressure gauge again indicates zero and the oil level noted so that ΔV can be determined. In creating this pressure differential across the porous plug there is a flow through the plug decreasing the pressure in the gas source volume. The error introduced by this flow into the determination of V was estimated using an expression similar to Equation (3.2.2) and found to be negligible for porous plugs whose conductance is less than 10^{-5} liters per second.

The volumes of the gas source with each of the plugs in place were determined to be:

$$V_1 = 1.383 \text{ liters, and}$$
$$V_2 = 1.309 \text{ liters.}$$

The relative probable error calculated from the error analysis given in Section 2.3 is 1.8%. The reason for this relatively large error is the multiplication of errors in pressure and temperature by the ratio $V/\Delta V$ where V is the gas source volume and ΔV is the incremental change in volume. In the measurements made, $V/\Delta V$ was greater than 50.

Measurements on the leak-down of the disc-type porous plug #2 were carried out over the pressure range 4 to 15 psi. From the slope of the pressure decay curve derived from 89 data points and the measured volume, V_2, the conductance of the porous plug was determined to be 6.84×10^{-6} ℓ/s. From the measured dimension

of the plug, a specific flow rate of 6.0×10^{-6} liter mm/sec cm^2 is calculated. This is greater than the value published[20] (oxygen data corrected to argon) for porous Vycor glass by a factor of 2.7, and larger than that obtained by Barrer and Barrie by a factor of 1.4. The reason for this discrepancy is not known although possibly 30% of the difference could be accounted for by uncertainty of tne area and thickness of the plug due to the type of mounting used and the fact that the rolled glass surface used is not flat. There may also be variations in the manufacturing procedure for different lots of glass. Several different characteristics were shown by Emett and Dewitt[21] for different samples of porous Vycor.

The experiments on the flow of argon in porous Vycor have shown its conductance to be constant with pressure over a very wide range of pressure and indications are that the conductance is not greatly affected by exposure to normal atmospheric conditions. It is concluded that the conductance of a porous plug of Vycor is not predictable a priori. However, by putting a differential pressure gauge between the pressure source and rotating piston gauge, the conductance of the porous plug in use in a calibration system may be measured at any time in an experiment as described above to any desired accuracy. Since the linear character of the decay has been proven, the measurement could consist of a few determinations of pressure and time over a period of a day. Such measurements could be periodically made to check system performance. In addition to the determination of conductance, this experiment would give a positive check on the pressure integrity of the gas source since as discussed above, non-linearity in the plot of $\ln p$ vs. t would be very evident if the pressure decay is due to flow through any other element except the porous plug.

4. INVESTIGATION OF MOLECULAR BEAM SOURCES

4.1 Deviations From Free Molecular Flow of an Orifice

In the derivation of the calibration equation (Equation (2.12)), there are several implicit assumptions which must be more carefully considered concerning the nature of gas flow in and from the molecular furnace. The constraints placed upon the operation of the system due to the result of these considerations may be

described, as for the porous plug, in terms of the ratio of the mean free path of the gas to some characteristic dimension. All of these constraints relate to the maximum allowable deviation from: 1) molecular flow conditions, and 2) thermodynamic equilibrium.

The most important constraint and the one given the most consideration both in the literature and in this investigation is that concerning the deviation from molecular flow through the orifice which defines the molecular beam. Postulating molecular flow conditions, the number of molecules passing out of the unit area of the orifice in unit time is

$$\frac{1}{4} n_f \bar{v}. \qquad (4.1.1)$$

This is a result derived from kinetic theory by M. Knudsen[1] for the number of molecules within an equilibrium gas that pass toward one side through unit area in unit time. The situation in the case of an aperture in the wall of a vessel containing an equilibrium gas, outside of which a relative vacuum is maintained, differs from the above in that a completely negligible number of molecules pass through the aperture with inward directed velocities. Therefore, the molecular density in the vicinity of the aperture is reduced, being $\frac{1}{2}n$ in the plane of the orifice and increasing to n, the equilibrium gas density, as one proceeds back into the gas. If the molecular mean free path is very large compared to the aperture diameter, the presence of the aperture has little effect on the molecular distribution function, and expression (4.1.1) yields the correct flow. Theoretical calculations of the correction to expression (4.1.1) have been made by Liepmann,[22, 23] Narishima,[24] Willis,[25, 26] and Probstein.[27] Their calculations are in general agreement with the fact that the deviation from the molecular flow limit (expression (4.1.1)) due to a finite ratio M (Knudsen number) of molecular mean free path, λ, to aperture diameter, d, for large M is

$$\frac{\text{Actual Mass Flow Rate}}{\text{Free Molecular Mass Flow Rate}} = 1 + \frac{1}{8M}. \qquad (4.1.2)$$

Willis gives an expansion in terms to order $(1/M)^2$ which is valid for smaller M than is Equation (4.1.2), but agreement with exact numerical computation is for $M \geq 3$. Willis' exact result (using the first iterate distribution function) for the mass flow rate at the center of an orifice normalized to the Knudsen flow rate is shown in Figure 28.

As Willis points out, since his is a first iterate treatment and a second order expansion of this shows large deviations for $M < 1.5$, therefore, it is expected that the second iterate problem should be considered for such small M values.

Experimental verification of the deviation from Equation (4.1.1) has been obtained by Liepmann. Scott, et al,[28] show that the deviation arises from a loss of molecules of low velocity from the Maxwell-Boltzmann distribution leading to a higher mean molecular speed and a more narrow distribution of speeds in the beam for low M values than in the collisionless limit ($M = \infty$). The scatter in their data is large. The free molecular limit conductance, C, is shown by Bureau, et al,[31] for an aperture of area, A, situated coaxially in a tube of length, L, diameter, D_o, and area, A_o, to be

$$\hat{C} = \frac{\left(\frac{kT}{2\pi m}\right)^{1/2} A}{\left[1 - \left(1 - \frac{3L}{4D_o}\right)\frac{A}{A_o}\right]}, \qquad (4.1.3)$$

In addition, a Clausing correction, K, should be included to account for finite thickness, ℓ, of the material in which the aperture is formed. This problem was first treated by Knudsen[32] and more completely by Clausing,[33] Smoluchowski,[34] and DeMarcus.[35] Miller[36] gives a Fortran program for Clausing's expression for the fraction of molecules entering a cylindrical orifice which diffuse out the other end into any given cone with half angles, θ, from 0^o to 90^o. He provides a table of values for various ℓ/r ratios. The value of this fraction for $\theta = 90^o$ is known as the Clausing factor. Clausing calculated the distribution from an orifice with $\ell/d = 1$. This is plotted in Figure 21 along with a cosine distribution function for comparison. Kennard[37] has shown that for short tubes, such as the orifices considered here, the Clausing factor, K, is

$$K = \frac{1}{1 + \ell/d}. \qquad (4.1.4)$$

where d is the diameter of the orifice. Thus, finally, from Equations (4.1.3) and (4.1.4), the orifice conductance, $\hat{C}$, is given by

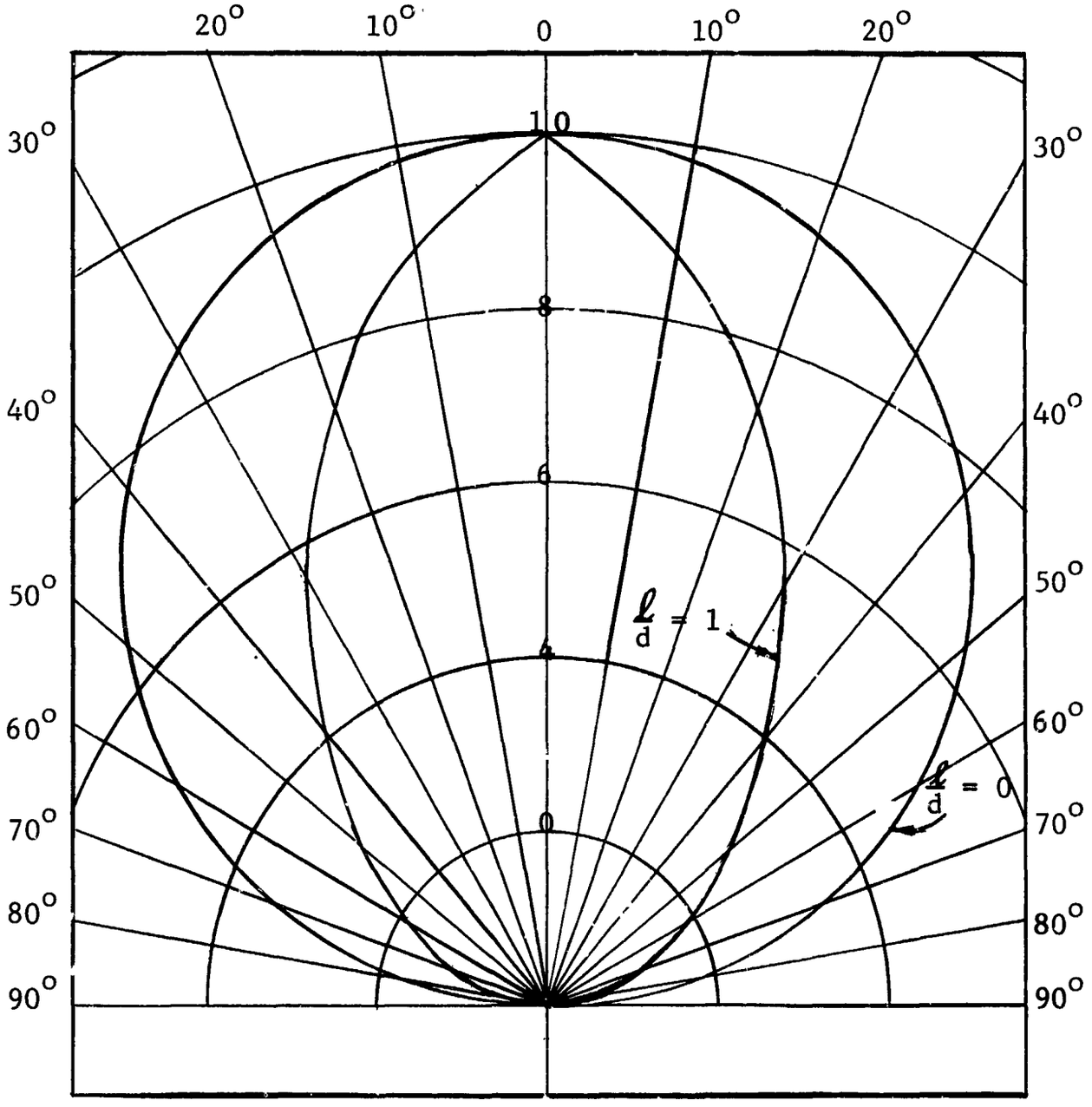

FIGURE 21

FLUX DISTRIBUTION OF MOLECULAR BEAM WITH ORIFICE THICKNESS TO DIAMETER RATIO $\ell/d = 0$ AND 1 (AFTER CLAUSING 33c)

$$\hat{C} = \frac{\left(\frac{kT}{2\pi m}\right)^{1/2} A}{\left[1 - \left(1 - \frac{3L}{D_c}\right)\frac{A}{A_o}\right]\left[1 + \ell/d\right]} \quad (4.1.5)$$

4.2 Experimental Measurement of Conductance

In order to more precisely evaluate these deviations from Equation (4.1.1), experiments were conceived in which the conductance of an aperture would be determined over a range of pressure corresponding to Knudsen numbers, M, from about 3.5 to 12. Consider a pressure source, molecular furnace, and pumping system as shown in Figure 22. C_i is the orifice whose conductance is to be determined. Anticipating that two experiments will be required to determine the conductance, the subscript i will take on the value 1 or 2, and other parameters will be treated similarly. A pressure p_{o_i} of argon measured by a rotating piston gauge is maintained in the gas source. The gas flows through a porous plug into a molecular furnace whose walls are maintained isothermal with the pressure source and plug. The gas then effuses from the orifice in question into a pumped cavity, the pressure of which is maintained at least two orders of magnitude smaller than the equilibrium furnace pressure, p_i, by maintaining an equally large ratio of pumping speed, S, to orifice conductance. The piston gauge which has a finite leak, as previously discussed, is maintained in a floating condition by a variable volume, piston-cylinder arrangement with which the total volume of the gas source and gauge chamber may be varied.

The pressure drop across the orifice is determined using a capacitance-type differential pressure gauge. The system reaches equilibrium shortly after the pressure p_o is established, the delay being all associated with the attainment of steady state flow in the porous plug, as previously discussed.

Under conditions of molecular flow through C_p and C_i it is seen that

$$C_p(p_{o_i} - p_i) = C_i(p_i - p_p). \quad (4.2.1)$$

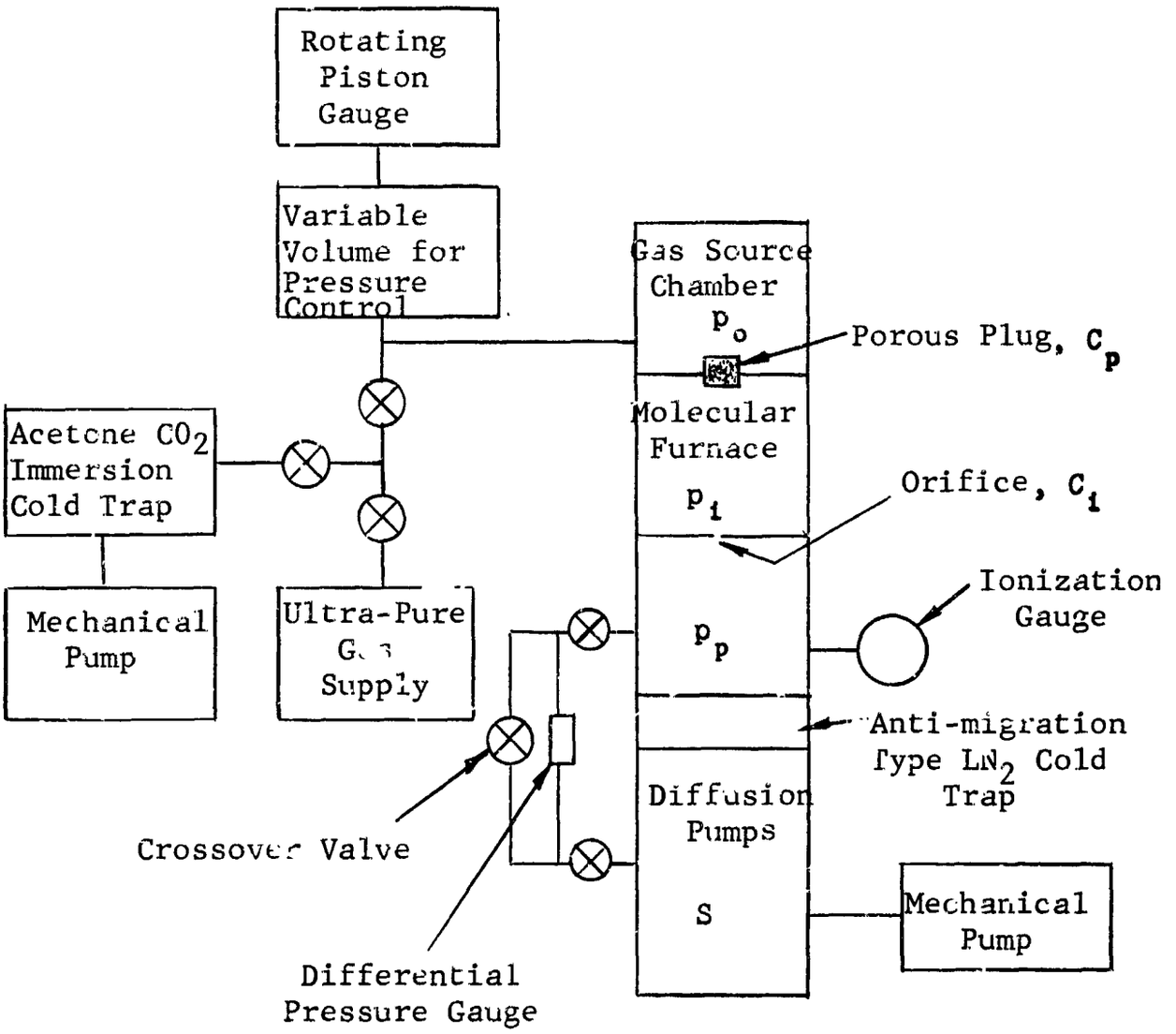

FIGURE 22

ORIFICE CONDUCTANCE MEASUREMENT EXPERIMENT (SCHEMATIC)

Also,

$$C_i(p_i - p_p) = Sp_p, \tag{4.2.2}$$

so that,

$$p_p = \frac{C_i}{C_i + S} p_i \equiv \alpha_i p_i, \tag{4.2.3}$$

and therefore

$$p_i = \frac{C_p}{C_i(1 - \alpha_i) + C_p} p_{o_i}. \tag{4.2.4}$$

Now, C_p is much smaller than C_i for any reasonable diameter of orifice, and we have, finally,

$$p_i = \frac{C_p}{C_i(1 - \alpha_i)} p_{o_i}. \tag{4.2.5}$$

The mounting and flange for the porous plug (see Figure 5) has a conductance C_M which is of the same order as the orifice conductance C_i. However, the geometry of this mounting and flange are such that p_i is determined by the series combination of C_M and C_p. It follows directly from the flux continuity equation that the total conductance is[29]

$$C'_p = \frac{C_p C_M}{C_p + C_M}, \tag{4.2.6}$$

and since $C_M > C_i$ then, as before, C_p may be neglected compared with C_M and no correction to Equation (4.2.5) is found necessary.

Consider an experiment in which the molecular furnace is operated over a range of pressure p_1 such that the ratio, M_1, of the mean free path,

$$\lambda_1 = \frac{\gamma}{p_1}, \tag{4.2.7}$$

to orifice diameter, d_1, is sufficiently large compared with unity, that there are negligible deviations from molecular flow, as given by Equation (4.1.1). γ here varies directly with temperature, and its value for various gases may be found in Dushman.[30]

Since C_p can be accurately measured, as shown in Section 3, Equation (4.2.5) may be used to calibrate a gauge which is arranged to measure p_1. Since it is desirable that the gauge have linear response characteristics over the range of pressure to be investigated, a capacitance-type differential pressure gauge, MKS Instruments, Inc., BARATRON, was chosen. The gauge is non-specific with respect to the gas to be measured. The particular model used (77H-1068) had high sensitivity and fast response over the range 2×10^{-5} Torr to 3 Torr, although the noise level was high at the low end of the range. A 1/4% chart recorder (Honeywell Electronik 17) was used as the indicator. The least count of the system is 2×10^{-5} Torr and short time zero drift variations of this order were found during zero check made before and after each of the data points measured. This also constitutes a hysteresis check since the zero check was made immediately following the removal of the measured differential pressure. A differential of 3 to 5×10^{-5} Torr, the origin of which is unknown, was measured across the orifice with the furnace evacuated. The range over which the differential pressure gauge was calibrated was 1.4×10^{-3} Torr to 5.0×10^{-3} Torr. Data was obtained over the range up to 1.5×10^{-1} Torr as will be described more fully below.

Now consider a second experiment performed with the same apparatus but with a different orifice such that the ratio $M_2 = \lambda_2/d_2$ is smaller than M_1. Equation (4.1.2) predicts for small M_2 values some variation from the specific flow rate, $\hat{C}_2$, obtained in the free molecular flow limit. In order to assess the magnitude of any such deviation, measurements of furnace pressure, p_2, must be made over the range for which the differential pressure gauge was calibrated in experiment 1, and since C_p and p_o are accurately known, then C_2 may be evaluated and compared with the predictions of Equation (4.1.2).

If μ is the multiplicative factor denoting the deviation from free molecular flow, then

$$C_2 = \mu \hat{C}_2 . \tag{4.2.8}$$

Now if measurement of p_i was made using a gauge which had a scale error η_j for the j scale, then the derived value p_i' is

$$p_i' = \eta_j \, p_i . \tag{4.2.9}$$

Using the j scale, Equations (4.2.5) and (4.2.9) yield

$$p_1' = \eta_j \frac{C_p p_{o_1}}{\hat{C}_1(1 - \alpha_1)}, \tag{4.2.10}$$

so that the gauge constant is

$$\eta_j = \frac{\hat{C}_1(1 - \alpha_1)}{C_p} \frac{dp_1'}{dp_{o_1}} \tag{4.2.11}$$

as long as the measurement is carried out for pressures low enough that C_1 is not a function of pressure. From Equation (4.1.2) this is seen to require that M be large.

For the second orifice experiment, the steady state solution, Equation (4.2.5), and Equations (4.2.8) and (4.2.11) may be combined to yield

$$p_2' = \frac{\hat{C}_1(1 - \alpha_1)}{\mu \hat{C}_2(1 - \alpha_2)} \frac{dp_1'}{dp_{o_1}} p_{o_2}, \tag{4.2.12}$$

where p_2' is the pressure across the orifice as measured using the j scale. Thus, by rearranging terms, the deviation from molecular flow may be determined from

$$\mu = \frac{\hat{C}_1(1 - \alpha_1)}{\hat{C}_2(1 - \alpha_2)} \frac{dp_1'}{dp_{o_1}} \frac{p_{o_2}}{p_2'}, \tag{4.2.13}$$

Using Equation (4.1.5), the orifice conductances for argon at 304°K are calculated to be for the two experiments performed

$$C_1 = 7.63 \times 10^{-2} \text{ liters per second}, \tag{4.2.14}$$

and

$$C_2 = 8.62 \times 10^{-1} \text{ liters per second}. \tag{4.2.15}$$

The system pumping speed, S, was determined during the porous plug experiments by measuring the pressure in the chamber below the plug with an NRC type 507 ionization gauge. The speed determined for 304°K argon is 104 liters per second. Correction was made for the series conductance of the spool piece interposed between the pump and the molecular furnace for the orifice experiments. The effective pumping speed in those experiments is then

$$S = 86 \text{ liters/second.} \tag{4.2.16}$$

Using Equations (4.2.3) and (4.2.14) - (4.2.16), the coefficients α_i are calculated to be

$$\alpha_1 = 8.9 \times 10^{-4} \tag{4.2.17}$$

and

$$\alpha_2 = 1.01 \times 10^{-2}. \tag{4.2.18}$$

Thus, Equation (4.2.13) becomes

$$\mu = 0.0893 \frac{dp_1'}{dp_{o_1}} \frac{p_{o_2}}{p_2'}. \tag{4.2.19}$$

Figure 23 is a picture of the experimental equipment shown schematically in Figure 22. Figure 24 shows one of the 0.0005" thick copper aperture plates mounted on a flange which joins it to the molecular furnace and Figure 25 is a 100X magnified picture of aperture #2 which was formed by drilling with fast spiral twist drills through the copper sandwiched between 1/8" thick ground and polished aluminum plates.

The deviation from free molecular flow, μ, was evaluated according to Equation (4.2.19) over the range $3.3 \leq M \leq 12.5$. The deviation from Knudsen flow was found to be less than 3% over this range. The uncertainty in this determination was slightly less than 2%. Since the deviation, μ, determined above was small, it was considered desirable to investigate the region of smaller M where the deviation is expected to be substantially larger. A repeat of the calibration procedure described above for a wider range of M is impractical with any reasonable set of system parameters, as can be shown from the results of Appendix 2. Therefore, the extension of the measurement of μ to smaller M values must depend on the assumed linearity of the differential pressure gauge. A measurement is also required of the multiplicative factor, ζ_{jk}, relating readings on scale k to those on scale j so that

$$p_{2j}' = \zeta_{jk} p_{2k}'. \tag{4.2.20}$$

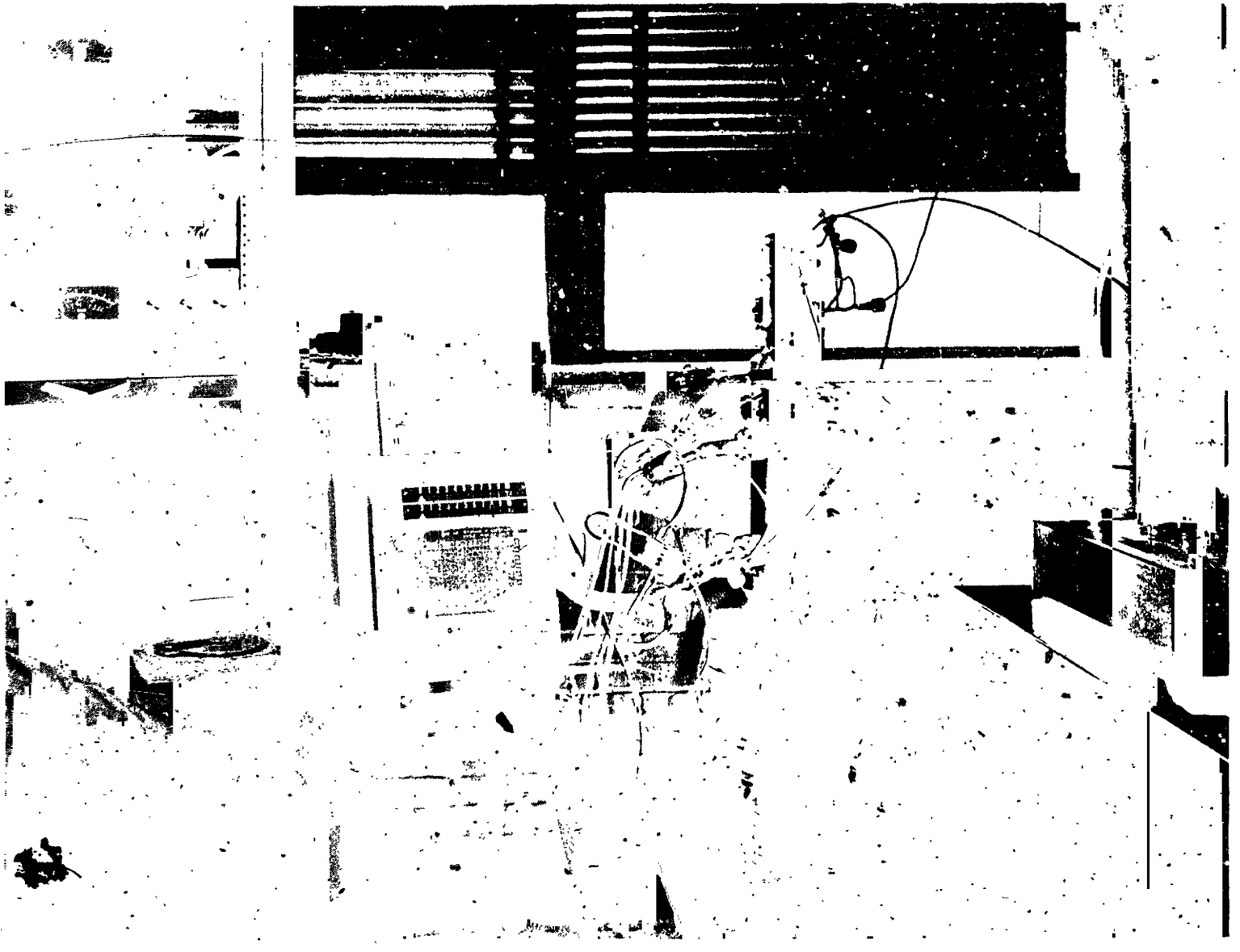

FIGURE 23
ORIFICE CONDUCTANCE MEASUREMENT EXPERIMENT

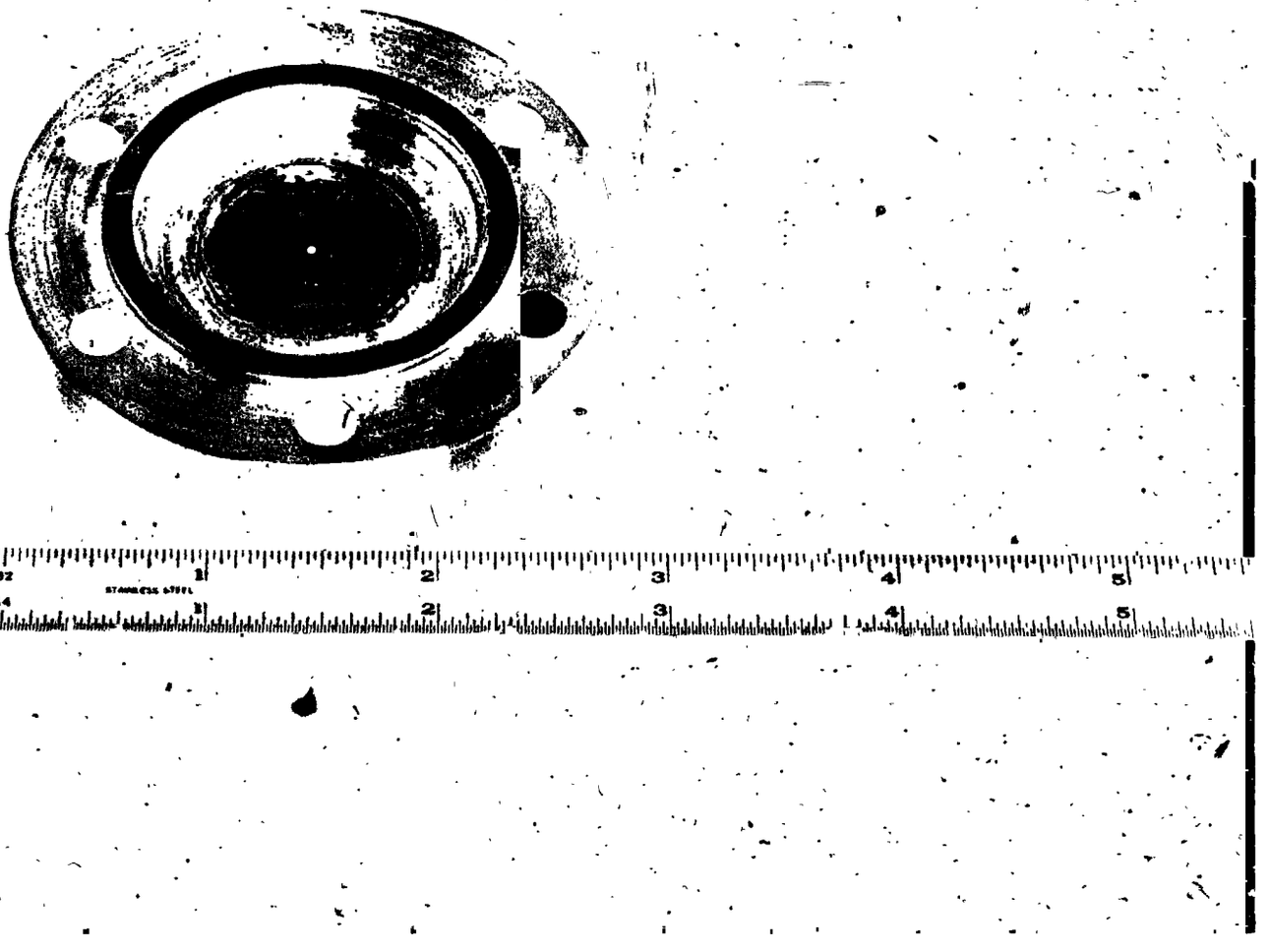

FIGURE 24
ORIFICE #1 MOUNTED ON GOLD O-RING SEAL FLANGE

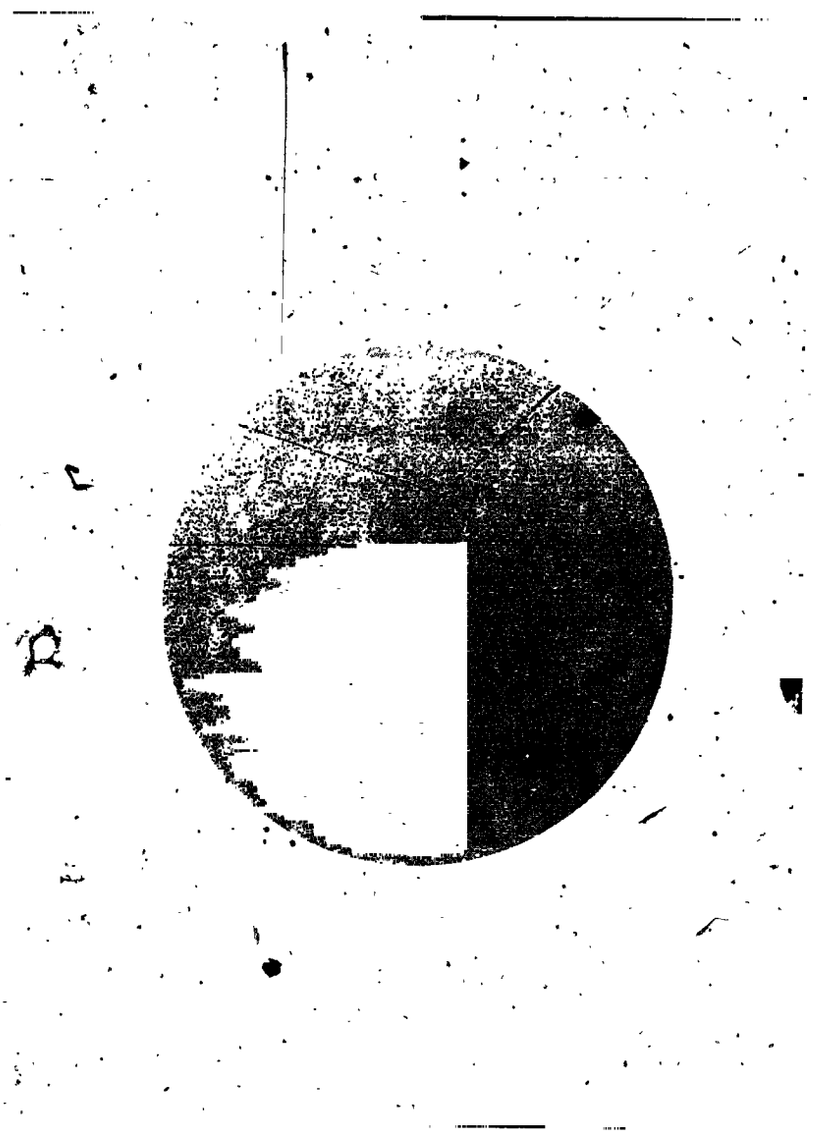

FIGURE 25
ORIFICE #2 100X MAGNIFIED

Determination of ratio ζ_{jk} was made by measuring p_2' for the same p_o but on 2 different scales, j and k. The relative standard error of the mean for a large number of such ratios ζ_{jk} was found to be less than 1.3%. As for linearity, the manufacturer's specifications indicate that it should be better than 1/2%, and since the lower scales were used for which the diaphragm deflection is small, the assumption of linearity should be even better. As may be seen from Figures 26 and 27, which show least squares fits of straight lines for the data of p' vs p_o for M from 12 to 40, the linearity assumption appears good; the relative standard error estimate for these least square fits is approximately 0.5%. A total of 266 data points were daken over the range 10^{-3} Torr to 10^{-1} Torr.

If measurements of p_1' in Equation (4.2.19) were made using scale j, then for the extension of measurements of M_2 below $M_2 = 3.3$, the factor μ is obtained by substitution of Equation (4.2.20) into Equation (4.2.19). The resulting expression for μ, the multiplicative factor denoting the deviation from free molecular flow through the orifice, is given by

$$\mu = 0.0893 \frac{dp'_{1j}}{dp_{o_1}} \frac{p_{o_2}}{p'_{2k}} \qquad (4.2.21)$$

Figure 28 is a plot of μ, given by Equation (4.2.21), versus M, where γ (Equation (4.2.7)) for argon at 304°K is found from Dushman[30] to be 5.42×10^{-3} cm/Torr. Also on Figure 28 is plotted μ as given by Willis' complete first iterate treatment of the orifice flow from upstream on the axis of the orifice in which second order corrections were applied to correct for flow from downstream. The latter correction procedure is probably in error for M less than about 3. Finally, on Figure 28 is plotted the curve representing Equation (4.1.2), the first order expression for μ given by Liepmann.

It is a temptation to conclude that Willis' correction to free molecular flow accounts well for the measured deviation. However, a measurement of the diameter of the orifices after the completion of the entire experimental program showed a 2.5% and 8% increase in the diameter of orifice 1 and orifice 2, respectively, which leads to undertainty in calculating the theoretical conductance. It was expected that orifice 2 would show yield, since while carrying out leak testing procedures in

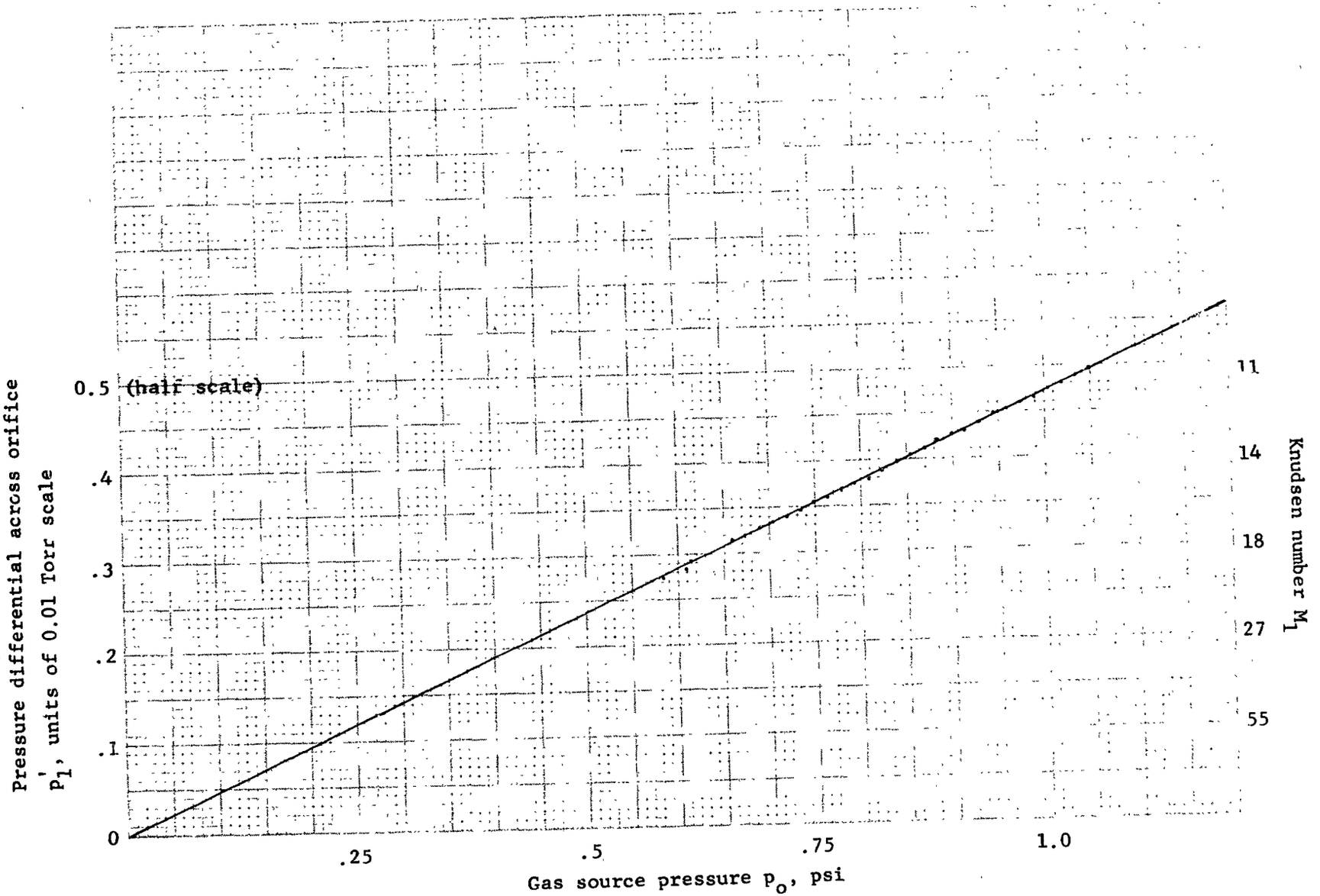

FIGURE 26. ORIFICE CONDUCTANCE MEASUREMENT RUN 1-6. Least squares fit to straight line.

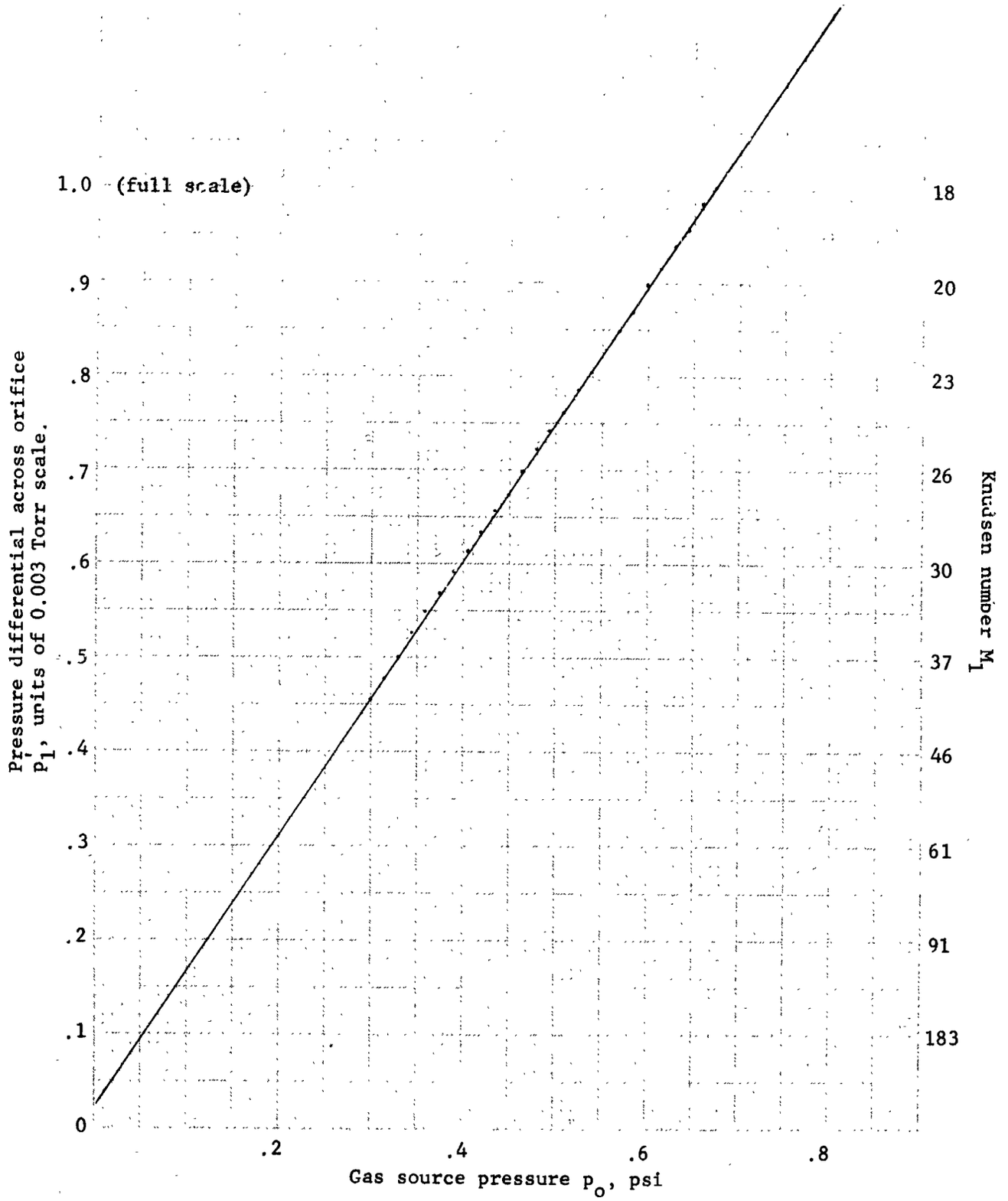

FIGURE 27. ORIFICE CONDUCTANCE MEASUREMENT RUN 1-7.
Least squares fit to straight line.

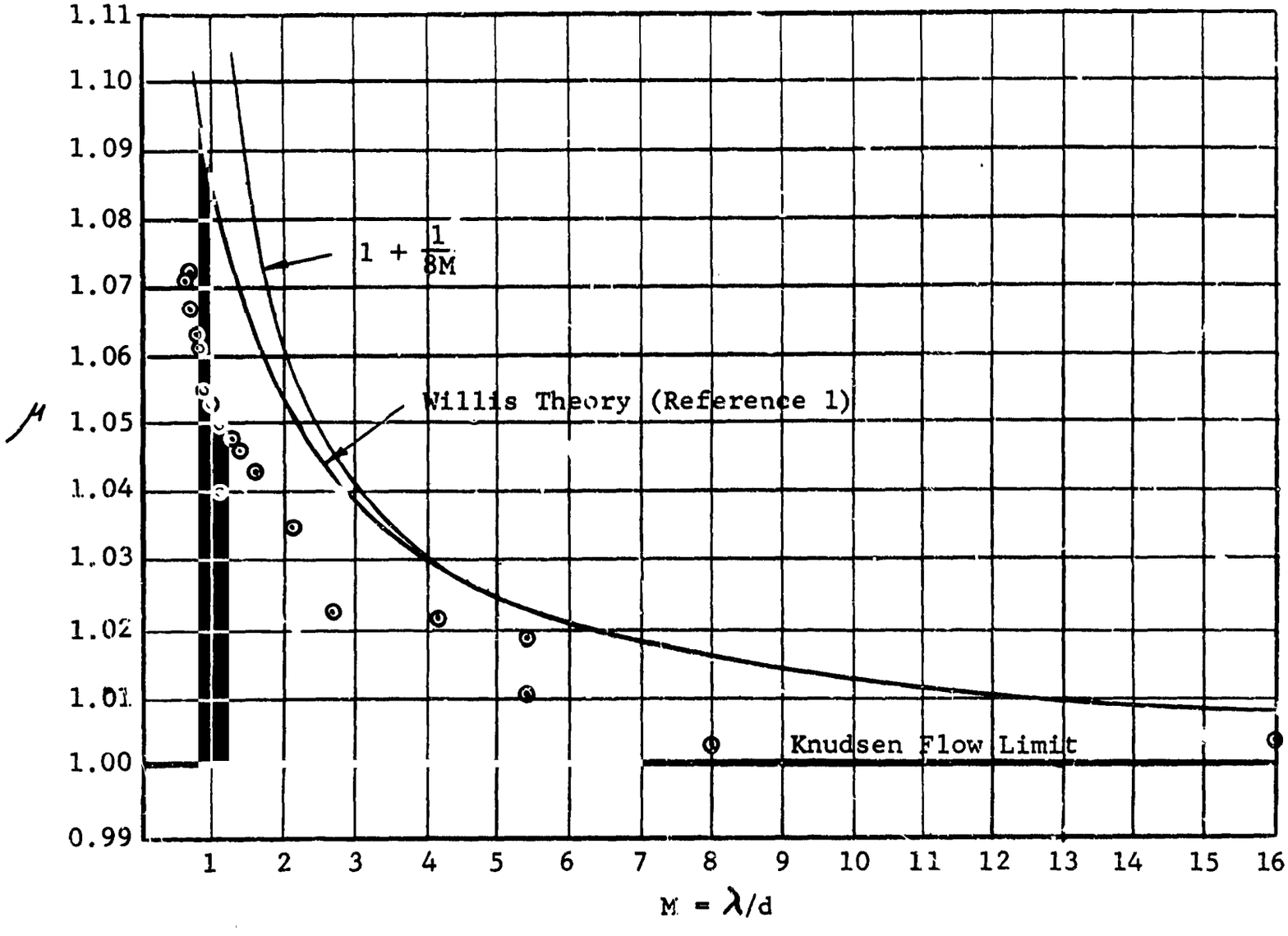

FIGURE 28. CALCULATED AND MEASURED DEVIATION FROM FREE MOLECULAR FLOW THROUGH AN ORIFICE.

the extreme high vacuum system, a large pressure differential was applied across the orifice.

However, in the previous orifice experiments, a conductance was put in parallel with the orifice to minimize such pressure differentials during pumpdown. Since orifice 1 was found to have been yielded much less than orifice 2, it is probable that most of the yielding of orifice 2 occurred after the orifice flow experiments were complete, that is, during the XHV experiments. If, for example, the fractional yield of orifice 2 during pumpdown for the orifice flow experiment was about the same as for orifice 1, then to first order there would be no correction to the treatment given above or to the experimental curve in Figure 28. Thus, depending on the fractional yield occurring during pumpdown for the orifice experiments, the experimental curve in Figure 28 could be in error up to about 11% which is much greater than the deviation that must be explained. It is for this reason, and because as M gets large, the measured deviation from Knudsen flow goes to zero, that it is assumed the yield of orifices 1 and 2 was nearly the same during the orifice experiments and u plotted in Figure 28 requires no correction. The problem of the yielding of the orifice must have a more satisfactory solution for the calibration system. Possible solutions are that the pressure differentials applied must be kept small enough, or perhaps a stronger material than copper may be used for the orifice and still maintain a sufficiently low temperature gradient in the orifice material. However, even the copper orifice used in the experiments described above showed a large temperature gradient.

4.3 Scattering Effects in Molecular Beam Sources

It is concluded from the results shown in Figure 28 that the deviation from Knudsen flow for small M may be estimated with some precision from Willis' first iterate solution. This gives one confidence in the range of pressure over which molecular flow theory may be applied. In the calibration system, measurement of the pressure in the molecular furnace is not carried out so that correction to the molecular flow throughput need not be made. The throughput of the orifice must be identical with the throughput of the porous plug which is always maintained in the molecular flow regime as shown in Section 3.

Thus, the correction to the downstream intensity of the beam becomes a question not of the throughput but rather of the angular distribution of the beam as it effuses from the orifice, and of the scattering that occurs downstream of the orifice. This is a distinct problem not connected with the total flow rate of the orifice as considered above, but rather with a secondary effect on the intensity of the molecular beam downstream of the orifice. With respect to total flow rate, the back scattered flow from downstream of the orifice which must occur due to gas-gas collisions in the vicinity of the orifice, has been considered by Willis and found for M = 3 to be nearly 10% in magnitude of the increased flow from upstream. The gas-gas collisions outside the orifice are expected to be increasingly more important as M is decreased. Knauer and Stern[38] were the first to show that as M is decreased, the intensity downstream is decreased. The reason for this decrease was claimed to be the formation outside the orifice of a "cloud," the area of which is the emitting surface for the molecular beam rather than that of the orifice. At any given value of M, the effect is dependent on the particular type of orifice used. For example, Knauer and Stern[39] dismissed Mayer's[40] criticism of their "cloud" theory on the basis that a stronger cloud formation should occur for their slit type of orifice than for Mayer's circular orifice, since the intensity, a distance r from an emitting slit, should vary as $1/r$, however for a circular orifice as $1/r^2$. Knauer and Stern, using a slit, showed for H_2O that the cloud effects appear at M = 3 and less. Kratzenstein,[41] using a circular orifice, showed for potasium that cloud formation was just detectable at M = 1.6.

Other experimental problems affecting the detection of cloud formation arise from scattering phenomena. Johnson[42] suggested that Knauer and Stern saw the cloud at large M values because of scattering from background gas near the orifice. He suggested the remedy of cryopumping in this area as is used in the present calibration system. In addition, the effect of small angle scattering is more noticable as one moves farther away from the orifice where all the scattering takes place. As the detector with its finite opening is brought close to the furnace orifice, molecules scattered through only small angles are still collected. Thus, since in the calibration system high pressures and, thus, small M will be used when the distance ℓ is small, therefore, the effect of the scattering or "cloud" formation will be least. It is expected that the effect of this scattering on the beam intensity would

not become evident before that of deviation μ, due to collisions inside the orifice. Therefore, Willis' theory may be used to estimate the M below which unacceptable deviations in the beam flux occur. From Figure 28 it may be seen that the deviation becomes 1% for M = 13.

4.4 Nonequilibrium Effects in Molecular Beam Sources

The last constraint on the molecular furnace and beam orifice system arises from the requirement that the gas be in thermal equilibrium with the isothermal furnace walls and that density gradients in the furnace be negligibly small. There are several distinct elements to this constraint.

The first element in maintaining density gradients small is that the conductance of the furnace be very great compared with that of the orifice. This is not difficult to attain for any reasonable aperture size.

Second, there is the requirement that the orifice area be small compared with the internal surface area of the furnace so that wall collisions will be orders of magnitude more frequent than will be passages through the orifice. This is analogous to the problem that arises when an exit hole is made in a black body cavity. Also, if a temperature gradient exists in the orifice material due to radiation to the 4°K cryopump, then it is required that the wall surface be large compared with the area of orifice material having an excessive temperature difference from the furnace temperature.

The third element is concerned with the finite mass flow rate of gas through the furnace and orifice which may lead to nonequilibrium of the gas with the furnace. Barnes[43] and also Cooke[44] using different methods have treated some problems arising from such mass flow. It may be seen that this non-equilibrium effect decreases and finally becomes negligible as the mean free path approaches and exceeds the furnace dimensions. In that limit, gas-wall collisions are more frequent than are gas-gas collisions and there is no opportunity for the molecules to deviate from a Maxwellian distribution characteristic of the temperature of the wall.

5. CALIBRATION EXPERIMENT OF PROTOTYPE SYSTEM

The prototype calibration system was installed in the extreme high vacuum system in order to make use of the low temperature helium gas cryopumping system for attaining conditions of low background density. Johnson,[42] in 1927, suggested that the deviation from molecular flow found by Knauer and Stern[38] in their molecular beam experiment was due to background gas collisions and could be eliminated by cryopumping between the furnace and detector. The cylindrical cryopumped cavity used in the present experiment is 45 cm. in diameter by 60 cm. long. It may be seen in Figure 29a. Previous experiments[45] carried out in this system have shown that if the wall were maintained at about 8°K the capture coefficient for argon would be greater than 0.999. This is supported by the work of Dawson, et al,[46] who show the capture coefficient for argon to increase to unity as the temperature is decreased below about 12°K. A different view is expressed by Foner, et al,[47] who give the capture coefficient for argon on a 4°K surface to be 0.6, but their experimental conditions are less well defined than those in the other experiments. Figure 1 is a schematic of the installation.

The molecular furnace and gas source was joined to the cryopump wall by means of a stainless steel bellows, as may be seen in Figure 29b. A conical radiation shield which operates at the temperature of the rest of the cryopumped cavity shields the 300°K beam orifice from the cryopump. The beam orifice may be seen beyond the radiation shield in Figure 29a. The axis of the molecular furnace, and thus, the axis of the molecular beam, was aligned toward the gauge in the cavity by adjusting three stainless steel turnbuckles. The gauge was enclosed in a copper cylinder which is shown mounted in the cryopumped cavity in Figure 29a. The theory of the calibration system using the gauge enclosure is given in Section 2.2. The gas source, molecular furnace, and gauge enclosure were maintained isothermal by a common heat transfer line which circulated fluid around them. Water was used as the heat transfer fluid and the temperature of the 30 liter bath was maintained at 304°K ± 0.03°K. The auxiliary equipment for maintaining constant temperature, supplying and measuring argon gas pressure, and measuring ion current of all ion gauges is shown in Figure 30.

The gauge in the enclosure was a hot filament suppressor grid gauge. The orifice on the enclosure was a 1.6 cm. diameter

FIGURE 29
(A) GAUGE AND ENCLOSURE IN CRYOPUMPED CHAMBER

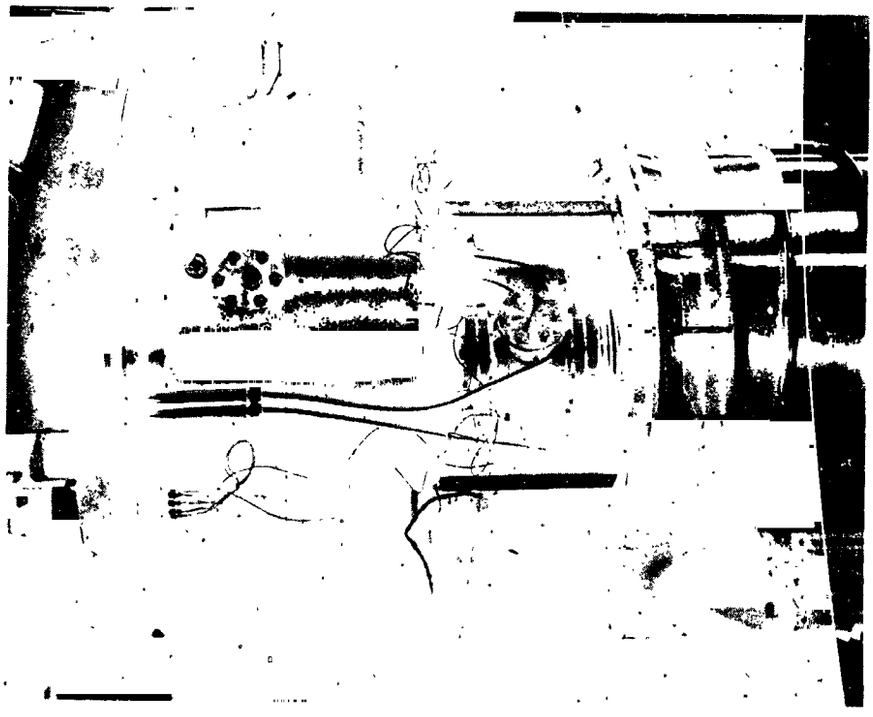

(B) MOLECULAR FURNACE AND GAS SOURCE CHAMBER MOUNTED ON CRYOPUMPING CHAMBER WALL

FIGURE 29
CALIBRATION RUN OF PROTOTYPE SYSTEM

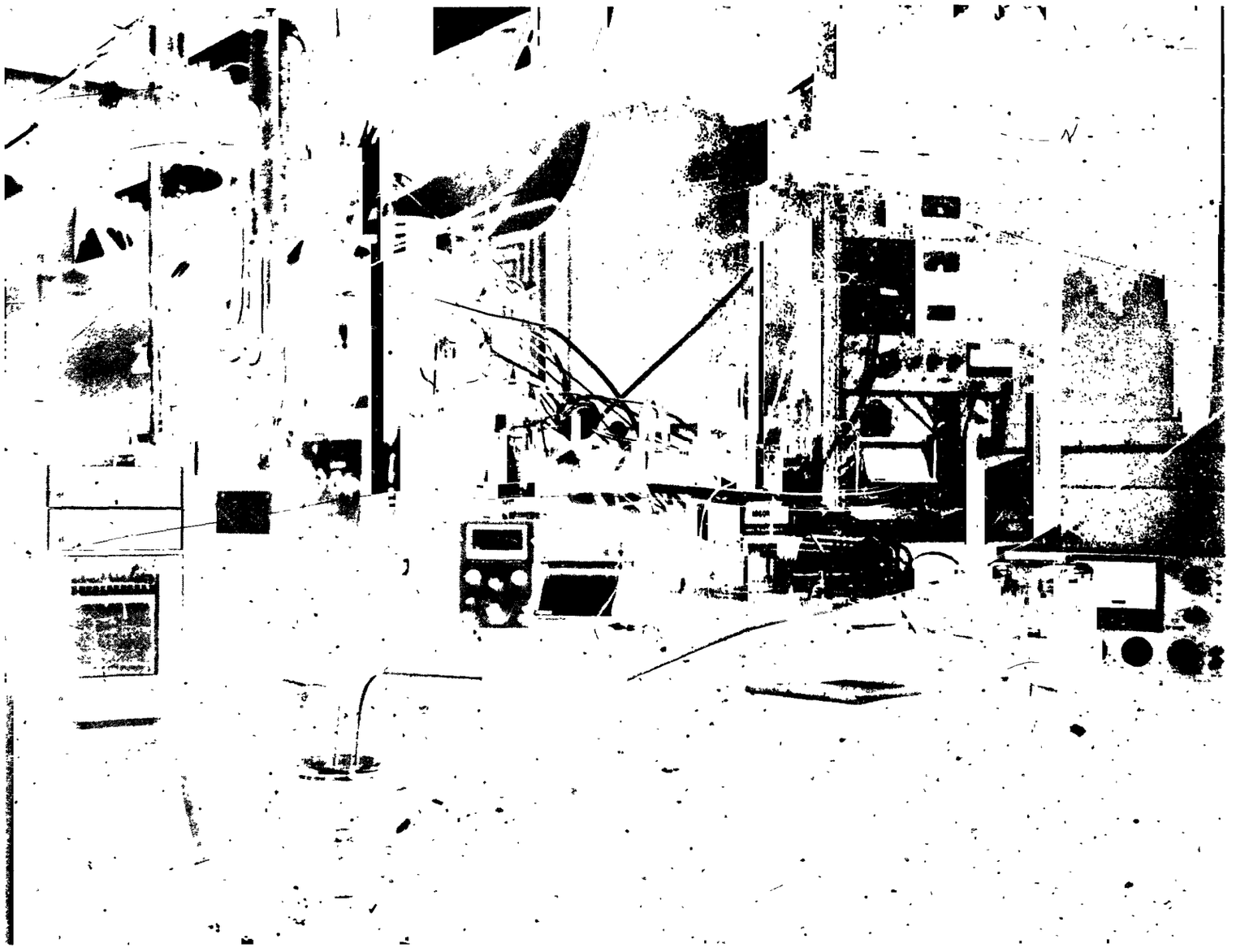

FIGURE 30
AUXILIARY APPARATUS FOR CALIBRATION RUN OF PROTOTYPE SYSTEM

hole in 10^{-3} cm. thick certified OFHC copper foil. The conductance of this orifice was sufficiently large that ionic pumping of argon by the gauge led to less than 0.5% variation of the enclosure pressure from that predicted by Equation (2.2.25). Bakeout of the enclosure was accomplished by electron bombardment from the gauge filament during which time the water cooling was diverted such that it flowed to the molecular furnace and gas source only. Bakeout of the gauge and enclosure was carried out at 350°C for several hours until activation of the electron bombardment at 10^{-9} Torr caused no increase in the collected ionization current.

Ultra-pure argon, as used in the experiments described in Sections 3 and 4, was admitted to the calibration system. With the porous plug ($C_p = 6.84 \times 10^{-6}$ liters/sec.) and the orifice (0.358 cm. diameter) used, the calibrated range attained, as determined from Equation (2.2.25), was 1×10^{-8} Torr to 2.2×10^{-7} Torr. Lower gauge pressures could be attained in the enclosure; however, due to electrical leakage in the collector electrode circuit of unknown origin within the extreme high vacuum system, data for pressures below 8×10^{-9} Torr were not measured. Table 3 gives the data for pressures from 1.38×10^{-8} Torr to 2.21×10^{-7} Torr. The potentials applied to the gauge electrodes with respect to ground (collector potential) were: grid, 150 volts; cathode, 45 volts; screen grid and suppressor grid, 0 volts; modulator connected to grid. The collector current versus enclosure pressure is plotted in Figure 31. Nonlinearity due to the electrical leakage is noticeable below 10^{-9} Torr. The gauge sensitivity derived from Figure 31 is 0.038 amperes per Torr.

The background gas density was monitored by a Redhead magnetron gauge (NRC 552A) which was mounted in the wall of the cryopumped cavity on which the molecular furnace was mounted. The axis of the gauge tubulation was parallel to the axis of the molecular beam. The background density thus determined was compared to the density in the gauge enclosure and the resulting signal-to-background gas density ratio is shown in Figure 32 where pressures, p_o, are varied from 1 to 40 psi. It is noted that the signal-to-noise ratio varies from 496 to 63. It is also noted that the signal-to-noise ratio measured for $p_o = 5$ psi was much smaller in the latter part of the experiment. The noticeable large decrease in signal-to-background gas density ratio is probably due to a change in the temperature of the cryopumped cavity. Sufficient argon had been deposited on the cavity, prior to collecting the data shown, to assure that the surface was covered with solid argon. A calculation using the reported[48]

TABLE 3

DATA OBTAINED ON CALIBRATION OF SUPPRESSOR GRID GAUGE

Gas Source Pressure, p_o psi, (Torr)	Gauge Enclosure Pressure, p_g, Torr	Gauge Collector Current, I, Amp	Background Pressure, Torr	$\frac{I}{P_g}$ $\frac{Amp}{Torr}$	$\frac{P_{Enclosure}}{P_{Background}}$
5(258)	2.76×10^{-8}	9.75×10^{-10}	5.56×10^{-11}	0.0353	496
2.5(129)	1.38×10^{-8}	5.50×10^{-10}	3.33×10^{-11}	0.0398	415
40(2070)	2.21×10^{-7}	8.3×10^{-9}	1.07×10^{-11}	0.0376	207
35(1810)	1.93×10^{-7}	7.3×10^{-9}	1.11×10^{-9}	0.0378	174
30(1550)	1.65×10^{-7}	6.15×10^{-9}	1.09×10^{-9}	0.0372	151
25(1290)	1.38×10^{-7}	5.08×10^{-9}	1.04×10^{-9}	0.0368	132
20(1030)	1.10×10^{-7}	4.02×10^{-9}	1.28×10^{-9}	0.0366	86
15(775)	8.25×10^{-8}	2.92×10^{-9}	9.33×10^{-9}	0.0354	88
10(517)	5.5×10^{-8}	1.92×10^{-9}	6.22×10^{-10}	0.0349	88
5(258)	2.76×10^{-8}	9.8×10^{-10}	4.00×10^{-10}	0.0355	63

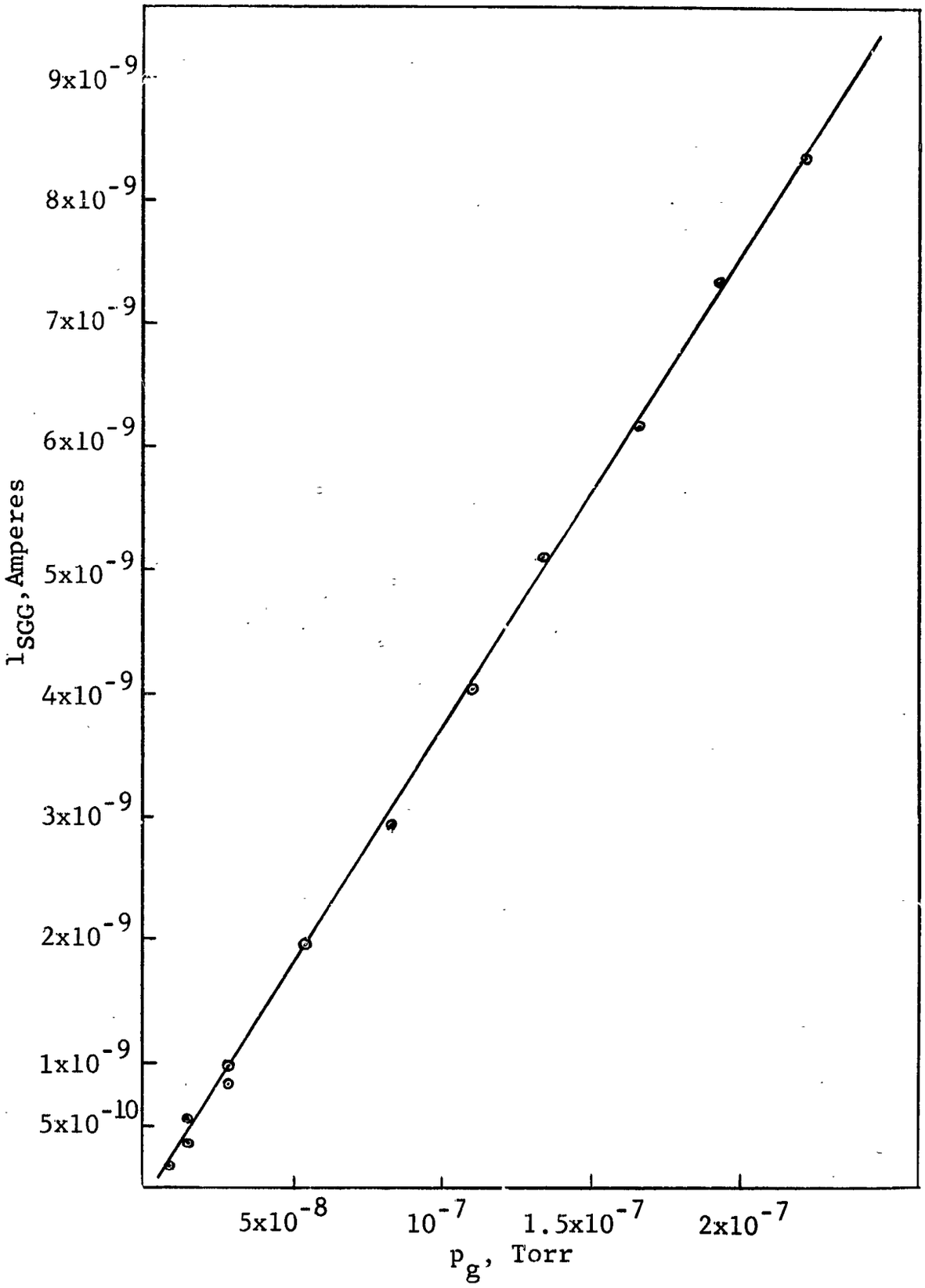

FIGURE 31
CALIBRATION DATA FOR SUPPRESSOR GRID GAUGE

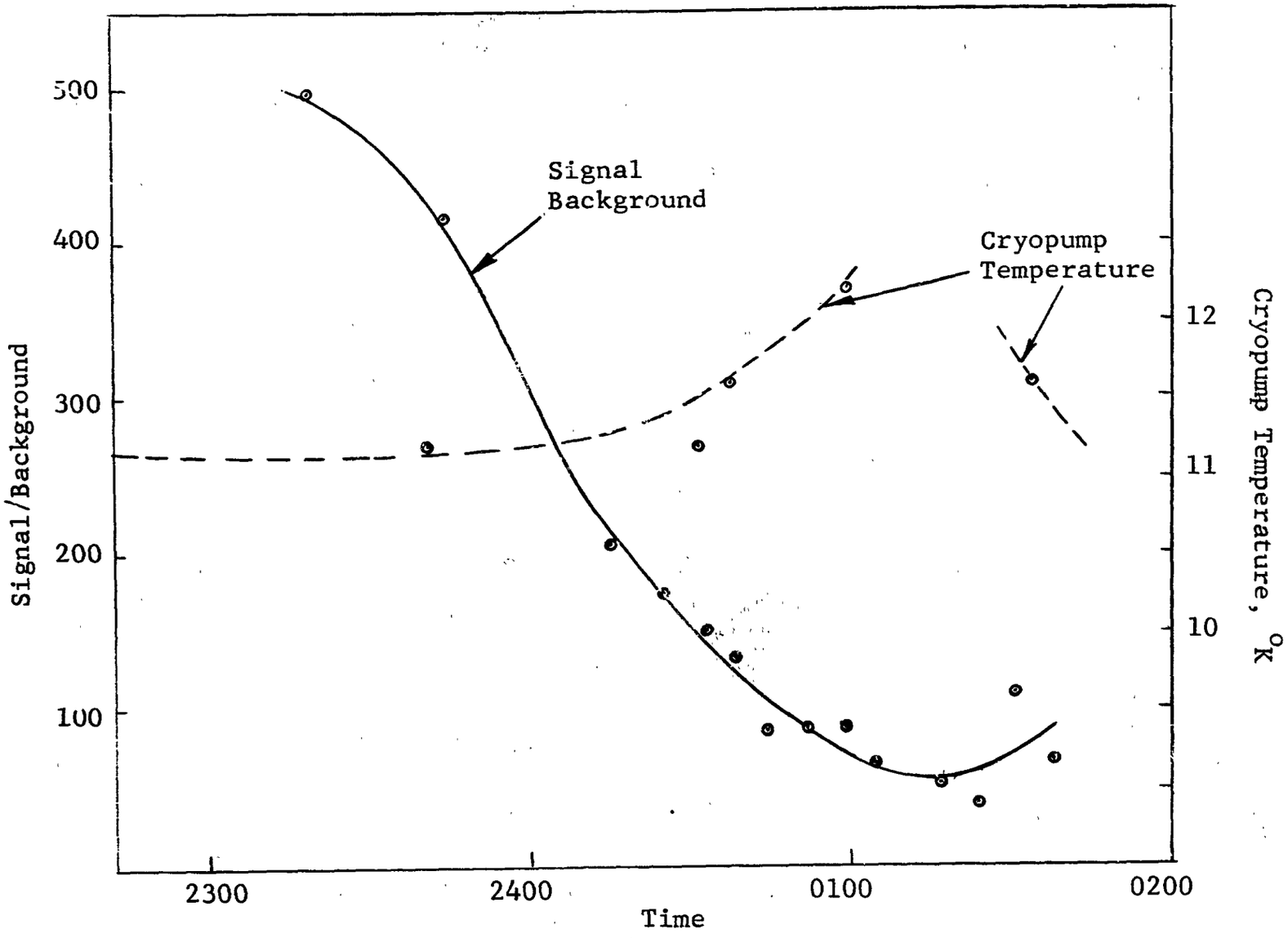

FIGURE 32
SIGNAL-TO-BACKGROUND GAS PRESSURE RATIO AND CRYOPUMP TEMPERATURE DURING CALIBRATION RUN

heat conductivity of solid argon shows that the heat of condensation or radiated heat available is insufficient to significantly increase the surface temperature. Due, however, to a failure in the helium heat transfer system there was a temporary increase in the temperature of the circulating gaseous helium. The measured increase was from approximately 11°K to approximately 12°K. The data of Dawson, et al,[46] indicate that a decrease in capture coefficient of argon from unity occurs in this range of temperatures. In addition, desorption of cryosorbed hydrogen could add a significant gas load. In order to investigate the possible effects of this on the data, the average of the temperatures of the helium gas out of the cryostat and the return gas is also plotted in Figure 32 on the same time scale as for the signal-to-background pressure ratio. It is seen that there is a rough correlation between the decrease in signal-to-background ratio and increase in average gas temperature.

6. DISCUSSION, RESULTS, AND CONCLUSIONS

During the construction and testing of the calibration system prototype apparatus, individual components of the system have been examined in detail. Those areas in which the problems considered have been resolved will be discussed below and the application of these results to calibration system design principles will be presented. Discussion of those areas in which future work is considered necessary will be deferred until Section 7.

6.1 Porous Plug

It was shown in Section 3 that a porous Vycor glass plug may be effectively used as a pressure attenuation element between the gas source chamber and molecular furnace for pressures at least as high as 5200 Torr for argon at 304°K. The lowest pressure in the gas source chamber that may be used is that for which the National Bureau of Standards will presently certify a measuring device, namely 15.5 Torr; therefore, the dynamic range of the calibration system that may be obtained by variation of the gas source chamber pressure is at least 350. The addition of a differential pressure gauge between the

rotating piston gauge and gas source chamber of the calibration system allows that system to be used to determine the porous plug conductance. Thus, the conductance of this very critical element of the calibration system could be measured at any time, providing a continuing on-site calibration of the system.

The apprehension that contamination due to exposure of the plug to atmospheric air may have a large effect on subsequent flow measurements has been found to be groundless. A deliberate attempt to contaminate a porous Vycor plug for more than 1/2 day by flowing humid atmospheric air through it was followed by a measurement that showed the conductance for argon to be within 1.5 times the standard deviation obtained by considering all conductance measurements.

A porous Vycor plug with a conductance smaller than 7×10^{-6} liters/sec was made and by combining the techniques used for fabricating the plugs in this investigation, a porous Vycor plug of less than 2×10^{-8} liters/sec probably could be made. Using well controlled heat treatment techniques it may then be possible to shrink the pore structure and reduce the conductance to a still lower value. This may be desirable for attaining the lowest level of pressure (10^{-15} torr) since it would mean that both the beam attenuation orifice and auxiliary cryopump could be eliminated and all the pressure attenuation could be accomplished with the porous plug and beam aperture conductances.

The two porous plugs used were subjected to a maximum stress level on the order of 1500 psi. Porous Vycor is many times stronger than this[7] even for long time loading, so that the gas source pressure attained is not limited on that basis. In the case of plug no. 2 which was sealed in a compression mounting with indium, a stress level of about 500 psi was reached in the indium which is approximately the tensile strength for pure indium.[50] A step increase was found in the measured conductance. Tightening the plug in the mounting caused the conductance to decrease to its former value. Since a higher strength material is desirable and since the low melting point of indium restricts the temperature attainable in degassing required for proper system preparation, future compression mountings should use a metal such as gold that does not have these undesirable characteristics.

6.2 Beam Orifice

It was found that various metal foils of sufficient quality for use as orifice materials are available in the thickness range down to 2.5×10^{-4} cm. This allows the fabrication of orifices with negligible ($\leq 1/2\%$) Clausing corrections (see Equation (4.1.4)) for diameters as small as 0.05 cm. An orifice as small as 0.10 cm diameter was fabricated in 10^{-3} cm thick OFHC copper foil. The circularity of the orifice was better than 1/2%. Two problem areas were found which require consideration in future work. The first was that during the pumpdown of the system a large enough pressure differential was attained across the orifice material to cause it to yield. Figure 33 shows the yielding of the 10^{-3} cm thick OFHC copper of orifice #2. The diameter of the orifice was found to be increased by 8 percent. The solution to this problem would be to provide a sufficiently large parallel conductance between the molecular furnace and cryopump cavity during pumpdown. The second problem was the relatively high thermal resistance of the thin orifice material leading to a noticeable radial temperature gradient due to heat radiation from the 300°K foil to the 11°K cryopump wall. This gradient is illustrated in Figure 33 where the condensation of diffusion pump oil resulting from a failure in the liquid nitrogen trapping system, may be seen. The pattern of condensation clearly indicates the temperature gradient that must have existed. The result of this was that the assumption of isothermal molecular furnace walls was violated. The most satisfactory solution is to increase the ratio of the area of isothermal walls and baffles to the area of orifice material. Another approach is to consider a knife edged type of orifice but the effect of such non-ideal aperture geometry would have to be carefully investigated in order to define the error introduced.

The results of the experiment to determine the departure from free molecular flow as the mean free path of the gas in the molecular furnace was made comparable with the diameter of the orifice, were presented in Section 4. It is seen from the results plotted in Figure 28 that the ratio of the measured flow to that calculated for free molecular flow is approximately that predicted by theory and the departure is less than one percent for Knudsen numbers greater than about M = 12. It is seen from Equation (2.2.25) that considering only the

FIGURE 33
ORIFICE #2 MOUNTED ON GOLD O-RING SEAL FLANGE

density of the molecular beam or gas enclosure density, not the total throughput, then for the case where the molecular furnace attenuation aperture conductance, C, is zero, the effect of transition flow through the beam orifice conductance, C_a, is at most of second order due to the appearance of $C = \pi d_a^2$ in the numerator and the denomenator. If $C \neq 0$ deviations from molecular flow lead to deviations in p_g which are not compensated as above when $C = 0$. Thus, it is desirable to operate the calibration system with $C = 0$. As will be shown below, in order to attain the lower limit of pressure desired (i.e., 10^{-15} Torr) the constraint that $C = 0$ requires that C_p be decreased by at least two orders of magnitude which may envolve substantial fabrication problems for porous plugs of Vycor glass. However, the minimum C_p required depends on the lower limit of gas source pressure, p_o, for which the National Bureau of Standards will certify a pressure gauge. At present the Pressure and Vacuum Measurements Sections of the National Bureau of Standards are not prepared to calibrate a commercially available absolute instrument below 15.5 Torr, but they expect, in the near future, to be able to certify certain gauges to 0.1 Torr with an accuracy of 1/2 percent.

The above conclusions were based on the assumption that deviations in beam intensity resulting from scattering downstream of the orifice are a weaker function of M than is the deviation in throughput. These deviations in beam intensity result from the formation of a "cloud" downstream of the orifice as discussed in Section 4. Experiments to determine the effect of the "cloud" on beam density were not made.

6.3 Molecular Furnace Equilibrium

In developing the theory of the calibration system and in carrying out the experiments on it, it was implicitly assumed that the gas in the molecular furnace was in thermal equilibrium with the (isothermal) walls. There are several distinct elements to this assumption: the conductance of the molecular furnace must be large compared with the conductance of the apertures; the area of the aperture and non-isothermal orifice material must be small compared with the furnace wall area; the center of mass velocity of the gas through the furnace must be sufficiently small compared to the mean thermal velocity that the gas may be considered in equilibrium with the furnace walls.

The problems associated with the first two elements above were solved by their proper consideration during the design of the molecular furnace. The problem of non-isothermal orifice material as discussed above in reference to Figure 33 must be more carefully considered in future work. The non-equilibrium condition due to finite mass flow rate of the gas is negligible if the gas mean free path greatly exceeds the molecular furnace dimensions, since the temperature of the molecules then becomes that of the wall. As the mean free path becomes smaller, the influence of gas-gas collisions becomes more important than gas wall collisions. In the absence of a quantitative measure of the extent to which the gas becomes non-equilibrium due to gas-gas collisions, an estimate of the effect may be made based on the ratio, R, of the collision probability in the gas phase to the collision probability with the furnace surface. This ratio is given by kinetic theory for a gas of mean free path λ in a spherical cavity of radius r_f as

$$R = \frac{2r_f}{3\lambda} . \qquad (6.3.1)$$

Thus, the probability for collision with another gas molecule is less than that for collision with the cavity wall if λ is about equal to the furnace dimension and becomes negligible with increasing λ. For a cylindrical cavity, R is still smaller. Thus, it is expected that for a gas whose mean free path is at least as large as the furnace dimension, the departure of the distribution from that of a gas in thermal equilibrium with the wall is small. Due to the relative insensitivity of the average velocity to small changes in the distribution, it is concluded that errors introduced into Equation (4.1.1) by molecule-molecule collisions will be negligible as long as $\lambda \geq d_f$ or in terms of the Knudsen number $M_f = \lambda/d_f \geq 1$.

6.4 Time to Establish Calibration System Equilibrium

In the practical application of the calibration system, it is necessary that the time to set up equilibrium in the system be reasonably short. The approach to equilibrium of a volume V filled or evacuated through a conductance C is exponential in time as was shown in Section 3. Equation (3.2.3) shows the time constant to be V/C. In the calibration system, the times to establish equilibrium in the following volumes are of interest:

1. Source chamber
2. Gauge enclosure
3. Molecular furnace

In changing the pressure in the gas source chamber, benefit is obtained from the fact that viscous flow conditions lead to a high effective conductance C. Thus, by providing a sufficiently large bore tube connecting the gas source chamber to its gas supply, the time lag in arriving at equilibrium in the gas source chamber can be made negligible.

Equation (2.2.20) shows that the diameter of the gauge enclosure must be maintained large for gauge pumping effects to be negligible. Even for gauges with pumping speeds as small as 0.1 liters/sec, the enclosure conductance must be at least 20 liters/sec so that the time constant of a 1 liter enclosure would be approximately 0.05 seconds.

The desired value of the conductance, C_a, of the molecular furnace will vary with the pressure range covered. As can be calculated from Equation (2.2.25), the smallest conductance, C_a, required in a calibration system to reach 10^{-15} Torr for an attenuation aperture diameter of 0.5 cm and $C_p = 1.6 \times 10^{-7}$ liters/sec is about 3.8×10^{-3} liters/sec. Thus, the time constant for a 1 liter molecular furnace is about 4.5 minutes. By decreasing C_p and p_o suggested in Section 6.2, C_a may be increased with a consequent decrease in the time delay in establishing equilibrium.

In addition to these time delays associated with the volumes discussed above, there can be a substantial delay associated with the attainment of equilibrium in the porous plug. It may be shown[15] that the time lag, τ_L, in establishing equilibrium for flow proceeding by a diffusion mechanism is directly proportional to the square of the length, L, of the element through which diffusion occurs and inversely proportional to the diffusion constant, D, that is,

$$\tau_L \alpha \frac{L^2}{D}. \qquad (6.4.1)$$

Barrer[15] has shown for 300°K argon diffusion through porous Vycor glass that $\tau_L = 44$ minutes for L = 2.69 cm. Therefore, for a porous Vycor plug as thick as the one used in this

investigation, namely 0.3 cm for porous plug #2, Equation (6.4.1) shows that

$$\tau_{0.3cm} < 30 \text{ seconds.} \qquad (6.4.2)$$

This is a reasonably short time lag and for porous plug #1 used in this investigation the expected time lag would be

$$\tau_{0.11cm} < 5 \text{ seconds.} \qquad (6.4.3)$$

It should be noted that the τ_L Barrer measured probably includes the effect of filling up the blind pores in the plug. During a change of pressure, p_o, from one level to another, the effect of filling these blind pores will be very much less than in the first introduction of gas into evacuated pores and thus the time lags calculated above are upper limits to τ_L.

During the experiments carried out and described in Sections 3, 4, and 5, the approximate time, τ', to attain 70% of the equilibrium system pressure was determined. Some of these times are given below.

Gas source chamber: $\tau' < 2$ seconds.
Porous plug #1: $\tau' < 5.5$ seconds.
Porous plug #2: $\tau' < 14$ seconds.
Porous plug #2, molecular furnace, and 0.1 cm diameter orifice: $\tau' < 45$ seconds.
Porous plug #2, molecular furnace, and 0.33 cm diameter orifice: $\tau' < 12$ seconds.
Response of gauge in enclosure using porous plug #2 and 0.33 cm diameter orifice: $\tau' < 60$ seconds.

6.5 Gas Properties

The performance of the calibration system depends on various properties of the gas to be used. Some of these properties will be considered here with respect to the behavior of the gas in the various parts of the calibration system.

6.5.1 Pressure-Volume-Temperature Relation for Gas

The virial equation of state may be written

$$PV = RT(1 + B_p p + C_p p^2 + - - - -) \qquad (6.5.1)$$

where B_p, C_p, etc. are the second, third, etc. virial coefficients. As may be seen by comparison of Equation (6.5.1) with Equation (2.0.10), a perfect gas has been assumed in deriving the calibration equation, that is:

$$B_p = C_p = . . . = 0.$$

For argon at room temperature the error introduced by this assumption is less than 1/2 percent for p_o = 5200 Torr. However, if the temperature is decreased to 200°K, the second virial coefficient for argon is[51]

$$B_p = - 0.002941. \qquad (6.5.2)$$

and at p_o = 5200 Torr, the error in Equation (2.0.10) is 2%. Virial coefficients for the various gases are tabulated in reference 51 and may be used to correct Equation (2.0.10). Referring to these tabulated values it is seen that the correction is only important for the gas source pressure, p_o, and may be neglected for the gauge enclosure pressure, p_g, since the correction is negligible for pressures as low as 10^{-5} Torr.

6.5.2 Adsorption and Desorption of Gas

Under some conditions of temperature and pressure, the amount of gas adsorbed on the walls of a chamber may be a substantial amount of the gas present. The calibration system can be adversely affected by such a situation since small temperature fluctuations could, as a result, provide a significant, uncontrolled, variable source or sink for gas. To investigate this situation the ratio, R, of the quantity of gas adsorbed on a surface of area, A cm^2, with relative coverage, θ, to that present in the volume V cm^3 at pressure P is considered. Since a monolayer of an elemental gas contains[52] approximately 8×10^{14} molecules per cm^2, the above ratio is therefore

$$R = \frac{8.4 \times 10^{-5} A\theta T}{PV} \qquad (6.5.3)$$

For a spherical volume of radius 10 cm maintained at 300°K, this ratio is less than 1/2% for pressures greater than 1.5 Torr, even for a complete monolayer. Thus, for the case of the gas source which is at a pressure at least an order of magnitude greater than this, the effects of such sources or sinks may be neglected. Taking into account the relative coverage θ as will be described below, it can be calculated that the quantity of gas adsorbed at the high pressures (5200 Torr) is small compared to that in the gas phase at low pressures (15 Torr) so that desorption-time effects in the gas source may be neglected. Of course, the gas source pressure, p_o, is always measured so that any desorption would be of little consequence in any case.

In the case of the porous plug and molecular furnace, the pressure decreases to less than 1.5 Torr, and these situations must be considered more carefully. The relative coverage of the wall θ, defined as the ratio of number of molecules adsorbed per cm^2 to the number in a complete monolayer, is not necessarily unity as assumed above. Hobson[53] has shown that θ is well represented for a gas at temperature T and pressure p by the Dubinin-Radushkevich equation,

$$\ln \theta = - BR^2T^2 \left[\ln \frac{p}{p_o}\right]^2, \qquad (6.5.4)$$

where B is a constant for the gas considered and p_o is the vapor pressure that would exist above the liquified gas at temperature T, given by the Clausius-Clapeyron equation,

$$p_o = d\, e^{-\frac{E_d}{RT}}, \qquad (6.5.5)$$

where d and E_d are constants for the gas.

Using the value of the constants found by Hobson, the solution of the relative coverage was calculated for the

highest pressure expected in the molecular f rnace, namely, $p = 3 \times 10^{-3}$ Torr, and log θ vs T is plotted in Figure 34. From Equation (6.5.3) it is seen that for R to be less than 1/2 percent, the following inequality must therefore hold for the 10 cm sphere:

$$\frac{\theta T}{p} \leq 198. \qquad (6.5.6)$$

Substituting for θ obtained from Equation (6.5.4), this becomes

$$\frac{T}{p} e^{-BR^2T^2\left[\ln \frac{p}{p_o(T)}\right]^2} \leq 198. \qquad (6.5.7)$$

The solution to this transcendental inequality may be obtained by graphical methods. From Figure 34 and using inequality (6.5.6) it is found that for $p = 3 \times 10^{-3}$ Torr, the inequality requires

$$T \gtrsim 103^{\circ}K. \qquad (6.5.8)$$

Investigation of inequality (6.5.7) for lower pressures shows the minimum allowed surface temperature T is yet smaller. The fact that low temperatures are allowed for the gauge enclosure is significant in attaining the lower limit of pressure in the calibration system. The outgassing rate due to the combination of permeation, diffusion and desorption of gas is an exponential function of temperature. For well outgassed stainless steel, the outgassing rate, Q', at 300°K is of the order of 10^{-13} Torr liters/sec cm^2. Thus, for a stainless steel gauge enclosure of area $A = 1000$ cm^2 which has a 200 liter/sec conductance, C, to the cryopumped cavity, the equilibrium pressure attained due to the outgassing of the enclosure is

$$p = \frac{Q'A}{S} = 5 \times 10^{-13} \text{ Torr.} \qquad (6.5.9)$$

To reach 10^{-15} Torr calibration pressure, the background pressure must be at least 200 times lower, so a pressure of 5×10^{-18} Torr must be reached in the gauge enclosure. It is thus required that either a material with a lower outgassing

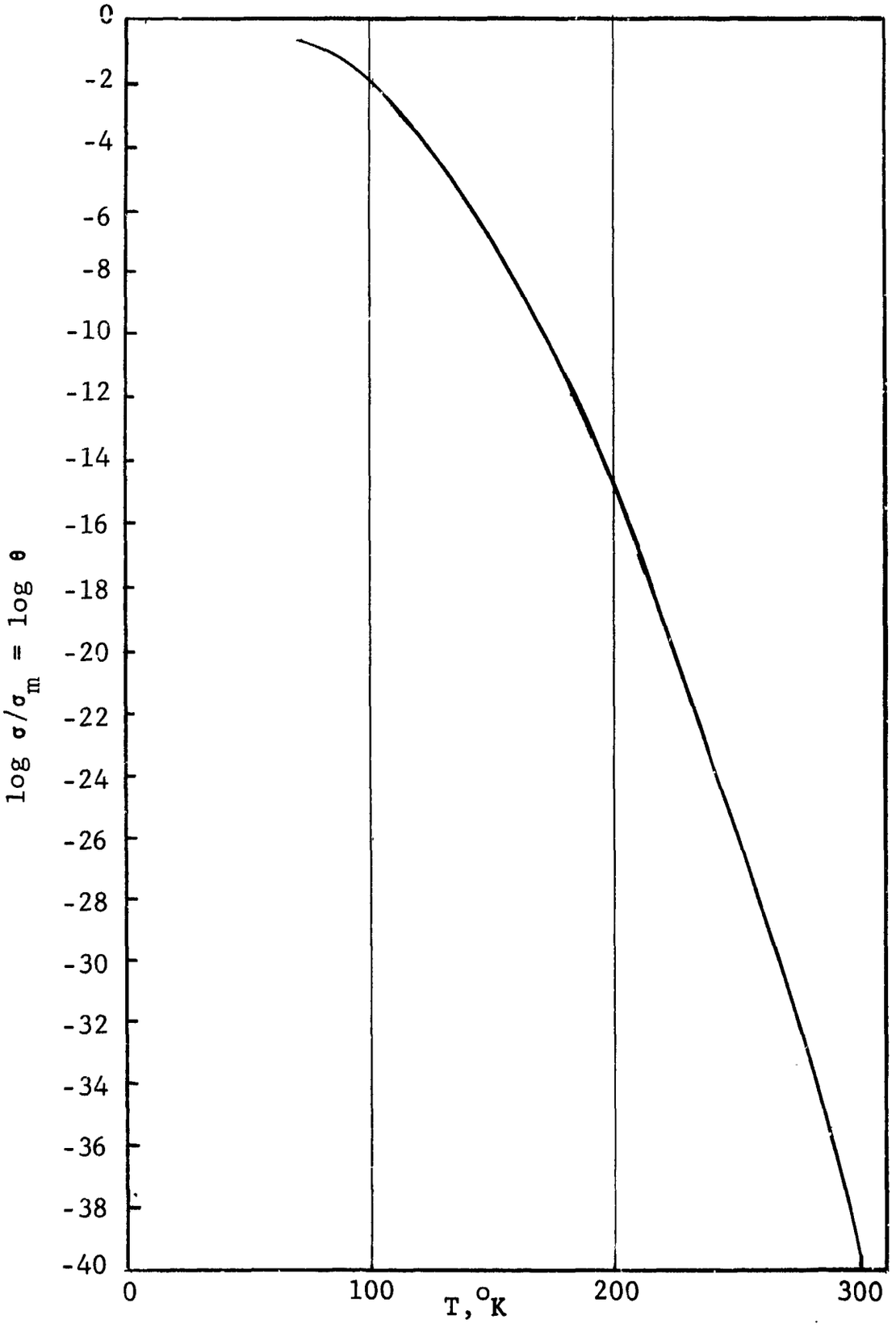

FIGURE 34
ARGON RELATIVE COVERAGE VERSUS TEMPERATURE
FOR A 10 CM RADIUS SPHERICAL CAVITY.

rate be used or that the outgassing rate of the stainless steel be lowered by decreasing the temperature. Reducing the temperature to 150°K reduces the total outgassing rate by three to four orders of magnitude.

If the pressure in the gauge enclosure were lowered and there were any time lag in arrival at equilibrium, the amount of gas adsorbed at the initial pressure may be significant compared with the equilibrium amount at the final pressure. In order to minimize this problem during operation of the calibration system, the pressure should initially be low, and the calibration conducted in the direction of increasing pressure. This may not always be the situation so that the time to reach equilibrium must be estimated. Due to the similarity of this problem to other adsorption processes, it is expected that if the desorption is retarded below the value expected on the basis of kinetic theory, it is probably due to an activation energy that must be provided. The rate of desorption of adsorbed gas from a surface at temperature T into a volume maintained at a pressure far below that corresponding to an equilibrium coverage N_o is given by first order theory [54]

$$\frac{dN}{dt} = -\frac{N}{\tau} e^{-E_d/kT}, \qquad (6.5.10)$$

where N is the number of molecules adsorbed, E_d is the activation energy for desorption, and τ is the effective period of oscillation of the adsorbed molecule in the potential field of the surface.

Solution of Equation (6.5.10) for N yields

$$N = N_o e^{-\frac{t}{\tau} e^{-\frac{E_d}{RT}}}, \qquad (6.5.11)$$

where N_o is the number of molecules adsorbed at time $t = 0$. Equation (6.5.11) obviously represents a decay of the number of molecules adsorbed with a time constant given by

$$\tau_1 = \tau e^{E_d/RT_1}. \qquad (6.5.12)$$

Now, the results of Section 6.4 show that after decreasing the pressure in the furnace at 304°K, equilibrium is set up in less than 1 minute. Thus, ζ_1 in Equation (6.5.12) will be taken to be 1/2 minute. Now consider the approach to equilibrium for temperature T_2. In a similar manner to Equation (6.5.12) the time constant in the pressure decay is given by

$$\zeta_2 = \tau e^{E_d/RT_2}. \qquad (6.5.13)$$

Therefore, from Equations (6.5.12) and (6.5.13) it is seen that

$$\zeta_2 = \zeta_1 e^{E_d/R(\frac{1}{T_2} - \frac{1}{T_1})}. \qquad (6.5.14)$$

Now, for argon, the heat of desorption is[53] 1558 calories/mole so that for $T_2 = 100°K$, Equation (6.5.14) yields a time constant,

$$\zeta_2 = 95.3 \text{ minutes}. \qquad (6.5.15)$$

This provides an upper limit to the time lag that could occur in the attainment of equilibrium when the pressure is suddenly decreased in the molecular furnace or gauge enclosure at 100°K. It is unlikely that such a delay would occur due to the relatively low activation energy for desorption.

Investigation of Equations (6.5.3) and (6.5.4) shows that the ratio, R, of gas adsorbed on the surface to that in the volume is negligible for most of the range of pressure over which the porous plug is operated. The result, observed in this and in other investigations and discussed in Section 3, that kinetic theory does not account for the observed porous plug conductance with respect to molecular mass is therefore surprising (see Equation (3.1.3)). If the ratio, R, for argon were significant, an increased conductance for argon over helium could be accounted for since the ratio of the relative coverages, θ, for argon and helium at, say, 15 Torr and 304°K from Equation (6.5.4) is $\sim 10^{23}$. The value of the argon to helium conductance ratio measured in this investigation is 0.344 which is 8% larger than that predicted by kinetic theory (see Equation (3.1.4)). The opposite trend

noted by Barrer and Barrie (see Equation (3.1.3)) can not be accounted for on the basis of surface flow but such observations could be accounted for by atomic size effects.

6.5.3 Background Gas Pressure

As was shown in Section 6.5.2, the background gas density must be kept as low as 5×10^{-18} Torr. This pressure level requires the use of cryosorption or cryopumping. The data on vapor pressure of gases shows that for helium the wall temperature must be $\sim 0.215^{\circ}K$, for hydrogen $0.48^{\circ}K$ and for neon not less than $3^{\circ}K$. Since these temperatures are economically impractical in large systems, these gases must be excluded from the system. For all other gases $10^{\circ}K$ is sufficiently low for the vapor pressure to be less than 5×10^{-18} Torr. Another requirement for low background pressure is that the capture coefficient, α, for the gas be sufficiently close to unity. In the case of several gases, α has been shown[46] to increase to unity for $T < 10^{\circ}K$. As discussed in Section 5, the measured signal-to-background ratio was at least 40 at about $12^{\circ}K$ implying a large value of α. The measurement of α should be performed for a $4.2^{\circ}K$ surface where α would be expected to rise above the desired value of 0.995. Previous experience[45] has shown that $8^{\circ}K$ is a sufficiently low temperature to attain at least this large a capture coefficient.

A calculation was made of the time required for the gas effusing from the furnace to form a uniform condensate of significant thickness (2.5×10^{-3} cm). For the condition of the largest throughput expected in practice, this time is 1000 hours so that the buildup is insignificant during a calibration experiment. Furthermore, a calculation of the temperature gradient across the condensate due to the heat radiated from contemplated gauges or the gauge enclosure is found to be completely negligible. On the other hand, due to the low heat of vaporization of liquid helium, the boil-off rate of liquid helium resulting from the radiative heat load would be at least several liters per hour.

The technique of beam chopping and synchronous detection may be used to solve the problem of background gas interference. This scheme may be unfeasible at the lowest pressure due to the relatively long time constant of measuring devices for extremely small currents.

6.6 Application of Results to Design Principles

Design of a calibration system to cover the desired pressure range was carried out based on the results of the present investigation. The maximum pressure, $p_{g_{max}}$, attained in a gauge enclosure at 304°K was calculated for argon. It was assumed that the diameter of the molecular furnace is maintained at least 25 times the beam aperture diameter so that the conductance of the furnace is less than 1/2 percent of C_a and, in addition, the mean free path of the gas in the furnace was not allowed to be smaller than the diameter of the furnace so that non-equilibrium effects are negligible. These two assumptions result in the condition that $M_a \geq 25$ which was seen in Section 4 to be sufficient to assure that the deviation from free molecular flow is less than 1/2 percent. As d_a was decreased, the above assumptions led to an impractically small furnace as can be seen from the results presented below.

It was assumed that: $p_{o_{max}} = 5200$ Torr; $r_g = 3.1$ cm, so that a Redhead magnetron gauge may be calibrated; and $\ell_{min} = 9$ cm was taken as a practical minimum, deferring a calculation of the error introduced for small ℓ until later. The results of the calculation of $p_{g_{max}}$ are shown in Figure 35. Also shown are the results of calculations in which the constraint that the mean free path, λ, of the gas remain larger than the furnace diameter, d_f, was relaxed. The conditions assumed were $\lambda \geq d_f/2$ corresponding to $M_a \geq 12.5$ and which would lead to at least 1 percent deviation from free molecular flow and also $\lambda \geq d_f/5$ which would lead to more than 2.5% deviation. Table 4 gives the maximum allowable molecular furnace pressure, p, and porous plug conductance, C_p, for a given da and for $M_a = 25$, 12.5, and 5.

It may be seen from Figure 35 that if da = 0.5 cm, then a maximum pressure of 3.1×10^{-7} Torr can be reached in the gauge enclosure. The porous plug conductance is 1.6×10^{-7} liters/sec and the pressure in the molecular furnace reaches 4.4×10^{-4} Torr. To reach a pressure of 10^{-6} Torr with the same aperture results in non-equilibrium conditions in the furnace and transition flow through the orifice with $M_a = 6$ and $\lambda/d_f = 1/6$. This would require the introduction of a porous plug of $C_p = 8 \times 10^{-7}$ liters/sec and the furnace pressure would reach 2.2×10^{-3} Torr.

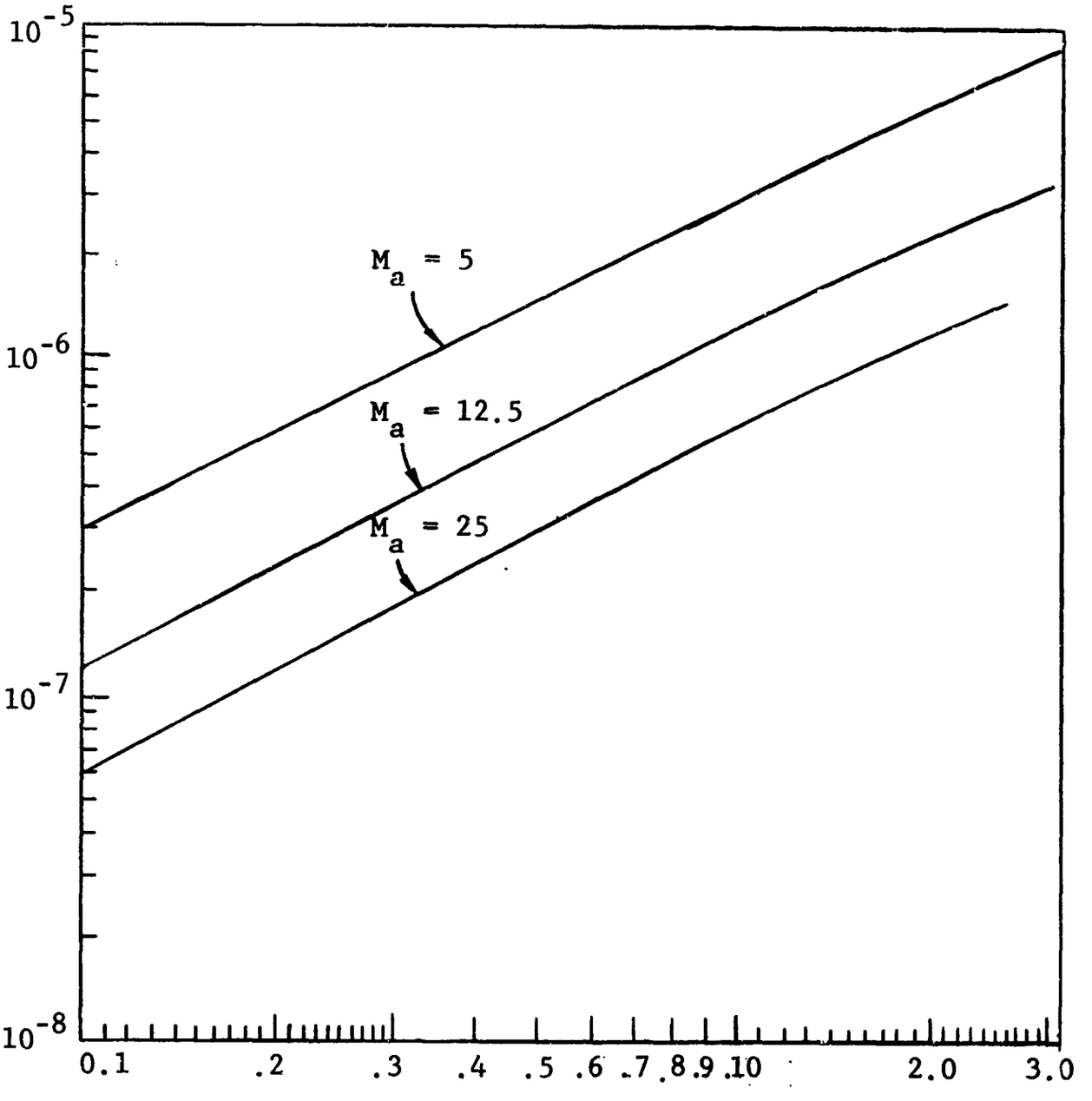

FIGURE 35

MAXIMUM GAUGE ENCLOSURE PRESSURE VERSUS BEAM APERTURE DIAMETER FOR VARIOUS CONSTRAINING CONDITIONS

TABLE 4

MAXIMUM FURNACE PRESSURE AND POROUS PLUG CONDUCTANCE FOR VARIOUS ALLOWED KNUDSEN NUMBERS

Beam Aperture Diameter d_a cm	Furnace Diameter cm	$M_a = 25$		$M_a = 12.5$		$M_a = 5$	
		C_p liters/s	p_{max}, Torr	C_p liters/s	p_{max}, Torr	p_{max}, Torr	C_p liters/s
0.1	2.5	3.2×10^{-8}	2.2×10^{-3}	6.5×10^{-8}	4.3×10^{-3}	1.1×10^{-2}	1.6×10^{-7}
0.25	6.3	8×10^{-8}	8.8×10^{-4}	1.6×10^{-7}	1.7×10^{-3}	4.4×10^{-3}	4×10^{-7}
0.5	12.5	1.6×10^{-7}	4.4×10^{-4}	3.3×10^{-7}	8.6×10^{-4}	2.2×10^{-3}	8×10^{-7}
0.75	18.8	2.4×10^{-7}	2.9×10^{-4}	4.8×10^{-7}	6.5×10^{-4}	1.6×10^{-3}	1.2×10^{-6}
1.00	25	3.2×10^{-7}	2.2×10^{-4}	6.5×10^{-7}	4.3×10^{-4}	1.1×10^{-3}	1.6×10^{-6}

Now, with the former C_p and by placing the gauge at ℓ = 200 cm and removing the enclosure, the beam pressure for $p_{o_{min}}$ = 15.5 Torr is

$$p_{g_{min}} = 4.24 \times 10^{-13} \text{ Torr.} \qquad (6.5.16)$$

There are several ways that the gauge enclosure pressure may be lowered to 10^{-15} Torr, including any one or a combination of the following:

1. provide another porous plug of lower C_p,
2. use a lower gas source pressure, $p_{o_{min}}$,
3. open another aperture of diameter, d, facing an auxiliary cryopump and simultaneously decrease da.

As will be shown in Section 6.7, the use of low C_p may lead to large errors in calibration. In addition, the fabrication of plugs with sufficiently small C_p may lead to significant practical problems. Alternative 2, above, is most attractive and is a distinct possibility in the near future when the National Bureau of Standards completes its plans to certify Bourdon gauges with better than 1/2 percent accuracy to 10^{-1} Torr. With respect to alternative 3, the smaller aperture would be quite fragile and would lead to time delays as shown in Section 6.4. In addition, the required auxiliary cryopump would complicate system construction.

To investigate the assumption ℓ_{min} = 9 cm in the above calculations, consider the error introduced due to increased furnace pressure resulting from gas emitted from the gauge enclosure. The expression for the fractional increase of molecular furnace pressure can be obtained by continuing the reasoning of Section 4, and is given by

$$\frac{\Delta p}{p} = \frac{(r_a^2 + r_g^2 + \ell^2)^2}{4 r_a^2 r_g^2} \left\{ 1 - \left[1 - \frac{4 r_a^2 r_g^2}{(r_a^2 + r_g^2 + \ell^2)^2} \right]^{1/2} \right\}^2 . \qquad (6.5.17)$$

Figure 36 shows $\Delta p/p$ of Equation (6.5.17) plotted versus ℓ for $r_a = 0.5$ cm and $r_g = 3$ cm. The calculation leading to Equation (6.5.17) neglects the re-emission of molecules which impinge on the warm orifice material and thus the results estimated for this situation are also plotted on Figure 36. In estimating this contribution, an expression similar to Equation (6.5.17) was used and the enclosure was taken to be a cylinder of radius $3r_g$ and length $6r_g$. It may be seen that with either assumed situation the error resulting from the re-emission is much less than 1/2 percent for the minimum value of ℓ of 9 cm assumed earlier.

6.7 Probable Error in Gauge Pressure

The complete error analysis was carried out in Section 2.3 for the case of a gauge in an enclosure. Evaluation of the relative probable error in gauge enclosure pressure, r_{p_g}, was made on the basis that the relative probable error in lengths is 0.5%, in pressure measurement is 0.03%, in time is 0.1%, and in temperature is 0.5%, except for in the measurement of gas source volume where it is 0.1%. It is found that the accumulated probable error given by Equation (2.3.16) for a porous plug of 10^{-6} liters/sec conductance is less than 2%. For C_p larger than 10^{-5} liters/sec, the relative probable error increases due to the flow through the plug during the volume measurement as discussed in Section 3.3, and for smaller C_p and a gas source volume of 1 liter, the relative probable error increases due to the small pressure decay that occurs during any reasonable period of time. The error is estimated at 5.7% for a porous plug of $C_p = 10^{-7}$ liters/sec for a gas source volume of 1 liter. The error tends to go approximately as $V/\tau C_p$ where τ is the length of time over which the measurement of C_p is made. It is thus seen that the use of porous plugs of $C_p < 10^{-7}$ requires the use of a smaller gas source volume if the porous plug calibration is to be completed in a reasonable time with the desired accuracy.

In the case of the nude gauge, there is an additional source of error associated with the non-uniform gas density over the length L of the ionizing region due to the $1/\ell^2$ variation of beam density. This was discussed in Section 2.1 where it was indicated the error could be as large as 2 percent for a distance of $\ell = 200$ cm and a gauge with L = 4 cm. That estimate derived in Section 2.1 represents an upper limit

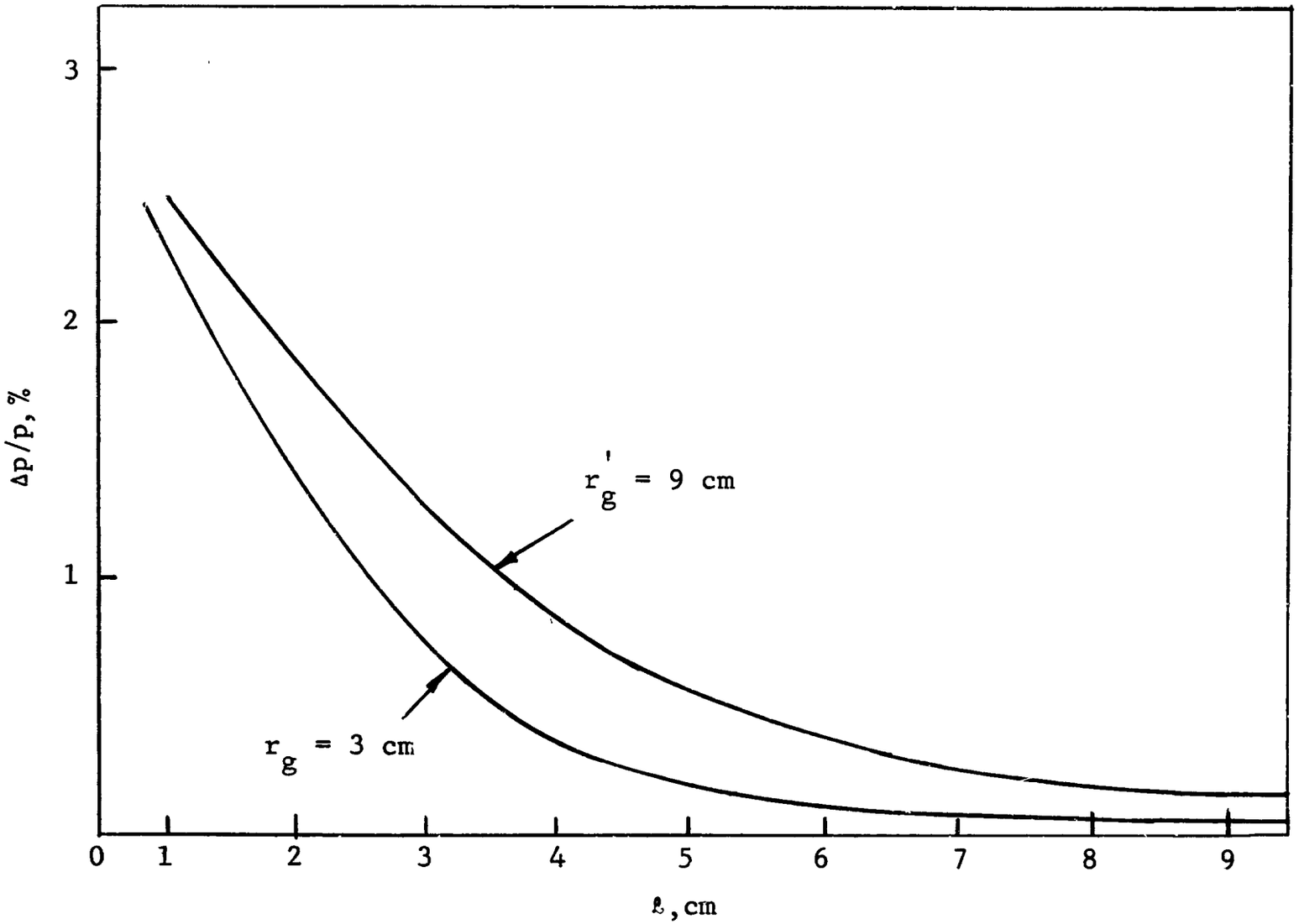

FIGURE 36

PERCENTAGE INCREASE OF FURNACE GAS DENSITY DUE TO EMERGENT FLUX FROM ENCLOSURE VERSUS ℓ

to the error in p_g, referred to the midpoint ℓ_m of the gauge due to the integrating effect of the gauge with respect to pairs of points equidistant from ℓ_m along a ray from the molecular beam aperture. The additional error due to the $1/\ell^2$ variation is thus expected to be much less than 2% for ℓ = 200 cm.

7. RECOMMENDATION FOR FUTURE WORK

From the results obtained in the work that has been completed and from the more complete understanding of the potential of this calibration method resulting from experience with the system, there has developed a clear need for additional research work. The recommendations for future research work are discussed separately below.

First, in the interest of achieving maximum operational efficiency and a wide calibration range, it is necessary to let the beam-forming furnace aperture approach as near as practicable to the upper bound of the free molecular flow regime. This upper boundary may be defined as that pressure at which the conductance of the aperture deviates by a prescribed amount from the free molecular flow conductance. Experiments were performed to determine the conductance properties of an aperture in the range of small Knudsen numbers. In these experiments it was found necessary to extrapolate the calibration of the gauge used to measure the pressure differential across the aperture beyond the range over which it was calibrated. Also, during these experiments some accidental yielding of the aperture occurred. However, from the results of this experimental work and some recent theoretical work, it now appears that fair agreement between experimental results and theoretical prediction of conductance deviation from molecular flow conductance for small Knudsen numbers may be possible. Therefore, an experiment should be performed in which the aperture conductance is measured as a function of Knudsen number over the range 1 to 25 and the deviation of the actual conductance from free molecular flow conductance determined as a function of Knudsen number. In order to maintain the aperture differential pressure gauge within its calibrated range, it is probable that three apertures will be required. Conductance around the aperture should be provided to prevent

yielding during pumpdown. The conductance deviation as a function of Knudsen number should be calculated from theory. The experimental deviation data should be correlated with deviation theory and the upper pressure limit for which the measured deviation departs from the theoretically predicted deviation by less than a prescribed amount established. If theory is not sufficiently precise at small Knudsen numbers, the experimental data alone may be used to establish the conductance deviation down to the minimum Knudsen number for which there is high confidence in the accuracy of the data. It is estimated that this will lower the limiting Knudsen number by about a factor of 8.

The second problem recommended for future research, which is closely related to the first, concerns the angular distribution of atoms effusing from an aperture operating at small Knudsen numbers. The deviation of the aperture conductance from its molecular flow value, to be determined in the above experiment, is actually a measurement of the deviation in the total flux effusing from the aperture as compared to free molecular flow. In atomic beam applications, it is necessary to know also the angular distribution of the effusing flux. Free molecular effusion through an aperture has a cosine angular distribution; however, it is expected theoretically that the distribution shifts toward the forward direction as small Knudsen numbers are approached. This has the effect of increasing the flux density near the beam axis at small Knudsen numbers. If full advantage is to be taken of driving the beam aperture into the range of low Knudsen numbers, an experiment must be performed to determine the deviation between the actual angular distribution of the flux effusing out of the beam aperture, and the free molecular flow distribution (cosine) as a function of Knudsen number (for small Knudsen numbers). If the angular distribution is a strong function of Knudsen number in a range which is acceptable with respect to all other considerations, this would impose a new constraint on the system in that a limit would be set on the minimum distance between the beam aperture and gauge enclosure aperture; however, if the deviation in angular distribution becomes substantial only at Knudsen numbers that are below limits imposed by other considerations, no new constraint is introduced.

The third problem that requires further investigation involves the signal-to-noise ratio (beam pressure to background

pressure ratio). It has already been determined experimentally that large signal-to-noise ratios are attainable. However, there exists some possibility that substantial density variations could occur in the background gas density in the cavity and thus introduce a spurious dependence of gauge enclosure density on the distance between the beam aperture and gauge enclosure aperture. It is therefore necessary to conduct further experiments in which a detailed density survey of the cryopumped cavity is made at various beam densities or to conduct a chopped-beam experiment at various beam densities in which the signal-to-noise ratio would be measured directly.

The fourth problem that requires further research is somewhat related to the above experiment in the sense that it is concerned with the ultimate background density attainable both in the cryopumped cavity and in the gauge enclosure. Cryopumping experiments have been conducted, under somewhat different conditions, in which the background density attained was below the limit of detectability of any gauge available ($\sim 10^{-13}$ Torr). Total surface gas desorption measurements have been made after applying ultra high vacuum processing techniques, from the results of which it is calculated that the background pressure inside the gauge enclosure due to outgassing and desorption of the enclosure should be no greater than $\sim 10^{-13}$ Torr. Using extremely rigorous processing techniques it is confidently expected that substantially lower background pressures are attainable inside the gauge enclosure. However, it is essential in establishing the accuracy and dynamic range of this method of calibration that the ultimate background pressure attainable be submitted to direct experimental determination in an actual system.

The fifth recommended investigation may be considered an overall proof of performance of the calibration system. After having completed the above experiments, sufficient data will be available to specify all known constraints and to apply accurate corrections for all known deviations from kinetic theory. An experiment should then be performed in which the beam density is varied over its complete allowed range and the beam aperture-to-detector distance is varied over its complete allowed range. The calibration system measured performance should then be correlated with predicted performance. The absence of substantial deviations between these two sets of data may be taken as proof that system performance is known and predictable within the prescribed accuracy.

Sixth, it is very desirable for calibration purposes that the conductance properties of porous Vycor be known for several gases over the range of temperature that may be useful in the laboratory. An experiment should therefore be performed on a porous Vycor diffuser in which its conductance is determined for several additional gases and in which the temperature of the gas source and porous plug is varied over a temperature interval which is a substantial fraction of normal temperature for at least one gas. It is also desirable to evaluate the problems encountered in fabrication and calibration of small conductance (10^{-8} to 10^{-7} liters/sec) porous plugs.

The final recommendation for future work is to synthesize the theory, experimental data, and experience developed in this program and apply it to the design and specification of a complete calibration system.

APPENDIX 1

MEAN MOLECULAR VELOCITY IN MOLECULAR BEAM

Maxwell's distribution law for an equilibrium gas gives the fraction of molecules with thermal velocity in the range dv to be

$$f(v)dv = 4\pi A v^2 e^{-\beta^2 v^2} dv \qquad (A1.1)$$

where

$$A = \left(\frac{m}{2\pi kT}\right)^{3/2}, \qquad (A1.2)$$

and

$$\beta^2 = \frac{m}{2kT} . \qquad (A1.3)$$

Calculation of the mean molecular velocity yields the well-known result:

$$\bar{v} = \frac{\int v f(v)dv}{\int f(v)dv} = \frac{\int 4\pi A v^3 e^{-\beta^2 v^2} dv}{\int 4\pi A v^2 e^{-\beta^2 v^2} dv} = \left(\frac{8kT}{\pi m}\right)^{1/2} . \qquad (A1.4)$$

Now consider an area S in this gas of volume V. The $N = nV$ molecules move equally in all directions, so a fraction $d\omega/4\pi$ moves into the solid angle $d\omega$ whose axis is inclined at θ to the normal to S.

The molecules that are included in a cylinder with base S and slant height vdt will cross S in dt; therefore, the number of molecules crossing S per unit area per unit time with velocities in dv passing into $d\omega$ at θ to the normal is

$$F(v,\theta)dvd\omega = n \frac{(Svdt \cos\theta)}{Sdt} \frac{d\omega}{4\pi} f(v)dv. \qquad (A1.5)$$

Using polar coordinates, the elementary solid angle, $d\omega$, may be expressed as

$$d\omega = \sin\theta \, d\theta \, d\phi. \qquad (A1.6)$$

Substituting Equations (A1.1) and (A1.6) into (A1.5) gives, finally,

$$F'(v,\theta)dvd\theta d\phi = nAv^3 e^{-\beta^2 v^2}\, dv \sin\theta \cos\theta\, d\theta\, d\phi. \qquad (A1.7)$$

Since v^3 appears in this expression, rather than v^2 as in Equation (A1.1), it is seen that concerning the gas molecules which pass through a plane from one side in a given time, the faster molecules pass through more frequently. This result is not surprising since the faster molecules traverse more of the volume in a given time and thus have a greater chance of being observed at plane S.

The mean molecular beam velocity, $\bar{v}_{beam}$, may now be calculated for those molecules passing through the area S into the half space beyond:

$$\bar{v}_{beam} = \frac{\int vF'(v,\theta)dvd\theta d\phi}{\int F'(v,\theta)dvd\theta d\phi}$$

$$= \frac{\int_0^{2\pi}\int_0^{\pi/2}\int_0^{\infty} nAv^4 e^{-\beta^2 v^2}\, dv \sin\theta \cos\theta\, d\theta\, d\phi}{\int_0^{2\pi}\int_0^{\pi/2}\int_0^{\infty} nAv^3 e^{-\beta^2 v^2}\, dv \sin\theta \cos\theta\, d\theta\, d\phi}$$

$$= \frac{3\pi^{\frac{1}{2}}}{4\beta}. \qquad (A1.8)$$

Now substituting for β from Equation (A1.3) and $\bar{v}$ from Equation (A1.4) gives

$$\bar{v}_{beam} = \frac{3\pi}{8}\,\bar{v}, \qquad (A1.9)$$

so that the mean molecular velocity of the beam molecules is about 18% higher than those in the volume from which the beam effuses.

APPENDIX 2

ANALYSIS OF ORIFICE CONDUCTANCE EXPERIMENT

In order to determine the $M = \lambda/d$ below which deviations from molecular flow are not negligible, the conductance of an orifice was measured for a range of small M's. A differential gauge was connected across an orifice and first calibrated (unprimed symbols) for large M such that deviations are negligible. A second orifice was then installed and the pressure varied over the calibrated range. In this second experiment (primed symbols), M may be varied over any chosen range by changing the source pressure and orifice size, as will be shown below. By maintaining $S >> C$, p_p is maintained negligible compared with p. The experimental setup is pictured in Figure 23 and shown schematically in Figure 22. A simplified schematic of the experiment is given in Figure 37.

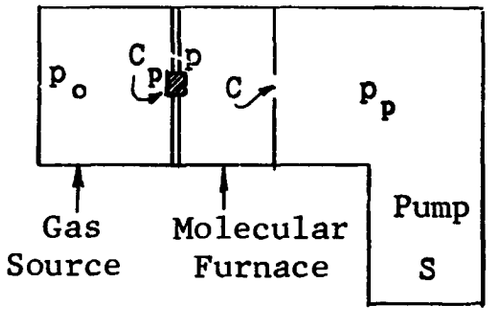

FIGURE 37

The following symbols are defined:

- λ = furnace mean free path
- p = furnace pressure (Torr)
- d = orifice diameter
- C = orifice conductance
- η = conductance of 1 cm diameter ideal aperture
- γ = mean free path at 1 Torr
- p_o = source pressure (Torr)
- C_p = porous plug conductance
- S = pumping speed of system.

The following relations are obvious:

$$Cp = C_p p_o \quad \text{(in the steady state)} \tag{A2.1}$$

$$M = \frac{\lambda}{d} = \frac{\gamma}{dp} \tag{A2.2}$$

$$C = \eta d^2 \tag{A2.3}$$

p' was restricted such that

$$\left.\begin{aligned} p'_{min} &= p_{min} \quad (a) \\ \text{and} \\ p'_{max} &= p_{max}. \quad (b) \end{aligned}\right\} \tag{A2.4}$$

Thus, from Equations (A2.1), (A2.2), and (A2.3)

$$p_o = \frac{Cp}{C_p} = \frac{\eta d^2 p}{C_p} = \frac{\eta \gamma^2}{M^2 C_p p}. \tag{A2.5}$$

Since $p_{o_{Min}}$ corresponds to p_{Min} and M_{Max}, from Equations (A2.4) and (A2.5)

$$\frac{p'_{o_{min}}}{p_{o_{min}}} = \frac{M^2_{max}}{M'^2_{max}}. \tag{A2.6}$$

Also, from Equations (A2.1) and (A2.2)

$$p_o = \frac{Cp}{C_p} = \frac{C\gamma}{MdC_p}, \tag{A2.7}$$

so that

$$\frac{p'_{o_{max}}}{p'_{o_{min}}} = \frac{M'_{max}}{M'_{min}}. \tag{A2.8}$$

Thus, combining Equations (A2.6) and (A2.8), we have

$$\frac{p_{o_{max}}'}{p_{o_{min}}} = \frac{M_{max}^2}{M_{min}' M_{max}'} . \qquad (A2.9)$$

Now, dividing Equation (A2.4b) by Equation (A2.4a) gives

$$\frac{p_{max}'}{p_{min}'} = \frac{p_{max}}{p_{min}} . \qquad (A2.10)$$

Combining Equations (A2.10) and (A2.2) gives

$$\frac{M_{max}'}{M_{min}'} = \frac{M_{max}}{M_{min}} . \qquad (A2.11)$$

Combining Equations (A2.9) and (A2.4) gives, finally,

$$\frac{p_{o_{max}}'}{p_{o_{min}}} = \frac{M_{min}^2 M_{max}'}{M_{min}'^3} . \qquad (A2.12)$$

$p_{o_{max}}'$ is the pressure above which unacceptable deviations in C_p occur due to transition flow in the plug., As shown in Section 3, it has been experimentally determined that $p_{o_{max}} \geq 5200$ Torr. $p_{o_{min}}$ is the lowest pressure for which a gauge may be certified by the National Bureau of Standards, namely, 0.3 P.S.I. (15.5 Torr).

It therefore follows that for $p_o' = 5200$ Torr,

$$\frac{M_{min}^2 M_{max}'}{M_{min}'^3} = 336. \qquad (A2.13)$$

Now in the first experiment, it was required that M_{min} be such that unacceptable deviations from free molecular flow through the orifice did not occur. From the results of experiment and theory presented in Section 4, it is known that $M \geq 25$ for deviations to be less than one-half percent.

Thus, choosing $M_{min} = 25$, Equation (A2.12) becomes

$$\frac{M_{max}'}{M_{min}'^3} \leq 0.537. \qquad (A2.14)$$

Equation (A2.13) may therefore be used to determine the allowable range of $M'_{min} \leq M' \leq M'_{max}$ over which departures from molecular flow through the orifice may be investigated. As an example, for $M'_{min} = 5$, Equation (A2.14) yields the range

$$5 \leq M' \leq 67.2 \ . \qquad \text{(A2.15)}$$

Obviously, there is no need for M' to be increased above $M'_{max} = 25$ since deviations are negligible above there.

If C_p is chosen to be 10^{-6} liters/sec, and d as 0.1 cm, then for argon gas at 298°K ($\eta = 7.8$ liters/sec, $\gamma = 5.31 \times 10^{-3}$ cm) Equation (A2.2) shows the differential pressure across the orifice will range over

$$2.12 \times 10^{-3} \leq p \leq 1.06 \times 10^{-2} \text{ Torr.} \qquad \text{(A2.16)}$$

The orifice conductance, C, is found from Equation (A2.3) to be 0.078 liters/sec.

To determine the orifice required in the second experiment, note that from Equation (A2.1)

$$C p_{min} = C_p \, p_{o_{min}} , \qquad \text{(A2.17)}$$

and

$$C' p'_{min} = C_p \, p'_{o_{min}} , \qquad \text{(A2.18)}$$

And taking the ratio of (A2.17) and (A2.18) and using Equation (A2.4) gives

$$\frac{C'}{C} = \frac{p'_{o_{min}}}{p_{o_{min}}} \ . \qquad \text{(A2.19)}$$

Recalling Equations (A2.6) and (A2.11), Equation (A2.19) becomes

$$\frac{C'}{C} = \frac{M^2_{max}}{M'^2_{max}} = \frac{M^2_{min}}{M'^2_{min}} \ . \qquad \text{(A2.20)}$$

Then, using Equations (A2.3) and (A2.20), gives

$$\frac{d'}{d} = \frac{M_{min}}{M'_{min}}. \qquad \text{(A2.21)}$$

Thus, for the example cited above, the second orifice must be 0.5 cm diameter and thus will have a conductance of 1.95 liters/sec. The required pumping speed determined from S = 200 C' is 390 liters/sec.

REFERENCES

1. M. Knudsen, Ann. Physik 28, 999 (1909), English Translation: AEC-tr-3715.

2. N. F. Ramsey, Molecular Beams, Oxford at the Clarendon Press, 1956, p. 11.

3. a) P. C. Carman, Flow of Gases Through Porous Media, Academic Press, Inc., New York, 1956; b) P. C. Carman and F. A. Raal, Trans. Faraday Soc. 50, 842 (1954).

4. a) R. M. Barrer, Disc. Faraday Soc. 3, 61 (1948); b) R. M. Barrer and D. M. Grove, Trans. Faraday Soc. 47, 826, 837 (1951); c) R. M. Barrer and E. Strachan, Proc. Roy. Soc. A 231, 52 (1955); d) R. M. Barrer, Brit. J. Appl. Phys., Supplement No. 3, 541, 549 (1954).

5. a) K. Kammermeyer and D. W. Brubaker, Chem. Eng. Prog. 50, 560 (1954); b) K. Kammermeyer and D. D. Wyrick, Ind. and Eng. Chem. 50, 1309 (1958).

6. M. B. Volf, Technical Glasses, Sir Isaac Putnam and Sons, Ltd., London, 1961, p. 176.

7. M. E. Nordberg, J. Amer. Cer. Soc. 27, 299 (1944).

8. T. H. Elmer and M. E. Nordberg, VYCOR Brand Porous Glass, Code 7930 - A Unique Drying Agent, Research and Development Division, Corning Glass Works, Corning, New York, June 29, 1961.

9. F. A. Schwertz, J. Amer. Cer. Soc. 32, 390 (1949).

10. K. R. Atkins and H. Seki, Phys. Rev. 102, 582 (1956).

11. D. F. Brewer and D. C. Champeney, Pro. Phys. Soc. (London) 79, 87 (1962).

12. P. H. Emmett and T. W. DeWitt, J. Amer. Chem. Soc. 65, 1253 (1943).

13. S. Dushman, Scientific Foundations of Vacuum Technique, Second Edition, J. M. Lafferty, Editor, John Wiley and Sons, Inc., New York, 1962, pp. 30-32.

REFERENCES (Continued)

14. P. C. Carman and P. le R. Malherbe, Proc. Roy. Soc. A., 203, 165 (1950).

15. R. M. Barrer and J. A. Barrie, Proc. Roy. Soc. A., 213, 250 (1952).

16. T. H. Elmer, Research and Development Division, Corning Glass Works, Corning, New York, Private Communication.

17. A. J. Mathews, Evaluation of Porous Materials as Molecular Leaks, Arnold Engineering Development Center Technical Documentary Report No. AEDC-TDR-64-94, Air Force Systems Command, U. S. Air Force.

18. S. Dushman, op. cit., p. 87.

19. L. H. Wilson, W. L. Sibbitt, and M. Jakob, J. Appl. Phys. 22, 1027 (1951).

20. Industrial Components Department, Corning Glass Works, Corning, New York, Bulletin IC-21, August 5, 1960.

21. P. H. Emmett and Martin Cines, J. Phys. Chem. 51, 1248 (1947).

22. H. W. Liepmann, A Study of Effusive Flow, Aeronautics and Astronautics, Proceedings of the Durand Centennial Conference, Stamford University 5-8 August, 1959, Pergamon Press, New York, 1960, p. 153.

23. H. W. Liepmann, J. Fluid Mech. 10, 65 (1961).

24. R. Narasimha, Phys. Fluids 3, 476 (1960).

25. R. Narasimha, J. Fluid Mech. 10, 371 (1961).

26. D. R. Willis, Center-Point Mass Flow Through a Circular Orifice Using the Integral Iteration Method, Technical Note No. 3, Division of Gas Dynamics, Royal Institute of Technology, Stockholm, Sweden, December 1960.

27. R. F. Probstein, The First Collision Orifice Problem and a Suggested Transformation for Rarefied Flow Analysis, Second International Symposium on Rarefied Gas Dynamics, Berkeley (1960).

28. J. E. Scott, Jr., H. S. Morton, Jr., J. A. Phipps, and J. F. Moonan, Project Squid Technical Report UNA-5-P, July 1964, Department of Aero Space Engineering, University of Virginia, Charlottesville, Virginia, ASTIA Document No. AD-602 977.

29. S. Dushman, op. cit., p. 82.

30. S. Dushman, op. cit., p. 32.

31. A. J. Bureau, L. J. Laslett, and J. M. Keller, Rev. Sci. Instr. 23, 683 (1952).

32. M. Knudsen, Ann. Physik, 28, 75 (1909). English Translation: AEC-tr-3303.

33. a) P. Clausing, Physica, 9, 65 (1929), English Translation: AEC-tr-2525 ; b) Ann. Physik, 7, 489 (1930); c) Zeits. f. Phys. 66, 471 (1930). English Translation: AEC-tr-2446 ; d) Ann. Phys. 52, 961 (1932), English Translation: AEC-tr-2447 .

34. M. v. Smoluchowski, Ann. der Physik u. Chemie 33, 1567 (1910).

35. W. C. deMarcus, The Problem of Knudsen Flow. Part III. Solutions for One Dimensional Systems. Report No. K-1302, March 19, 1957, Union Carbide Nuclear Company, Oak Ridge, Tennessee, ASTIA Document No. AD 124 579.

36. A. R. Miller, The Fraction of Effusing Molecules Striking a Collector Plate Over a Circular Capillary, Report An-1328, Aerojet-General Nucleonics, San Ramon, California, December, 1964, ASTIA Document No. AD 454 732.

37. E. H. Kennard, Kinetic Theory of Gases, McGraw-Hill Book Co., Inc., New York, 1938, p. 307.

38 a) F. Knauer and O. Stern, Zeits. f. Physik 38, 764 (1926); b) F. Knauer, Zeits. f. Physik 53, 766 (1929), English Translation: AEC-NP 2400.

39. F. Knauer, Zeits. f. Physik 60, 414 (1930).

40. H. Mayer, Zeits. f. Physik 58, 373 (1929).

41. M. Kratzenstein, Zeits. f. Physik 93, 279 (1935).

42. a) T. H. Johnson, Nature 119, 745 (1927); b) Phys. Rev. 31, 103 (1928).

43. C. B. Barnes, Jr., Vacuum 14, 429 (1964).

44. N. E. Cooke, An Inherent Error in the Knudsen Effusion Manometer and a Method of Correction, Vacuum Symposium Transactions, 1956, Pergamon Press, London, 1957, p. 82.

45. F. Feakes, F. L. Torney, Jr., and F. J. Brock, Gauge Calibration in Extreme High Vacuum, NASA Contractor Report, NASA CR-167.

46. J. P Dawson, J. D. Haygood, and J. A. Collins, Jr., Temperature Effects on the Capture Coefficients of Carbon Dioxide, Nitrogen, and Argon, Advances in Cryogenic Engineering, Volume 9, K. D. Timmerhaus, Editor, Plenum Press, New York, 1964, p. 443.

47. S. N. Foner, F. A. Mauer, and L. H. Bolz, J. Chem. Phys. 31, 546 (1959).

48. V. J. Johnson, General Editor, A Compendium of the Properties of Materials at Low Temperatures. Part 1. Properties of Fluids, July 1960. Wright Air Development Division Technical Report WADD TR 60-56 (Part I). U. S. Air Research and Development Command, United States Air Force, Wright-Patterson Air Force Base, Ohio.

49. E. H. Kennard, op. cit., p. 61.

50. Indalloy Intermediate Solders, The Indium Corporation of America, Utica, New York, 1957, p. 19.

51. American Institute of Physics Handbook, D. E. Gray, Editor, McGraw-Hill Book Co., Inc., New York, 1957, p. 4-118.

52. Dushman, op. cit., p. 422.

53. J. P. Hobson and R. A. Armstrong, J. Phys. Chem. 67, 2000 (1963).

54. J. H. de Boer, The Dynamical Character of Adsorption, Oxford University Press (1953).